1969

The cross section for the formation of H [Superscript +] [Subscript 2] in the reaction of fast protons with methane

Smyth, Norman Robert Anton

Monterey, California. U.S. Naval Postgraduate School

http://hdl.handle.net/10945/11903

THE CROSS SECTION FOR THE FORMATION OF H_2^+ IN THE REACTION OF FAST PROTONS WITH METHANE

by

Norman Robert Anton Smyth

United States Naval Postgraduate School

THESIS

THE CROSS SECTION FOR THE FORMATION OF H_2^+ IN THE REACTION OF FAST PROTONS WITH METHANE

by

Norman Robert Anton Smyth

June 1969

The Cross Section for the Formation of H_2^+

in the Reaction of Fast Protons with Methane

by

Norman Robert Anton Smyth
Captain, Canadian Armed Forces
B.Sc., University of Alberta, 1963

Submitted in partial fulfillment of the
requirements for the degree of

MASTER OF SCIENCE IN PHYSICS

from the

NAVAL POSTGRADUATE SCHOOL
June 1969

ABSTRACT

The capture cross section for the formation of H_2^+ in the reaction $\underline{H}^+ + CH_4 \rightarrow \underline{H}_2^+ + CH_3$ was measured at incident proton energies of 70, 85, 100, 150 and 200 eV and covering the scattering angles of 43^o to 49.5^o (lab coordinates). At 100 eV and below the curve of the cross section versus angle shows a sharp peak at about 46^o whose position approaches the theoretical limit of 46.9^o with increasing energy. Above 100 eV the peak was too small to be observed and only an upper limit can be placed on the value of the cross section. Typical values of the total cross section are 2.0×10^{-21} cm^2 at 70 eV and 7.6×10^{-22} at 100 eV. The magnitude and energy dependence of the cross section as well as the angular position of the peak all are in essential agreement with the classical theory of ion-molecule rearrangement collisions proposed by Bates, Cook and Smith.

TABLE OF CONTENTS

LIST OF TABLES

LIST OF FIGURES

Figure

ACKNOWLEGEMENTS

I wish to express my sincere gratitude and appreciation to my thesis advisor, Dr. Otto Heinz, for his confidence, encouragement and friendship, and for giving me the opportunity of working on this particular research project. My special thanks is also directed to Dr. Charles Cook of Stanford Research Institute, Palo Alto, California for the many days he devoted to assisting and advising me throughout this experiment. I am also grateful to Dr. Thomas Bush (LCDR USN) of the Lawrence Radiation Laboratory, Livermore, California for imparting to me much of his knowledge and understanding of the theory and operation of the experimental apparatus. I want to thank Mr. Thomas Maris of the Naval Postgraduate School, Physics Department Technical Staff for his patience, his technical competence, and his constant assistance.

I am very grateful to my wife Karen, whose interest in this project made the long hours seem less demanding and whose love and understanding made the disappointments and frustrations less traumatic and the final success more rewarding.

I would like to dedicate this work to the memory of the man who built and tested the ion-source I used; my friend and associate, Capt. Thomas Carter USMC, who was killed in action in the Republic of Viet Nam in November 1968.

I. INTRODUCTION

The correct description of complex atomic and molecular interactions is one of the major achievements of modern quantum theory. While there appears to be little doubt about the correctness of the theory in principle, it has become evident in practice that the mathematical complexity is such that only the very simplest cases can be treated with anything approaching complete rigor. Therefore many approximations are employed to simplify these mathematical computations. The question then, of the accuracy, nature and range of applicability of these approximations is of considerable practical importance. In general these questions can only be answered by comparison of the experimental results and the predictions of a specific approximate calculation.

This paper presents the results of a series of measurements which confirm the predictions of a classical theory of ion-molecule rearrangement collisions at high impact energies as proposed by Bates, Cook and Smith [1]. This theory uses an impulse type approximation to obtain the cross section for the capture of a light atom or ion from a target molecule by a fast moving projectile. Applying this theory to the reaction:

$$\underline{H}^{+} + CH_4 \rightarrow \underline{H}_2^{+} + CH_3 \qquad (1)$$

the cross section is predicted to show a sharp peak at 46.9° with an upper limit on the magnitude of the cross section of 1.4×10^{-20} cm^2 at 100 eV incident proton energy. It is further

predicted that the magnitude of the cross section should decrease rapidly with increasing proton energy, approaching an energy dependence of $E^{-5.5}$ asymptomatically at high energies (above 500 eV). The range of validity of the theory extends from about 50 to 800 eV when applied to reaction (1).

Our measurements were carried out at 70, 85, 100, 150, and 200 eV, covering the angles of scatter from 43° to 49.5°. We found essential agreement between the predictions of the theory and the experimental data, indicating that the classical impulse approximation proposed by Bates, Cook and Smith is a valid model for reaction (1) in the energy region considered.

II. THEORY

A. CLASSICAL THEORY OF ION-MOLECULE REARRANGEMENT COLLISIONS

A classical theory of ion-molecule rearrangement collisions at high impact energies has been proposed by Bates, Cook and Smith [1]. The impact energies are assumed to be high enough so polarization forces and chemical binding energies of the colliding molecules can be ignored. The theory applies to various ion molecule rearrangement reactions of the type:

$$\underline{X'X_i} + YZ_kZ' \rightarrow \underline{X}' + \underline{X_iY} + (\underline{Z_k} + Z') \qquad (1)$$

where X_i and Y are simple atoms or ions. The bar indicates which ions are fast in the laboratory coordinate system. An example of a rearrangement reaction of this type is:

$$\underline{H}^+ + CH_4 \rightarrow \underline{H}_2^+ + CH_3 \qquad (2)$$

The basic assumption made by Bates, Cook and Smith, is that process (1) may be described by a classical impulse approximation similar to that developed by Thomas [2], for the description of electron capture, where each composite system is regarded as a loose cluster of atoms and ions. (Eg $H_2^+ = H + H^+$ and $CH_4 = C + 3H + H$).

According to this model, we can consider the reaction to occur in the following manner: consider a particle of mass M_1 moving with velocity $\vec{v}_1$ through molecules of loosely bound particles of mass M_2 and M_k. Figure 1 shows the sequence of collisions that lead to

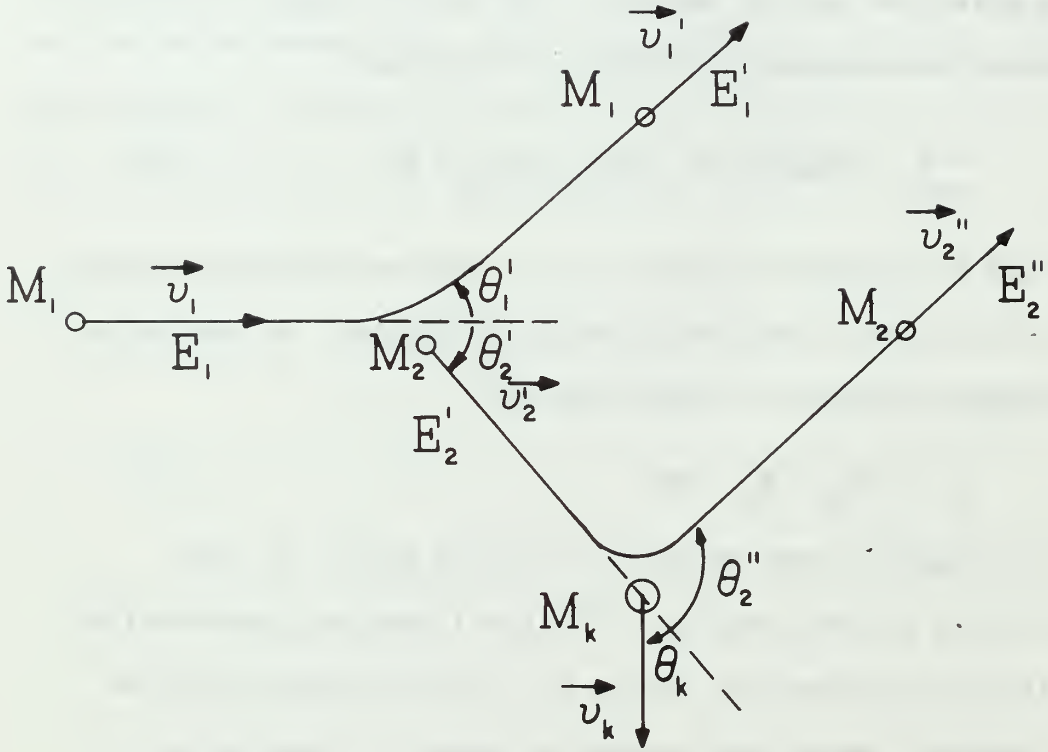

FIGURE I THE CAPTURE MECHANISM

the capture of M_2 by M_1. First mass M_1 collides with mass M_2. This causes M_1 to be scattered at an angle θ_1' and velocity $\vec{v}_1'$ while M_2 recoils at an angle θ_2' with velocity $\vec{v}_2'$. Mass M_2 then suffers a second binary collision with mass M_k. This causes M_2 to scatter at an angle θ_2'' with velocity $\vec{v}_2''$.

$$\left.\begin{array}{l} \text{Now if: (a) } \theta_2'' \approx \theta_2' + \theta_1' \\ \\ \text{And if: (b) } v_1' \approx v_2'' \end{array}\right\} \text{ or } \vec{v}_1' = \vec{v}_2'' \tag{3}$$

then masses M_1 and M_2 may have a relative energy of motion below that required for separation, and so, the two particles may combine and proceed on as one. If the particle with mass M_1 is a composite particle then its disruption can be avoided if

$$\vec{v}_1' \approx \vec{v}_1 \ . \tag{4}$$

In the particular case of:

$$M_2 = M_1 << M_k$$

condition (3) is satisfied if $\theta_1' \approx 45^\circ$ and $\theta_2'' \approx 90^\circ$ (see Section II of this Chapter), but then condition (4) is violated. In the case of the reaction:

$$\underline{H}^+ + CH_4 \rightarrow \underline{H}_2^+ + CH_3$$

where $M_1 = M_{H+}$, $M_2 = M_H$ and $M_k = M_{CH_3}$, the violation of condition (4) is not relevant since M_1 is not a composite particle.

Consider now, the first binary collision between M_1 and M_2 as shown in Fig. 2. The probability of scattering M_2 into the solid angle $d\Omega(\theta_2')$ with velocity between $\vec{v}_2'$ and $\vec{v}_2' + d\vec{v}_2'$ is:

$$q = \sigma_{12}(\theta_2')\ d\Omega(\theta_2') \tag{5}$$

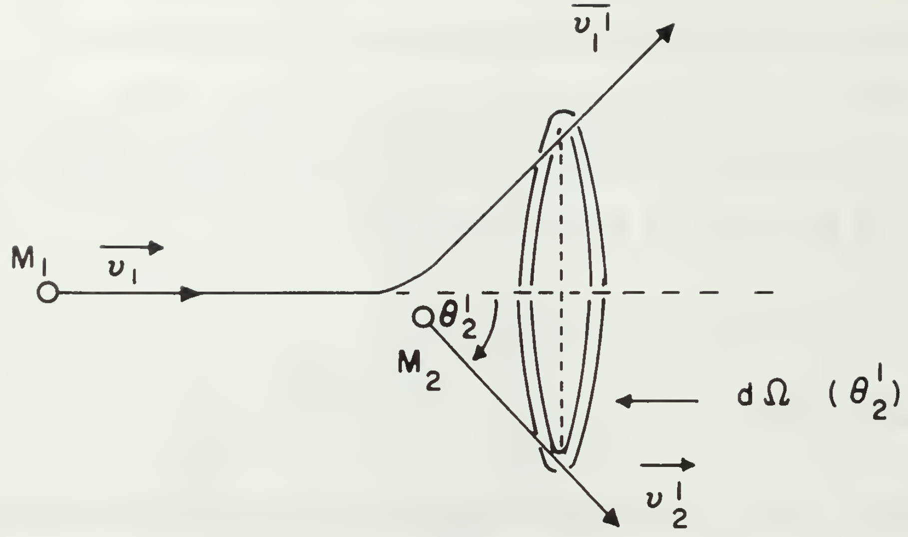

FIGURE 2. THE FIRST BINARY COLLISION

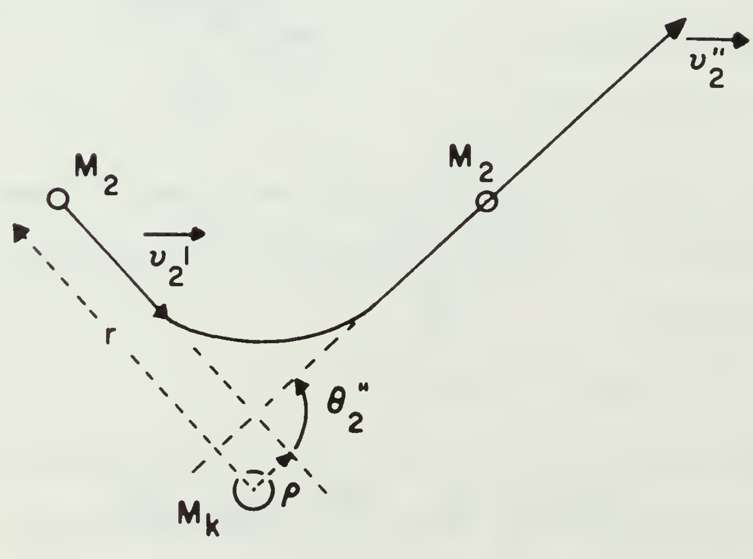

FIGURE 3. THE SECOND BINARY COLLISION

where $\sigma_{12}(\theta_2')$ is the appropriate differential scattering cross section. Since the solid angle is the cone of semi-angle θ_2' within $d\theta_2'$ then:

$$d\Omega(\theta_2') = 2\pi \sin \theta_2' \, d\theta_2'$$

and equation (5) becomes:

$$q = 2\pi\sigma_{12}(\theta_2') \sin \theta_2' \, d\theta_2' \, . \tag{6}$$

Consider now, the second binary collision between M_2 and M_k as shown in Fig. 3. The probability of M_2 having an impact parameter between ρ and $\rho + d\rho$ and an azimuthal angle between ψ and $\psi + d\psi$ at a distance r from M_k is given by:

$$p = \rho \, d\rho \, \frac{d\psi}{4\pi r^2} \tag{7}$$

where r is the M_2-M_k equilibrium internuclear separation. But particles incident on M_k with impact parameter ρ and azimuthal angle ψ are scattered into the solid angle $dr(\theta_2'')$ at θ_2''.

Hence: $$\rho \, d\rho = \sigma_{2k}(\theta_2'') \, d\Omega(\theta_2'')$$

where $\sigma_{2k}(\theta_2'')$ is the appropriate differential scattering cross section.

But: $$d\Omega(\theta_2'') = \sin \theta_2'' \, d\theta_2''$$

Hence equation (7) becomes:

$$p = \sigma_{2k}(\theta_2'') \sin \theta_2'' \, d\theta_2'' \, \frac{d\psi}{4\pi r^2} \tag{8}$$

Now, for M_1 to capture M_2, $\vec{v}_1' - \vec{v}_2''$ the relative velocity of M_1 and M_2 must be contained within a volume of velocity space

determined by D, the mutual affinity of these two systems. In the high velocity limit, Bates, Cook and Smith [1], state this requirement as:

$$(v_2'')^2 \sin \theta_2'' \, d\theta_2'' \, d\phi \, dv_2'' = \lambda \frac{4}{3} \pi \left(\frac{2D}{\mu}\right)^{3/2} \tag{9}$$

where $\lambda = \frac{1}{2}$ and $\mu = \frac{1}{2}M_2$ in the case of $M_2 = M_1 < M_k$. (10)

Substituting equation (9) into equation (8) we get

$$p = \frac{\sigma_{2k}(\theta_2'')}{3r^2} \left(\frac{2D}{\mu}\right)^{3/2} \frac{\lambda}{(v_2'')^2 dv_2''} . \tag{11}$$

Now, the capture cross section arising from the M_1-M_2-M_k sequence of binary collisions is:

$$Q(M_1\text{-}M_2\text{-}M_k) = \gamma p q \tag{12}$$

where γ is a dimensionless factor, less than, or equal to unity, which allows for the fact that M_1 and M_2 may approach each other such that in the resulting state, the affinity is less than that assumed.

Substituting equations (6) and (11) into (12) one gets:

$$Q(M_1\text{-}M_2\text{-}M_k) = \gamma\lambda \frac{2\pi \, \sigma_{12}(\theta_2')\sigma_{2k}(\theta_2'')}{3r^2} \sin \theta_2' \, d\theta_2' \, 2\left(\frac{2D}{\mu v_2''}\right)^{3/2} \frac{v_2''}{dv_2''} . \tag{13}$$

Changing from Lab. to Center of Mass coordinates, one gets for the case of $M_1 = M_2 << M_k$

$$Q(M_1\text{-}M_2\text{-}M_k) = \gamma \frac{16\pi \, \bar{\sigma}_{12}(90^\circ) \, \bar{\sigma}_{2k}(90^\circ)}{3r^2} \left(\frac{2D}{M_2 v_1^2}\right)^{3/2} \tag{14}$$

where $\bar{\sigma}_{12}$ and $\bar{\sigma}_{2k}$ denote the differential scattering cross sections in the center of mass coordinate systems. This

differential cross section is at an energy of relative motion of $\frac{1}{4} M_2 v_1^2$ and the affinity D is at an M_2-M_k internuclear distance of $\sqrt{2}\, r$. To obtain the total cross section for capture, Q, one now sums over all binary collision sequences which lead to the same final capture process. For example, the total cross section for process (2) is

$$Q = 4Q(H^{+}\text{-}H\text{-}C) + 4Q(H\text{-}H^{+}\text{-}C).$$

This represents the two possible collision sequences shown below:

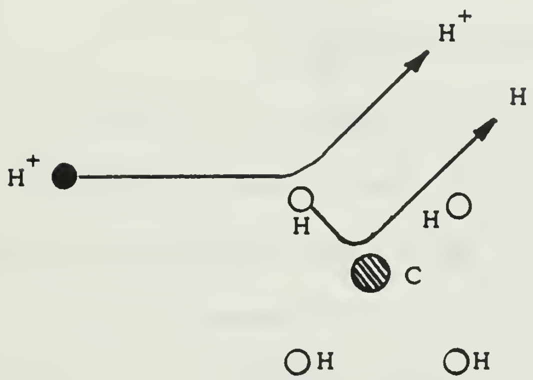

The $(H^{+}$- H - C) Sequence

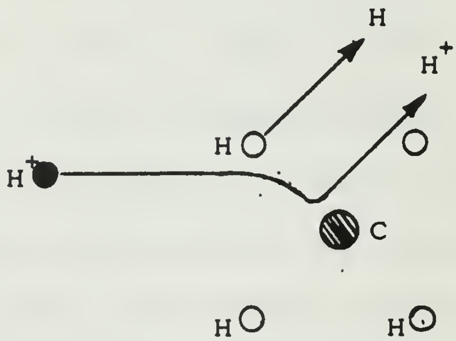

The (H- H^{+} - C) Sequence

Solution of Rutherford's expression for the differential scattering cross section when v_1 is high enough for the atomic field to be Couloumbic, shows that:

$$Q(M_1\text{-}M_2\text{-}M_k) \sim v_1^{-11} . \tag{15}$$

The range of validity of (14) does not extend indefinitely as v_1 increases. Two requirements must be satisfied:

(i) The De Broglie wavelength limitations,

(ii) The Heisenberg uncertainty relations.

Bates, Cook and Smith [1], computed the required differential scattering cross sections $\bar{\sigma}_{12}(90^{\circ})$ and $\bar{\sigma}_{2k}(90^{\circ})$ using classical methods and the analytic representation of the relevant Hartree potentials as given by Byatt [3]. From the results of these computations listed in Ref. 1, the cross section for the rearrangement reaction:

$$\underline{H}^{+} + CH_4 \rightarrow \underline{H}_2^{+} + CH_3$$

is determined to be as shown in Fig. 4.

B. THE $\underline{H}^{+} + CH_4 \rightarrow \underline{H}_2^{+} + CH_3$ REACTION KINETICS

The rearrangement mechanism for the reaction is shown in Fig. 1, where M_1 represents the H^{+}, M_2 the H and M_k represents the CH_3. To determine the exact value of the scattering angle θ_1' one has to consider the kinematics of the arrangement process.

If the speed v_1 is assumed to be large enough so the binding energy of M_2 to M_k can be ignored, then the conservation laws can be applied in the usual manner.

Consider the first binary collision of the reaction shown in Fig. 1. From conservation of energy and momentum we have:

$$\tfrac{1}{2}M_1 v_1^2 = \tfrac{1}{2}M_1 (v_1')^2 + \tfrac{1}{2}M_2 (v_2')^2 \qquad (16)$$

$$M_1 v_1 = M_1 v_1' \cos \theta_1' + M_2 v_2' \cos \theta_2' \qquad (17)$$

$$0 = M_1 v_1' \sin \theta_1' - M_2 v_2' \sin \theta_2' \qquad (18)$$

Now: $\quad M_1 = M_2 = M_H$

Hence: the above equations become

$$v_1^2 = (v_1')^2 + (v_2')^2 \qquad (19)$$

FIGURE 4

PREDICTED CROSS SECTION FOR

$H^+ + CH_4 \longrightarrow H_2^+ + CH_3$

FROM BATES COOK SMITH'

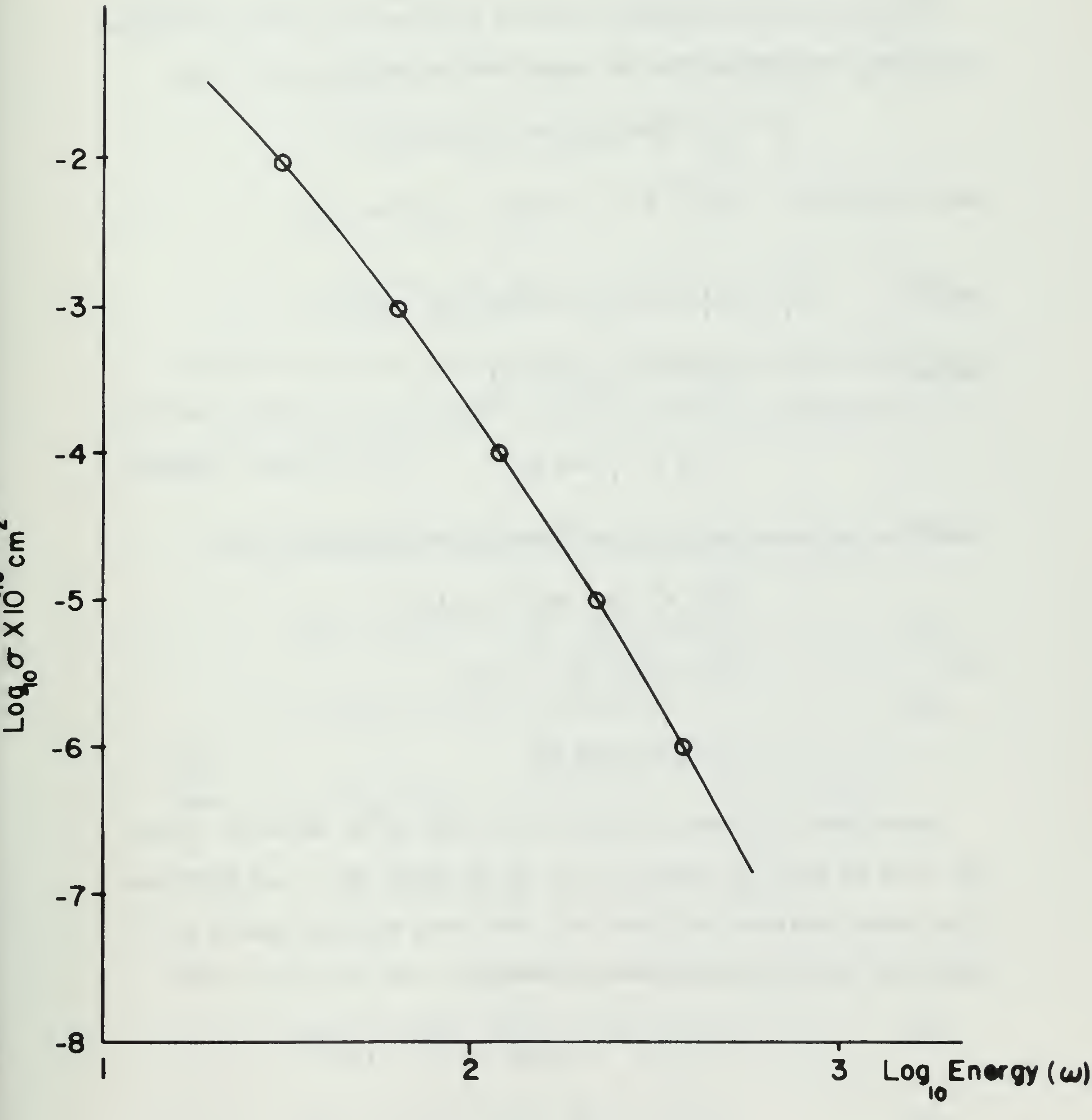

$$v_1 = v_1' \cos \theta_1' + v_2' \cos \theta_2' \qquad (20)$$

$$0 = v_1' \sin \theta_1' - v_2' \sin \theta_2' \qquad (21)$$

Now θ_2' can be eliminated between (20) and (21) by rearranging, squaring, and adding the two equations to yield:

$$v_1^2 + (v_1')^2 - 2v_1 v_1' \cos \theta_1' = (v_2')^2 \ .$$

But from (19): $(v_2')^2 = v_1^2 - (v_1')^2$

Thus: $v_1^2 + (v_1')^2 - 2v_1 v_1' \cos \theta_1' = v_1^2 - (v_1')^2$

Hence: $(v_1')^2 = v_1 v_1' \cos \theta_1'$

$$\therefore\ v_1' = v_1 \cos \theta_1' \qquad (22)$$

Substituting equation (22) back into equation (19) we get:

$$v_1^2 = v_1^2 (\cos \theta_1')^2 + (v_2')^2$$

or: $v_1^2 (1-\cos^2 \theta_1') = (v_2')^2$

$$\therefore\ v_2' = v_1 \sin \theta_1' \qquad (23)$$

Equations (22) and (23) give us v_1' and v_2' in terms of v_1 and θ_1'. Now we wish to obtain v_1' and v_2' in terms of v_1 and θ_2'. Thus we arrange equation (20) and (21) such that when we square and add them, we eliminate θ_1' and so obtain:

$$v_1^2 + (v_2')^2 - 2v_1 v_2' \cos \theta_2' = (v_1')^2 \ .$$

But from (19) we have: $(v_1')^2 = v_1^2 - (v_2')^2$

Thus: $v_1^2 + (v_2')^2 - 2v_1 v_2' \cos \theta_2' = v_1^2 - (v_2')^2$

Hence: $v_2' = v_1 \cos \theta_2'$. (24)

Substituting equation (24) back into equation (19) gives:

$$v_1^2 = (v_1')^2 + v_1^2 \cos^2 \theta_2'$$

or: $$v_1^2(1-\cos^2\theta_2') = (v_1')^2$$

$$\therefore \quad v_1' = v_1 \sin \theta_2' \quad . \tag{25}$$

Consider now, the second binary collision. Again ignoring the binding energies we can write the conservation of energy and momentum equations as:

$$\tfrac{1}{2} M_2(v_2')^2 = \tfrac{1}{2} M_2(v_2'')^2 + \tfrac{1}{2} M_k v_k^2 \tag{26}$$

$$M_2 v_2' = M_2 v_2'' \cos \theta_2'' + M_k v_k \cos \theta_k \tag{27}$$

$$0 = M_2 v_2'' \sin \theta_2'' - M_k v_k \sin \theta_k \tag{28}$$

Now: $M_1 = M_2 = M_H$

and: $M_k = M_{CH_3}$

Thus the above three equations reduce to:

$$(v_2')^2 = (v_2'')^2 + \frac{M_k}{M_H} v_k^2 \tag{29}$$

$$(v_2') = v_2'' \cos \theta_2'' + \frac{M_k}{M_H} v_k \cos \theta_k \tag{30}$$

$$0 = v_2'' \sin \Theta_2'' - \frac{M_k}{M_H} v_k \sin \Theta_k . \quad (31)$$

As we are not interested in Θ_k we can eliminate it by suitably rearranging equations (30) and (31) and then squaring and adding. Thus we get:

$$(v_2')^2 + (v_2'')^2 - 2v_2' v_2'' \cos \Theta_2'' = \left(\frac{M_k}{M_H}\right)^2 v_k^2 . \quad (32)$$

But from equation (29):

$$\frac{M_k}{M_H} v_k^2 = (v_2')^2 - (v_2'')^2.$$

Thus (32) becomes:

$$(v_2')^2 + (v_2'')^2 - 2v_2'v_2'' \cos \Theta_2'' = \frac{M_k}{M_H} (v_2')^2 - \frac{M_k}{M_H} (v_2'')^2$$

or

$$(v_2')^2 \left(1 - \frac{M_k}{M_H}\right) + (v_2'')^2 \left(1 + \frac{M_k}{M_H}\right) - 2 v_2'v_2'' \cos \Theta_2'' = 0$$

Multiplying through by: $\frac{M_H}{M_k + M_H} \left(\frac{1}{v_2'}\right)^2$ yields:

$$\frac{M_H - M_k}{M_H + M_k} + \left(\frac{v_2''}{v_2'}\right)^2 - 2 \frac{v_2''}{v_2'} \left(\frac{M_H}{M_H + M_k}\right) \cos \Theta_2'' = 0 \quad (33)$$

Now, let: $a = \frac{M_H}{M_k + M_H}$ and $b = \frac{M_k - M_H}{M_k + M_H}$.

Then (33) becomes:

$$\left(\frac{v_2''}{v_2'}\right)^2 - 2\left(\frac{v_2''}{v_2'}\right) a \cos \Theta_2'' - b = 0 \quad (34)$$

But now, for capture, we require that: $\Theta_2'' \approx \Theta_1' + \Theta_2'$

thus: $\cos \Theta_2'' \approx \cos (\Theta_1' + \Theta_2')$

ie., $\cos \Theta_2'' \approx \cos \Theta_1' \cos \Theta_2' - \sin \Theta_1' \sin \Theta_2'$ and using (24) and (25) to eliminate Θ_2' we have:

$$\cos \Theta_2'' \approx \cos \Theta_1' \left(\frac{v_2'}{v_1}\right) - \sin \Theta_1' \left(\frac{v_1'}{v_1}\right).$$

Hence equation (34) becomes:

$$\left(\frac{v_2''}{v_2'}\right)^2 - 2a\left[\frac{v_2''}{v_2'}\,\frac{v_2'}{v_1}\cos \Theta_1' - \frac{v_2''}{v_2'}\,\frac{v_1'}{v_1}\sin \Theta_1'\right] - b = 0$$

$$\text{or:}\quad (v_2'')^2 - 2av_2'\left[\frac{v_2''v_2'}{v_1}\cos \Theta_1' - \frac{v_2''v_1'}{v_1}\sin \Theta_1'\right] - b(v_2')^2 = 0\ . \quad (35)$$

But now, the second capture criteria is that: $v_2'' \approx v_1'$.

But, from equation (22) we have: $v_1' = v_1 \cos \Theta_1'$.

Hence, we require for capture: $v_2'' \approx v_1 \cos \Theta_1'$. (36)

Substituting equations (22) and (36) into (35) we get:

$$v_1^2 \cos^2 \Theta_1' - 2av_2'\,[v_2' \cos^2\Theta_1' - v_1 \sin \Theta_1' \cos^2\Theta_1'] - b(v_2')^2 = 0.$$

Using (23) to eliminate v_2' from this equation we get:

$$v_1^2\cos^2\Theta_1' - 2av_1\sin\Theta_1'\,[v_1\sin\Theta_1'\cos^2\Theta_1' - v_1\sin\Theta_1'\cos^2\Theta_1'] - bv_1^2\sin^2\Theta_1' = 0$$

which reduces to: $v_1^2 \cos^2 \Theta_1' - b\, v_1^2 \sin^2 \Theta_1' = 0.$

Hence, for capture to occur we must have:

$$\tan \Theta_1' = \sqrt{\frac{1}{b}} = \sqrt{\frac{M_k + M_H}{M_k - M_H}}\ . \quad (37)$$

Now $M_k = M_{CH_3} = 15.03506$ and $M_H = 1.00797$ amu. Thus the angle at which capture occurs is:

$$\theta_1' = 46.926^{\circ} \tag{38}$$

Hence we expect the capture cross section to show a pronounced peak at this angle. From Fig. 4, the magnitude of the cross section is predicted to be approximately 1.4×10^{-20} cm^2 if the energy of the incident proton beam is 100 eV.

C. THE RANGE OF VALIDITY OF THE CLASSICAL DESCRIPTION

A lower limit on the range of validity of the classical treatment of the rearrangement collision is imposed by the assumption made in the theoretical development that the energies involved in the collision are much larger than the binding energies. Hence, when the energy of the incident proton beam E_1 is less than, or equal to about 10 times the binding energy we expect the peak in the cross section to become less pronounced and more spread out. Thus the theory is valid when $E_1 \geq 50$ eV.

An upper limit on the range of validity of the theory is determined by the two requirements:

(i) The Di Broghlie Wavelength λ of any particle involved must be much less than the smallest distance involved in the collision S.

Hence we require: $\lambda << S$ (39)

(ii) The uncertainty in energy introduced by specifying the transverse position of the proton must be much less than the binding energy of the final product. Now, from (39)

we know the uncertainty in the proton position λ is less than the distance of closest approach S.

But we can write the uncertainty relation:

$$\Delta x \Delta p = \frac{\hbar}{2} \tag{40}$$

as

$$S \Delta p >> \frac{\hbar}{2}$$

Thus

$$\Delta p >> \frac{\hbar}{2S} \tag{41}$$

or

$$\Delta E = \frac{\Delta p^2}{2M_H} >> \frac{\hbar^2}{8M_H S^2} . \tag{42}$$

We then demand that the binding energy D be greater than ΔE, or:

$$D >> \frac{\hbar^2}{8M_H S^2} \tag{43}$$

To find what restrictions equations (39) and (43) place on the energy of the incident proton beam we have to relate the distance of closest approach S to the energy of the proton beam E_1. This can be done quite readily in the case of coulomb collisions. By considering the collisions to be coulomb it will be shown that: $S = \frac{C_1}{E_1}$

and $\lambda = \frac{C_2}{\sqrt{E_1}}$

where C_1 and C_2 are constants. Because S decreases faster than λ as E_1 increases we see that equation (39) will indeed place an upper limit on the energy E_1.

In a Coulomb collision the point of closest approach is yielded by solving the equation:

$$1 - \frac{b^2}{S^2} - \frac{\emptyset(S)}{U_1} = 0 \tag{44}$$

(see equation 3-4-3 of Ref. 4)

U_1, the Center of Mass energy, can be expressed as $U_1 = \frac{1}{2} \mu v_{rel}^2$ where μ is the reduced mass and v_{rel} is the relative speed of approach. $\emptyset(S)$, the potential energy at the distance of closest approach, is:

$$\emptyset(S) = \frac{(Ze)(Z'e')}{S}$$

The impact parameter b is given by:

$$b = \frac{(Ze)(Z'e')}{\mu v_{rel}^2} \cot \frac{\Theta}{2} \tag{45}$$

(see equation 3-8-8 of Ref. 4)

Where Θ is the Center of Mass scattering angle.

Now we have two collisions to consider:

(i) In the first binary collision (H^+-H) we have (see Fig. 1)

$$\Theta = 90^o, \mu = \frac{M_H}{2}, v_{rel} = v_1 \tag{46}$$

(ii) In the second binary collision (H-C) we have (see Fig. 1)

$$\Theta \approx \theta_2'' = 90^o, \mu \approx M_H, v_{rel} = v_2' \tag{47}$$

and since $E_2' \approx \frac{1}{2} E_1$ we have $v_2' \approx \frac{1}{\sqrt{2}} v_1$.

Making these substitutions in (45) we get:

$$b_{H^+ - H} = \frac{e^2}{E_1} \tag{48}$$

$$b_{H-C} = 12 \frac{e^2}{E_1} \tag{49}$$

where: $E_1 = \frac{1}{2} M_H v_1^2$.

Hence for the $H^+ - H$ collision, equation (45) yields

$$S^2 - \frac{2e^2}{E_1} S - \frac{e^4}{E_1^2} = 0$$

Which gives: $S(H^+ - H) \approx 2.4 \frac{e^2}{E_1}$. (50)

Similarily, for the H-C collision we get:

$$S^2 - \frac{12e^2}{E_1} S - \frac{144 e^4}{E_1^2} = 0$$

which gives: $S(H\text{-}C) \approx 7.4 \frac{e^2}{E_1}$. (51)

Hence the $H^+ - H$ collision has the smallest distance of closest approach and hence equation (50) will establish the upper limits of validity of the classical approximation.

Consider first the restrictions imposed by equation (39). We require that: $\lambda << S$

or:

$$\frac{h}{\sqrt{2M_H E_1}} << 2.4 \frac{e^2}{E_1}$$

$$\therefore E_1 << 2.32 \times 10^{-8} \text{ Ergs} \qquad (52)$$

$$\text{or} \quad E_1 << 1.45 \times 10^{+4} \text{ eV.}$$

Thus the wavelength considerations require $E_1 << 1.45 \times 10^4$ eV if our classical approximation is to be valid.

Consider now the restrictions imposed by equation (43). We require that:

$$D >> \frac{\hbar^2}{8M_H S^2}$$

or $$D \gg \frac{\hbar^2 E_1^2}{8M_H (2.4)^2 e^4} .$$

The binding energy of H_2^+ is 2.6 eV. Thus we get:

$$E_1 \ll \sqrt{8M_H D} \left(\frac{2.4e^2}{\hbar}\right) \tag{53}$$

$$= 3.93 \times 10^{-9} \text{ Ergs}$$

$$= 2.46 \times 10^{+3} \text{ eV.}$$

Hence equations (39) and (43) are satisfied if the energy of the incident proton beam is less than 1,000 electron volts. Thus the classical description of process (2) is valid in the 75 to 200 eV range where the experiment was performed.

III. EXPERIMENTAL APPARATUS

The experimental apparatus used in this experiment is the result of the work of many people. The overall apparatus, as shown in Fig. 5, was assembled by Bush [5], who demonstrated its satisfactory operation.

A reasonably mono-energetic beam of hydrogen ions ($\Delta E \sim 2$ eV) is produced in the Duoplasmatron, which was built and investigated by Carter [6]. The beam is mass analyzed in the mass spectrometer constructed by Strohshal [7], and H^+ ions proceed on to the scattering chamber which contains the target gas, CH_4. The scattering cell is placed on the magnetic axis of a large cylindrical magnet at the position of maximum field. H_2^+ ions, produced by the collision of H^+ with CH_4, exit from the scattering cell and are focused by the axially symmetric non-uniform field of the focusing magnet to a point on the magnetic field axis, a distance Z_o from the scattering cell. The detector which is located at Z_o, is an electron multiplier capable of gains up to 10^6.

A. THE DUOPLASMATRON

The duoplasmatron is shown in Fig. 6. With hydrogen in the source and filament power at 35 watts, one has about .1 amp of electron emission from the filament. An arc voltage of 400 volts between the filament and the Z-electrode accelerates these electrons through the hydrogen gas, ionizing the hydrogen and forming a plasma. Once the plasma has been formed, an arc current of

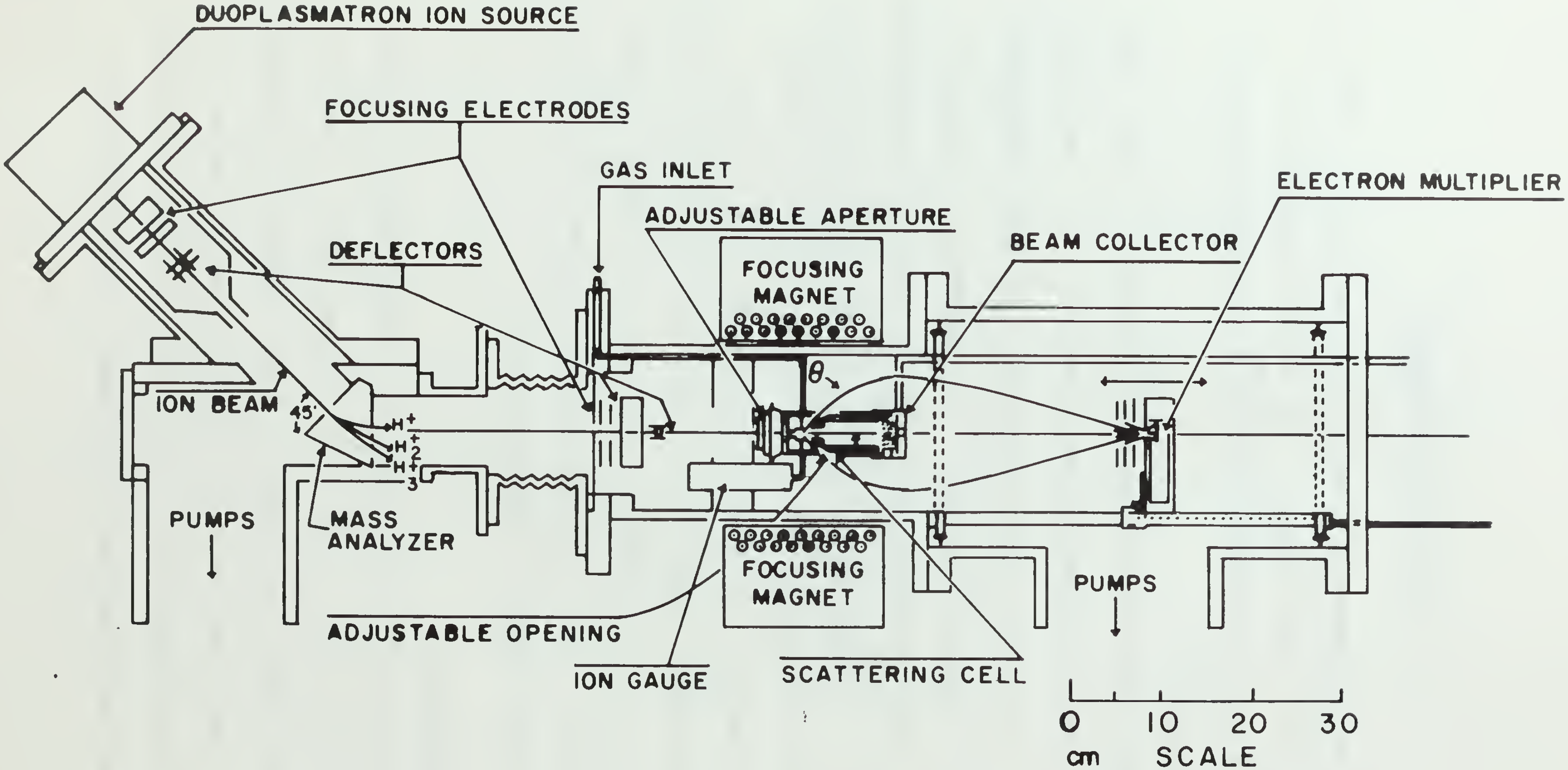

FIGURE 5. SCHEMATIC OF THE EXPERIMENTAL APPARATUS.

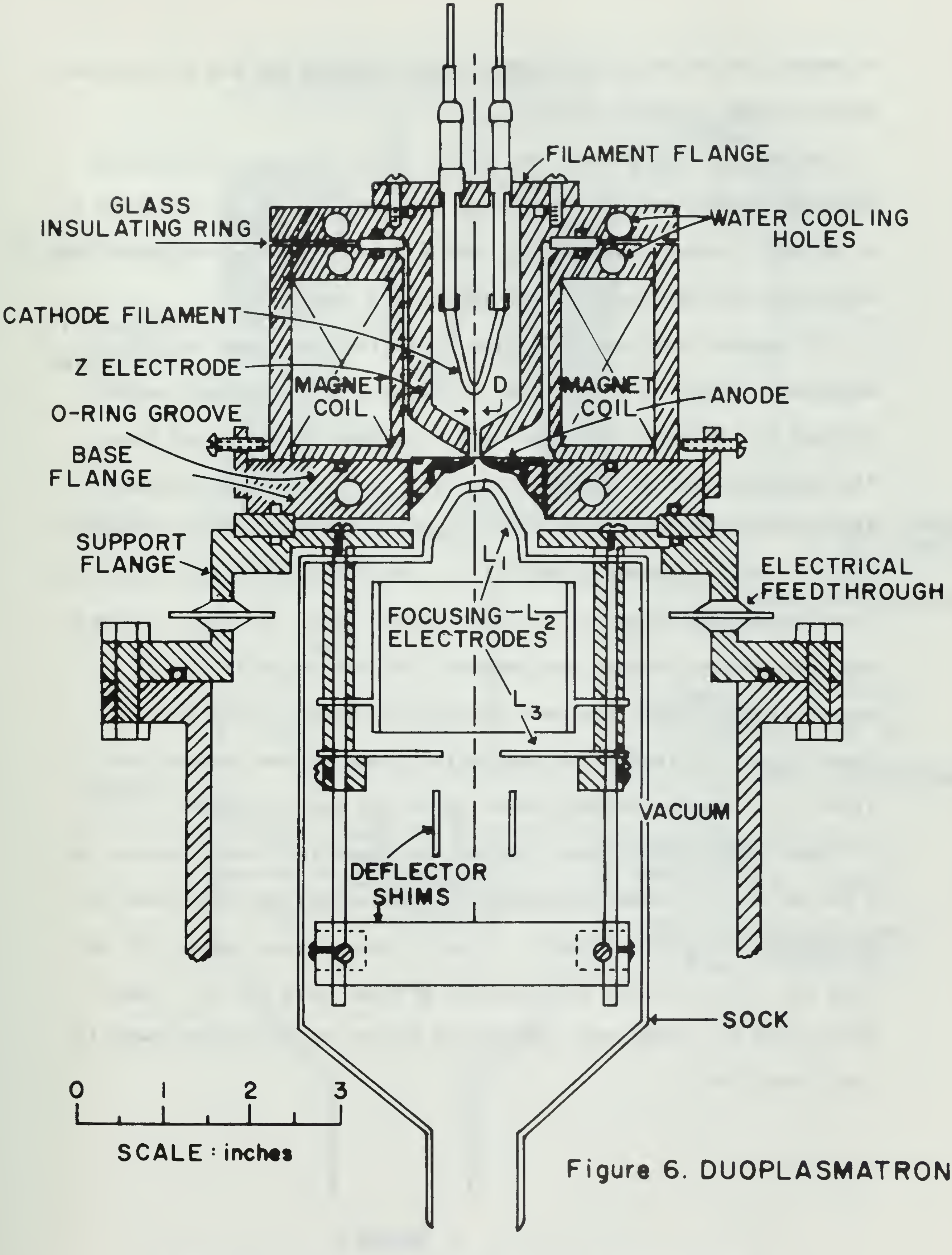

Figure 6. DUOPLASMATRON

1 ampere can be sustained between the filament and the Z-electrode by a voltage of about 250 volts.

To extract the plasma, the positive arc voltage is switched from the Z-electrode to the anode, (see Fig. 7) which is itself at a voltage E above ground. The energy of the hydrogen ion beam thus extracted will be (Ee) for singly charged ions.

To enhance the beam intensity a simple accel-decel system is employed. Figure 7 shows lens 1 at some arbitrary negative potential V. Thus the hydrogen ions are actually extracted from the duoplasmatron at an energy (V+E)e. A "sock" is fitted over the focusing and deflector lenses and attached to lens 1 so as to float at this negative potential V, and thus prevent the beam from "seeing" ground potential in this region. Thus the beam of hydrogen ions passes through the focusing and deflector lenses at an energy (V+E)e. Once the beam leaves the region of the sock it "sees" ground potential on the walls of the vacuum chamber and slows to an energy Ee and passes on to the mass analyzer.

This simple accel-decel system increased the beam intensity by a factor of 40. Thus we were able to obtain an analyzed beam of 100 eV protons (with diameter .5 cm at the scattering cell 80 cm from the source) which was slightly greater than 1×10^{-7} amps. Carter [6] has shown that the energy spread of the proton beam is less than 2.5%.

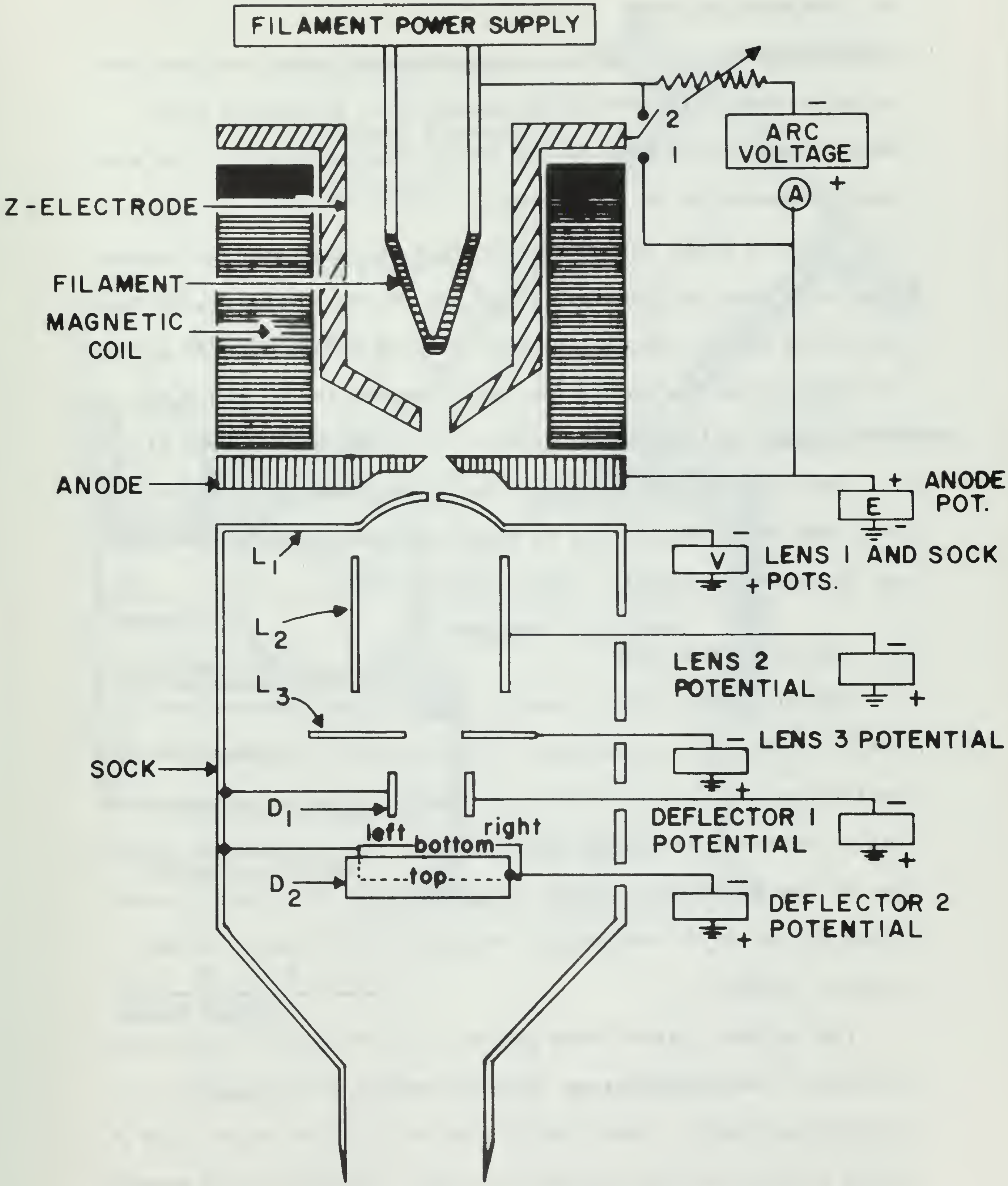

FIGURE 7.
CIRCUIT DIAGRAM FOR DUOPLASMATRON

B. THE MASS ANALYZER

The hydrogen ion beam is mass analyzed in the analyzer constructed and calibrated by Strohsahl [7]. It employs a 45° bending angle (see Fig. 8) and has a resolution of $\frac{m}{\Delta m} = 40$ with beam transmission of about 90%.

Figure 9 shows the current through the mass analyzer magnet that will pass any particular species in the energy region from 50 to 650 volts. Hence .45 amps allows a 100 eV beam of protons to travel into the scattering cell, whereas the H_2^+ and H_3^+ are not bent enough by the magnetic field to be transmitted (see Fig. 5).

The mass analyzer is carefully aligned with the scattering cell and the detector, all of which are positioned on the axis of the focusing magnet. (See section F below.)

C. THE SCATTERING CELL

The scattering cell, shown in Fig. 10, was designed and tested by Bush [1]. The target gas, methane, is bled into the scattering cell and is accurately controlled by a Variable Leak valve constructed by Granville Philips. The pressure of the CH_4 gas in the scattering chamber (approximately 10^{-3} torr) is measured by the VG 1A ion gauge. The gas is of research grade, (purity 99.65%).

The incident proton beam passes first through an adjustable aperature (generally set at .5 cm diameter) and then into the scattering chamber. Here the H^+ reacts with the CH_4 to form H_2^+ whose escape from the scattering cell is limited by the geometry of the exit slit. The exit slit is an annular opening of 360°,

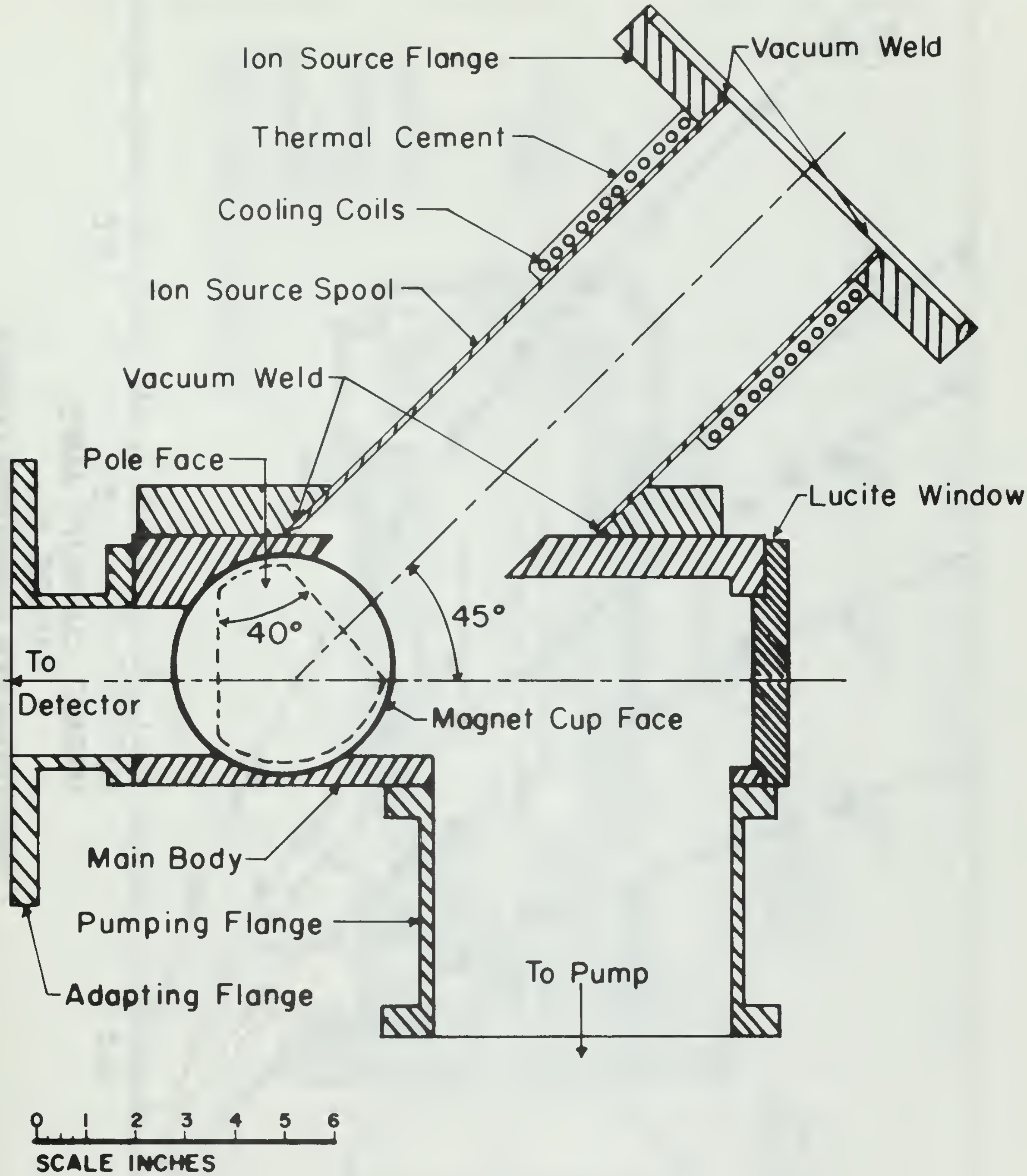

Figure 8. Schematic of Mass Spectrometer.

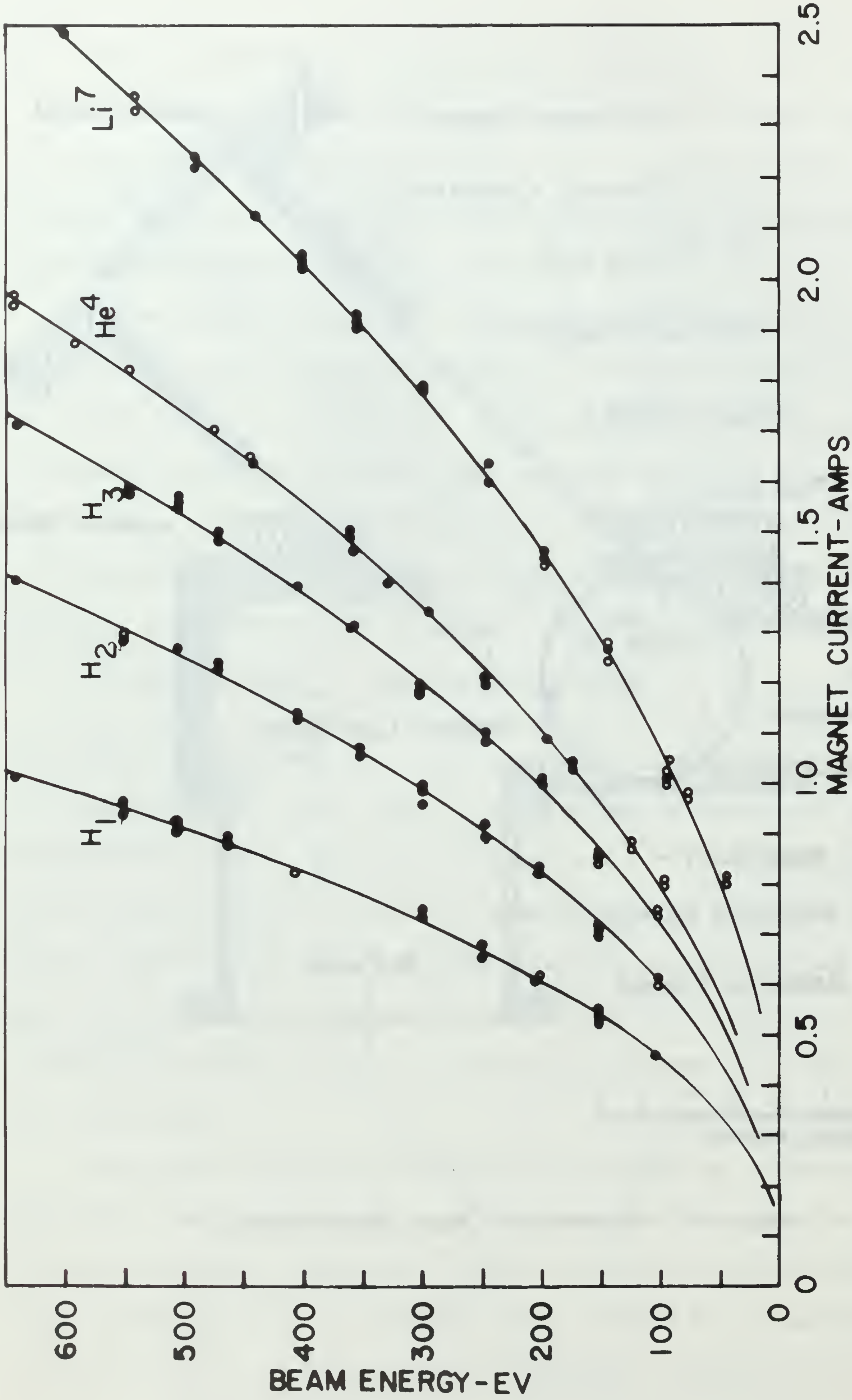

FIGURE 9
SPECTROMETER OPERATION CURVES

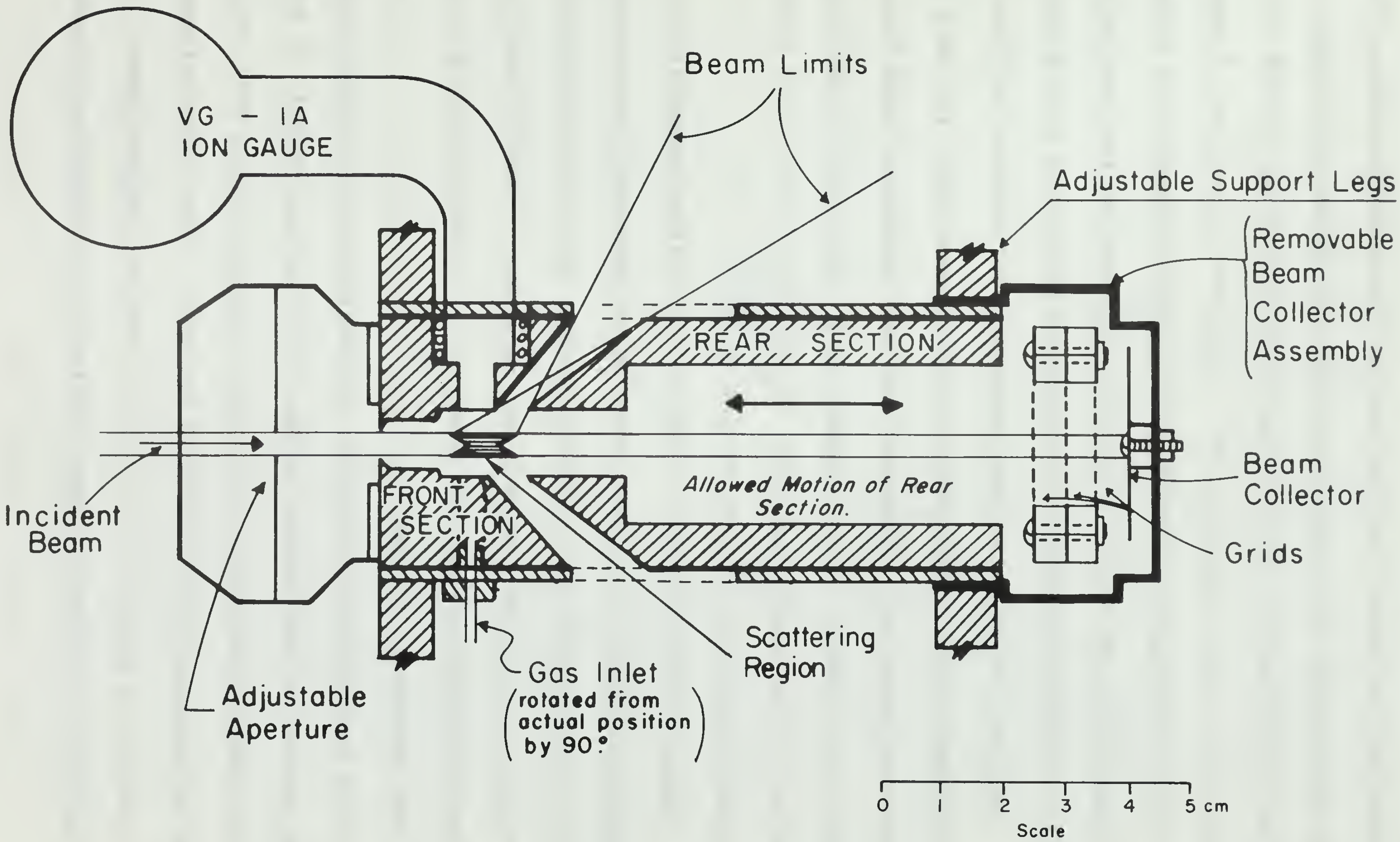

Figure 10. The Scattering Cell and Beam Collector

reduced by support legs to about 290^{o}, around the scattering cell, separating the front from the rear of the scattering cell. The exit wall of the front section of the scattering cell slopes upwards at 49^{o} and the exit wall of the rear section of the scattering cell slopes upward at 36^{o}. Appendix III of Ref. 5 shows how these two angles determine the target thickness. By varying the separation of the front and rear sections of the scattering cell, the target thickness can be increased from 0 to 0.8 cm.

The ions collected by the front and rear sections of the scattering cell are measured by separate ammeters. The beam collector collects the unscattered beam that passes through the scattering chamber. This current, plus the current from the rear section of the scattering cell, is recorded as the total proton current incident on the CH_4 target molecules.

Three grids on the beam collector are given potentials to suppress secondary electron emission and prevents slow background ions from reaching the collector plate. The beam collector and its grids are placed inside a metal cup which shields them from other charged particles and also acts as a gas cap over the rear of the scattering chamber.

The beam collector assembly is mounted on a rod which passes to the outside of the vacuum system, allowing the assembly to be pulled away from the rear section of the scattering cell and swung out of the path of the incident ion beam. This allows alignment of the entire apparatus and also allows the incident beam to fall directly on the detector when desired for calibration purposes.

D. THE FOCUSING MAGNET

The magnetic field of the focusing magnet is nonuniform and axially symmetric and has the focusing property of bending the trajectories of charged particles so they follow a path similar to that shown in Fig. 11.

If one considers the simpler case of an axially symmetric uniform magnetic field, it can be shown that the trajectory of a charged particle is a helix (see Ref. 5). The particle will cross the field line on which it originated after one complete revolution. Then, as shown in Fig. 11, particles of charge q leaving the source with momentum $p = mv$ at an angle θ will cross the magnetic axis at a distance Z_o given by:

$$Z_o = \frac{2\pi\, p \cos\theta}{qB} \qquad (1)$$

where B is the magnetic field strength. Thus a detector located at Z_o will only sense these ions scattered out of the scattering cell placed at $Z = 0$ which have momentum p, charge q, and scattering angle θ. If one now holds the detector fixed at Z_o and increases B then particles of larger $p \cos\theta$ values will strike the detector. Alternately by holding B fixed and varying Z_o we can detect particles scattered from the source at different values of $p \cos\theta$. Since equation 1 is independent of azimuthal angle ϕ, the entire 360^o can be observed at Z_o. For most conventional scattering experiments $\Delta\theta \approx 1^o$. Hence, the solid angle is enhanced by a factor of approximately 300.

In our experimental apparatus the magnetic field is NOT uniform, as it is produced by a "thin" solenoid shown in Fig. 5.

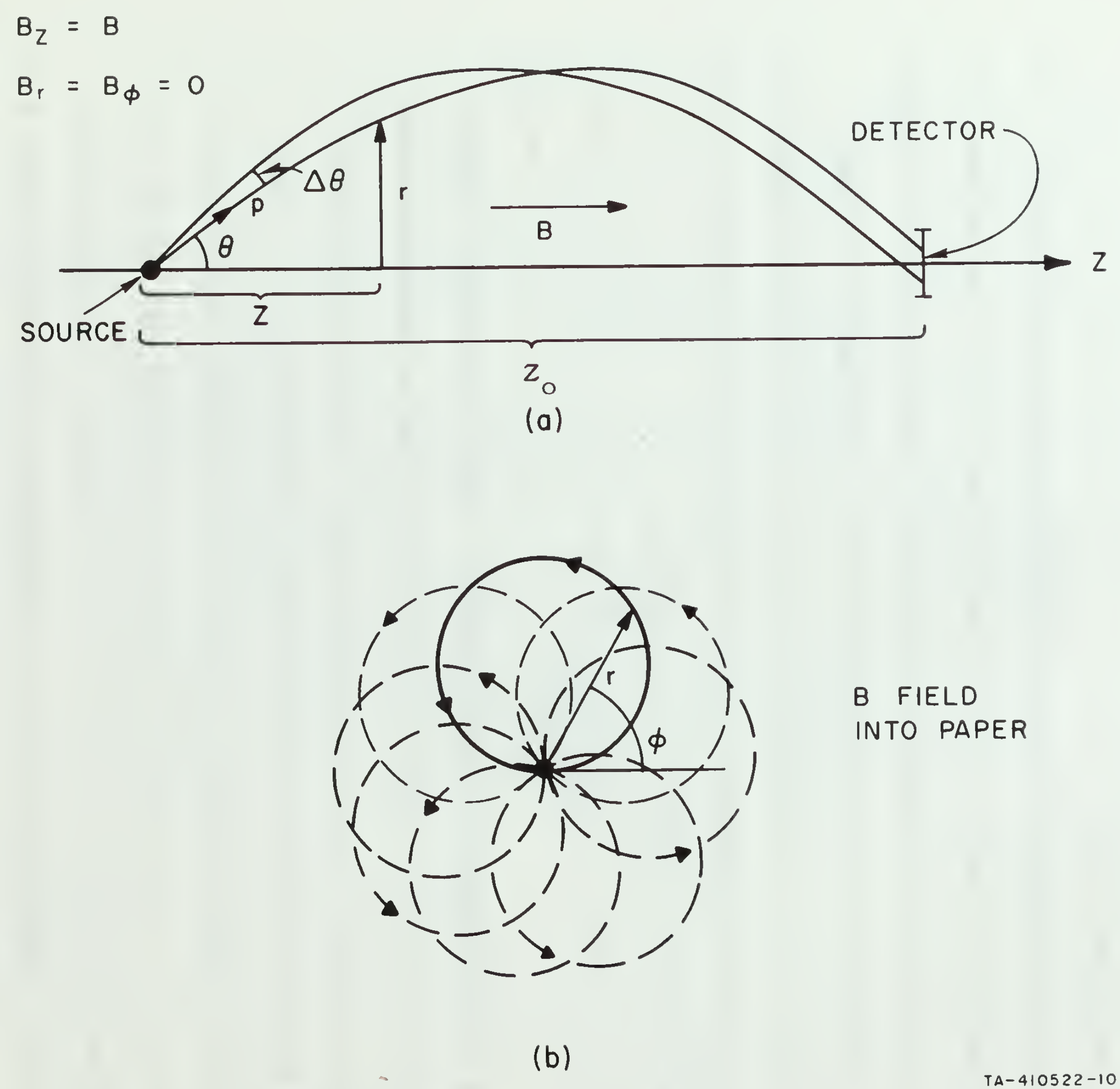

Figure 11. Orbit of Charged Particle in Uniform Magnetic Field

This complicates the trajectory equations and makes numerical intergrations necessary. The results of numerical intergrations for the H_2^+ ion are shown in Fig. 12. However, equation 1 the result obtained for the uniform field case is qualitatively the same as in our NON-uniform field configuration.

The magnetic field of the focusing magnet was measured by Kelly [8]. Figure 13 shows the axial component of the magnetic field on the magnetic axis. Figure 14 shows the values of the axial component of the magnetic field measured at various r and Ø values at the center of the coil. Figure 15a and b show the radial components of the magnetic field as measured with a Hall Probe(at Z_o = 34 cm) across the geometric axis of the coil, both vertically and horizontally. This demonstrates that the magnetic and geometric axis of the magnetic coil are aligned to within 0.1%. This allows use of the coil geometric axis and the coil center-line as reference for alignment of the entire system along the magnetic field axis.

E. THE SCATTERED ION DETECTOR

The beam detector and amplifier is a Model 306 Magnetic Electron Multiplier whose schematic is shown in Fig. 16. The multiplier is connected to a Bendix 1122 Power Supply as shown in Fig. 17. The output of the multiplier is fed to the input head of a Keithly 640 Vibrating Capaciter Electrometer.

The Multiplier, developed by Goodrich and Wiley, provides reproducible current gains up to 10^5 when operated at the potentials shown on Fig. 17. When operating as the detector of scattered

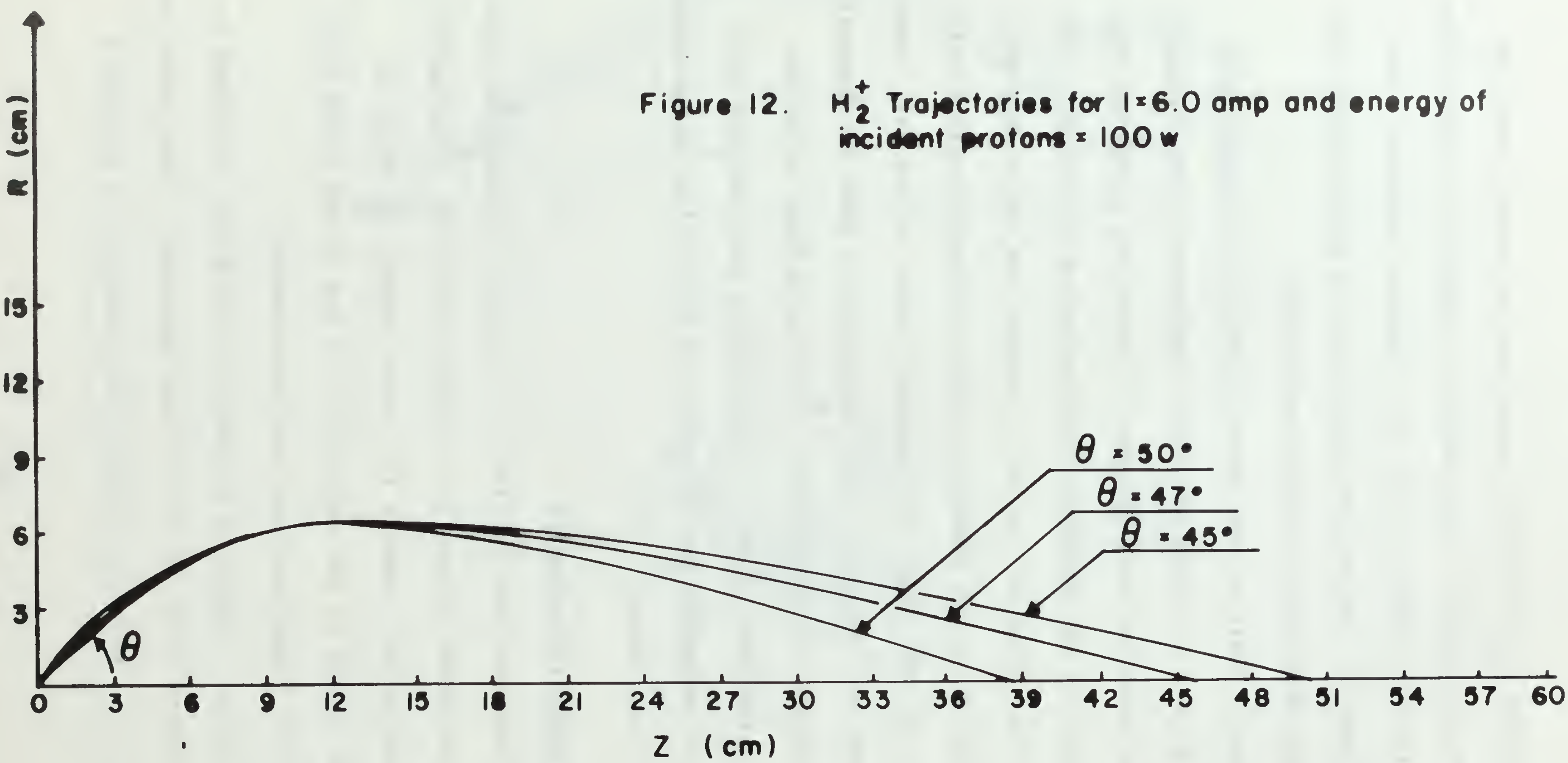

Figure 12. H_2^+ Trajectories for I = 6.0 amp and energy of incident protons = 100 w

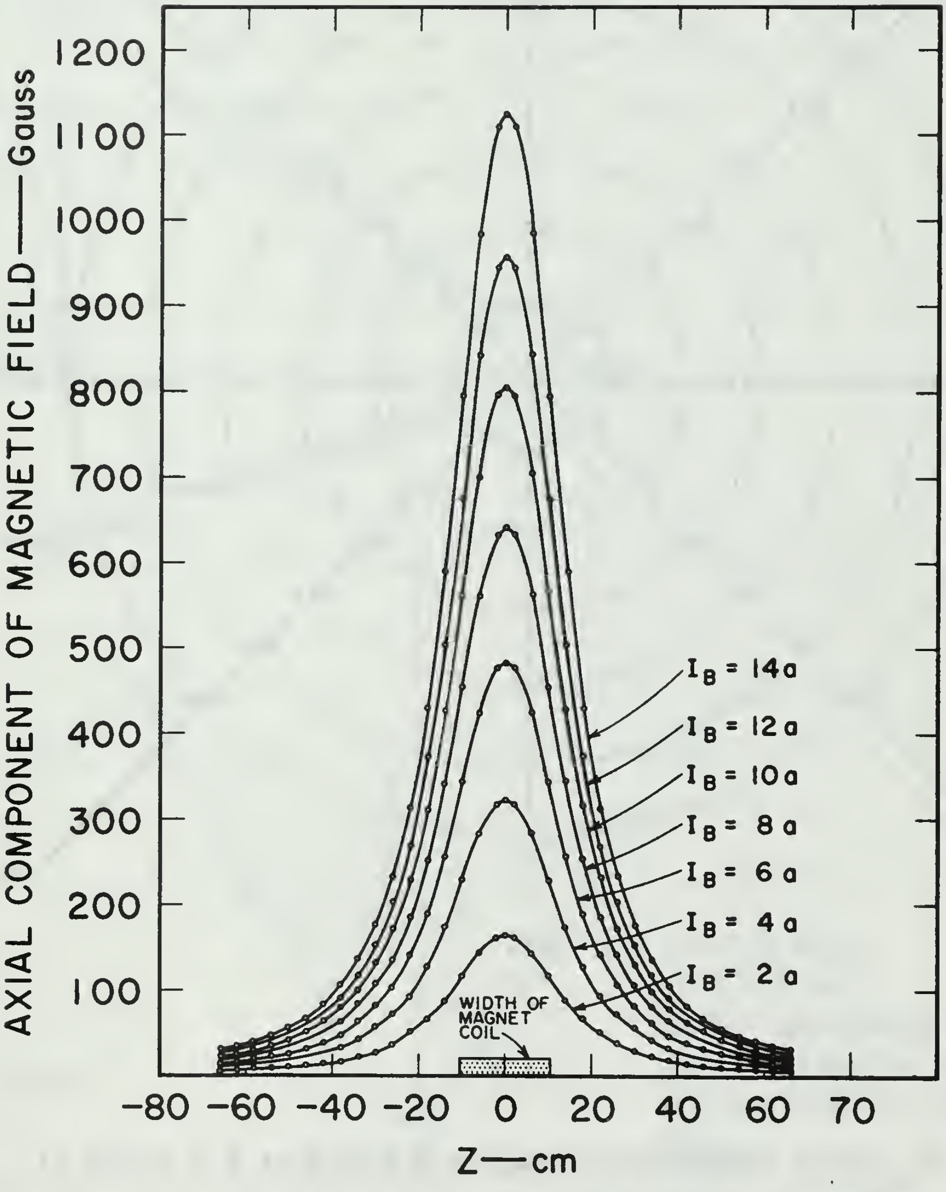

Figure 13. Magnetic Field Strength at Various Distances Along the Magnetic Axis for Various Currents

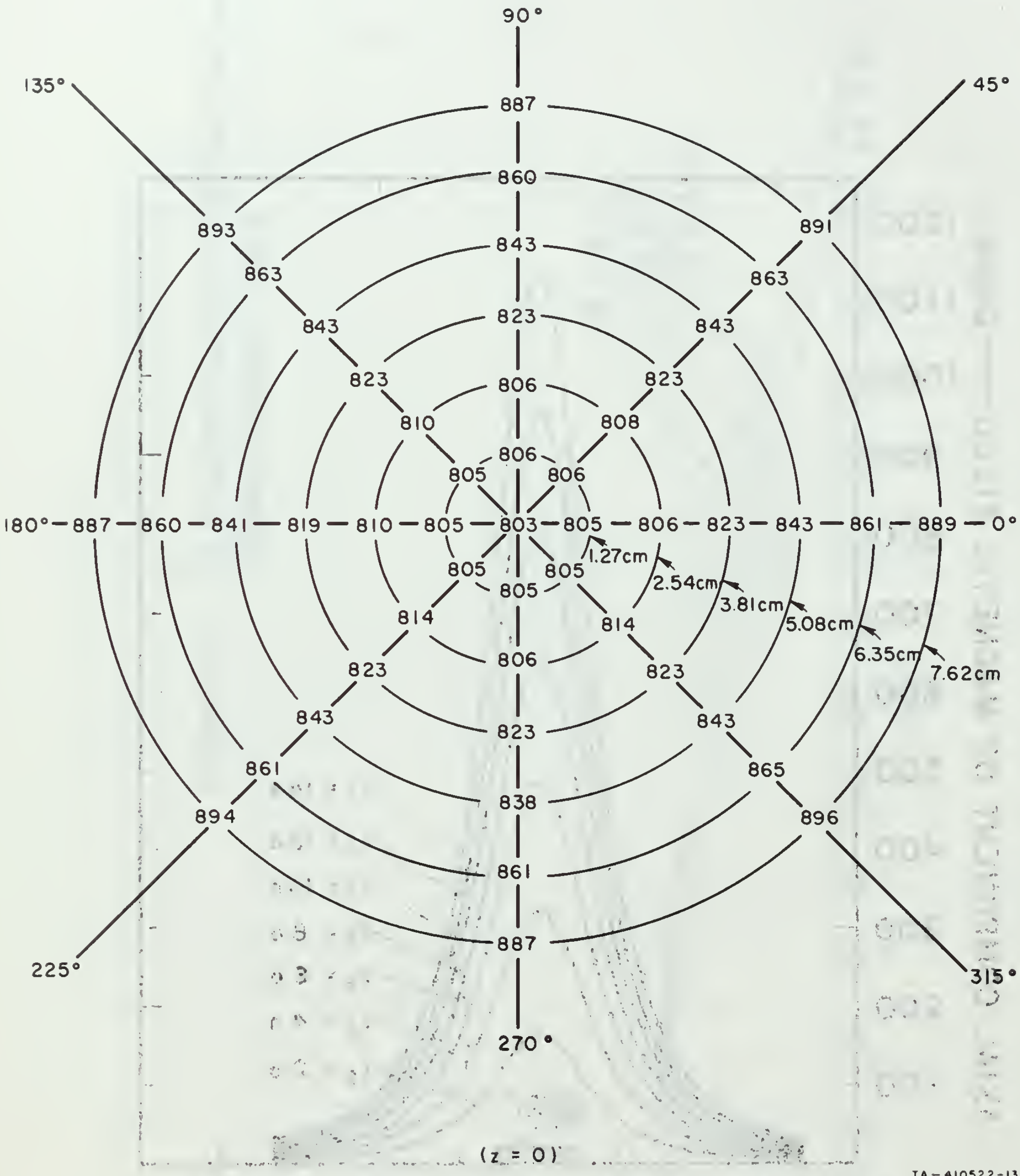

Figure 14. Axial Component of Magnetic Field at Z = 0 and at Various R and Ø Values.

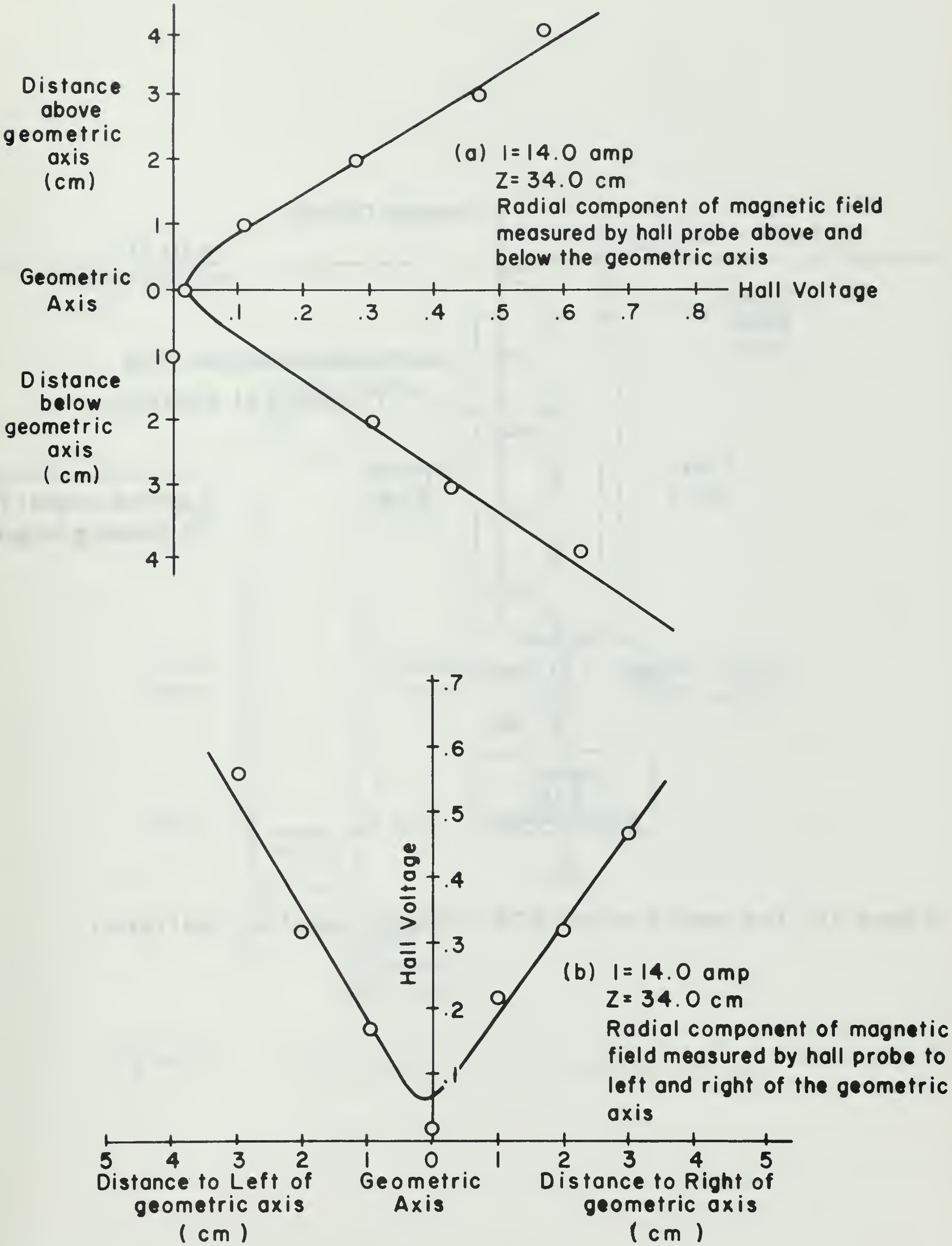

Figure 15. Radial magnetic field components

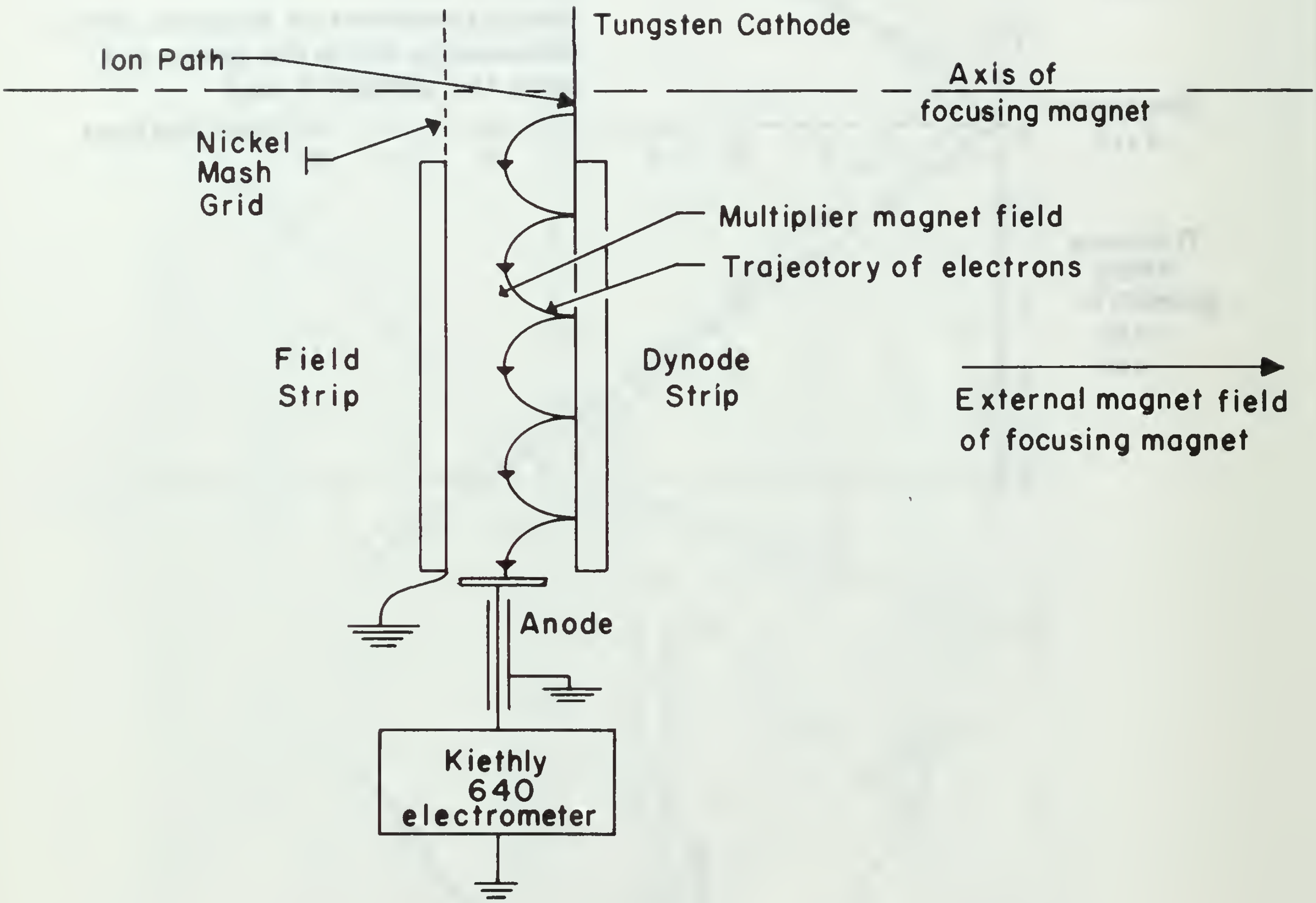

Figure 16. The bendix model 306 magnetic electron multiplier

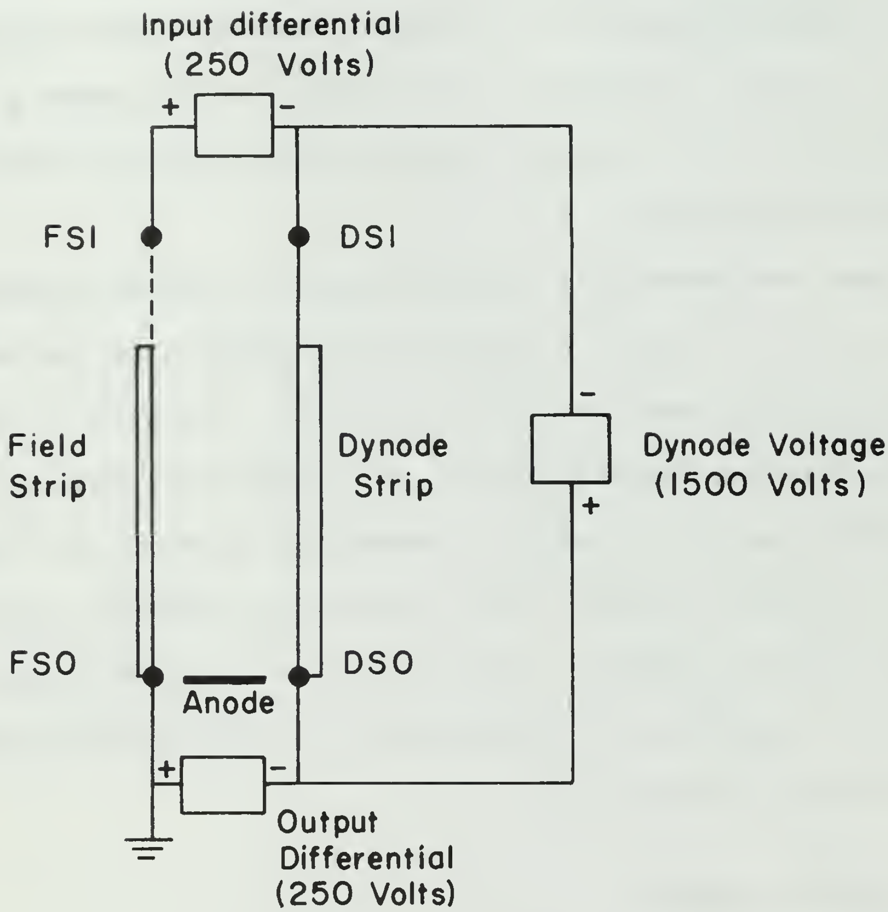

Figure 17. Circuit Diagram for Electron Multiplier.

ions in our experimental apparatus, the multiplier has to be operated in a magnetic field of up to 200 gauss. The effect of this magnetic field is to reduce the gain of the multiplier; increasing field, causes the gain to decrease.

The multiplier is operated inside an aluminum shield to protect it from random background. The various strip potentials were chosen to give the highest gain and the lowest noise. The multiplier gain was measured at different magnetic field values in the manner listed in Appendix I and fitted by a 12th order polynomial. See Fig. 18. The fitted polynomial was used in the actual cross section calculations.

Bush, has shown that the gain does not vary with gas pressure up to 2.0×10^{-4} torr, a pressure much higher than the multiplier ever encounters when data is being taken. The gain is independant of the incident ion mass and of the incident current, provided the anode current is below its saturation value of 10^{-5} amperes.

To prevent slow ions from reaching the detector, a grid is placed over the detector shield aperature as shown in Fig. 19. The grid also permits a crude analysis of the scattered beam energy. See section A, Chapter IV.

F. SYSTEM ALIGNMENT

In order to detect particles scattered at a particular angle the detector must be placed on the focusing magnetic field axis at the point Z where the scattered particles focus on the axis. The program SOLANG which calculates the intercept distance assumes that the scattering took place on the axis at the center of the

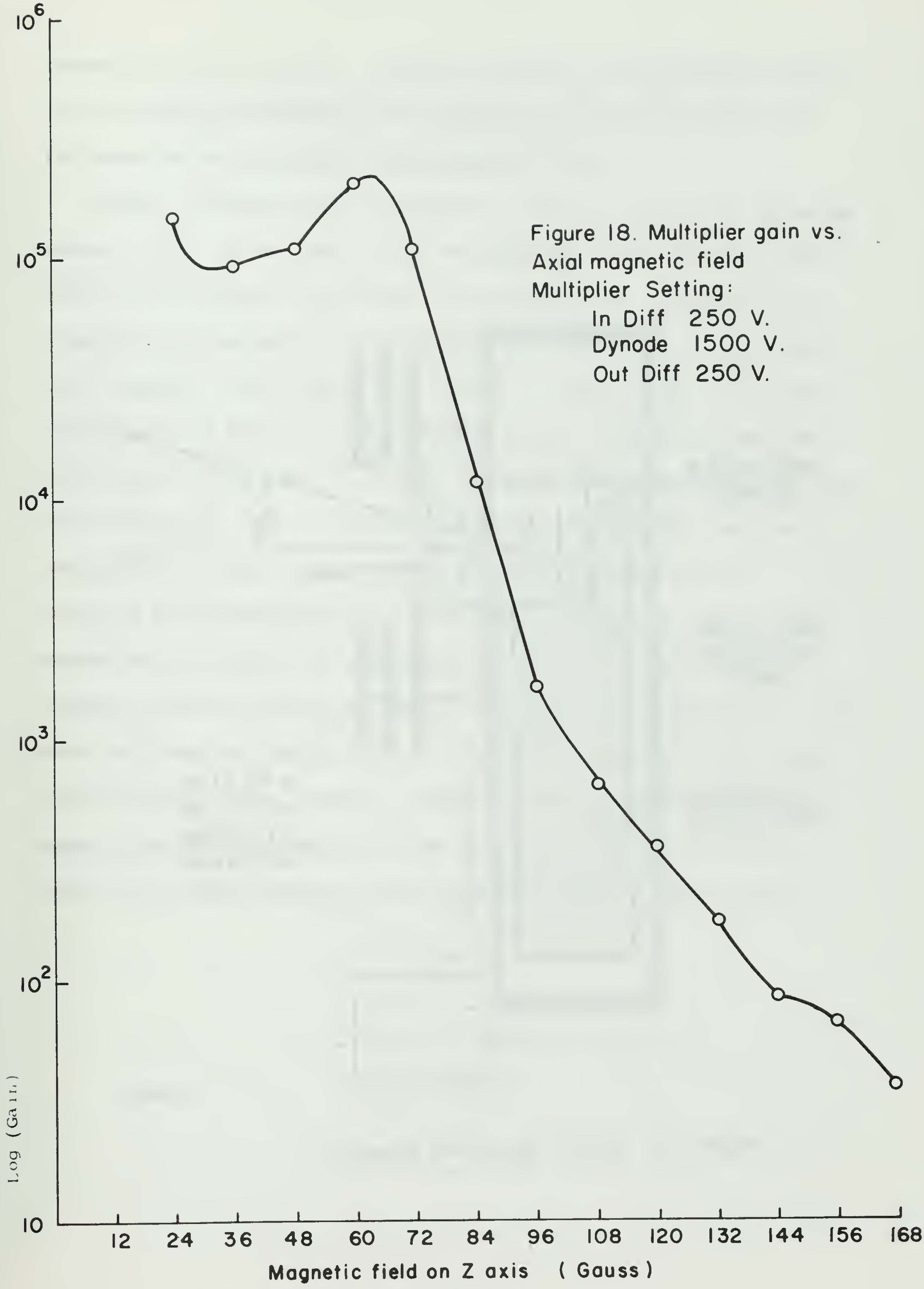
Figure 18. Multiplier gain vs.
Axial magnetic field
Multiplier Setting:
In Diff 250 V.
Dynode 1500 V.
Out Diff 250 V.
10^6
10^5
10^4
10^3
10^2
10
Log (Gain)
12 24 36 48 60 72 84 96 108 120 132 144 156 168
Magnetic field on Z axis (Gauss)

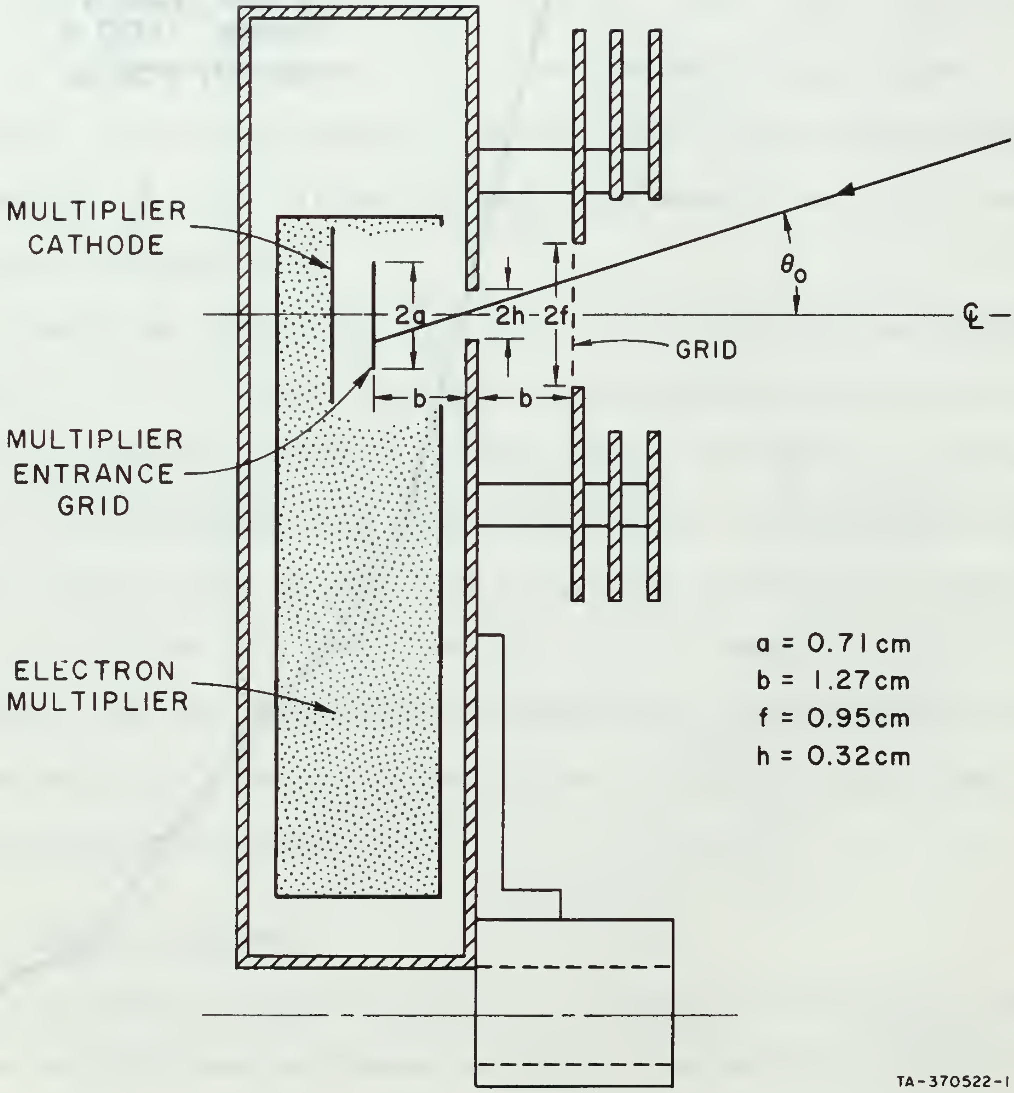

Figure 19. Dector Aperature Geometry.

focusing magnetic field. Therefore accuracy in the angle of scatter determination depends on how well the scattering center and the detector are aligned to the magnetic field.

Figure 15 shows that the geometric center line of the focusing magnetic coil is collinear with the magnetic field axis to within 0.1%. This geometric centerline was used as the reference for aligning all components to the magnetic field axis. To perform the alignment, cross hairs were placed on either side of the magnetic spool to mark its axis. Then a small laboratory laser was positioned so its beam lay on the magnetic axis established by the two crosshairs. The crosshairs were then removed and the line established by the laser beam was used as the reference for aligning all other components to the focusing magnet axis. This method made possible the alignment of the scattering cell, the detector, and the focusing lenses to the magnetic field axis. The mass analyzer was constructed by Strohsahl, (see Ref. 7) so that the ion beam, after analysis, travels down the geometric axis. Hence attaching crosshairs to the front and rear of the mass analyzer, it was adjusted into alignment with the laser beam.

IV. THE EQUATIONS DESCRIBING THE MOTION OF THE H_2^+ ION AND THEIR SOLUTION

A. THE TRAJECTORY EQUATION

The equation of motion of the H_2^+ ion in the nonuniform axially symmetric magnetic field of the focusing magnet, (equation (5)), is expressed in terms of the magnetic vector potential $\vec{A}$. Therefore the measured magnetic field $\vec{B}$ of the focusing magnet must be related to this quantity before the trajectory equation can be solved. The expansion of $\vec{A}$ in terms of the field $\vec{B}$ is shown by Bush [5] to be:

$$A_\phi(r,z) = \sum_{n=o}^{\infty} \frac{(-1)^n}{n!(n+1)!} \left(\frac{r}{2}\right)^{2n+1} \frac{\partial^{2n} B_z(r=0,z)}{\partial z^{2n}} \tag{1}$$

$$A_r(r,z) = 0 \tag{2}$$

$$A_z(r,z) = 0 \tag{3}$$

Gagliano [9] fitted the actual magnetic field measurements along the r = 0 axis with a 12th order polynomial in z such that:

$$B_z(r=0,z) = \frac{I}{10} \sum_{n=1}^{13} C_n z^{n-1} \tag{4}$$

where I is the current through the magnetic coil. Hence we know $B_z(r = z)$ and $A_\phi(r,z)$ for any given focusing magnet current I. Gagliano, and subsequently, Bush, has shown that the equation of motion of a particle of charge q and mass m with momentum p in our field configuration is given by:

$$\frac{\frac{d^2 r}{dz^2}}{1 + \left(\frac{dr}{dz}\right)^2} [k^2 - A_\phi^2] - \frac{dr}{dz}\left[A_\phi \frac{\partial A_\phi}{\partial z}\right] + A_\phi \frac{\partial A_\phi}{\partial r} = 0 \qquad (5)$$

where $k^2 = \frac{p^2}{q^2}$ (6)

To solve this second order nonlinear differential equation by means of the digital computer, it must be reexpressed as two first order differential equations. This is done by rewriting equation (5) as follows:

$$\frac{d}{dz}\left(\frac{dr}{dz}\right) = \frac{\frac{dr}{dz}\left[A_\phi \frac{\partial A_\phi}{\partial z}\right]}{k^2 - A_\phi^2} + \frac{\left(\frac{dr}{dz}\right)^3\left[A_\phi \frac{\partial A_\phi}{\partial z}\right]}{k^2 - A_\phi^2} - \frac{A_\phi \frac{\partial A_\phi}{\partial r}}{k^2 - A_\phi^2} - \frac{\left(\frac{dr}{dz}\right)^2\left[A_\phi \frac{\partial A_\phi}{\partial r}\right]}{k^2 - A_\phi^2} \qquad (7)$$

Define: DERY (1) $= r$

DERY (2) $= \frac{dr}{dz}$

FUNC (4) $= \frac{A_\phi \frac{\partial A_\phi}{\partial z}}{k^2 - A_\phi^2}$

FUNC (5) $= \frac{A_\phi \frac{\partial A_\phi}{\partial r}}{k^2 - A_\phi^2}$

Then equation (7) becomes

$$\frac{d}{dz}\left[\text{DERY}(1)\right] = \text{DERY}(2) \qquad (8)$$

$$\frac{d}{dz}\left[\mathrm{DERY}(2)\right] = \mathrm{DERY}(2) \times \mathrm{FUNC}(4) + \left[\mathrm{DERY}(2)\right]^3 \times \mathrm{FUNC}(4) - \mathrm{FUNC}(5) - \left[\mathrm{DERY}(2)\right]^2 \times \mathrm{FUNC}(5) \quad (9)$$

We now have two first order nonlinear differential equations which can be solved by the use of the digital computer.

From equation (6) we see we need to know the momentum of the scattered particle. But $p = \sqrt{2mE_s}$ where E_s is the energy of the scattered particle. Hence

$$k^2 = \frac{2m}{q} E_s' \quad (10)$$

where E_s' is the energy of the scattered particle expressed in electron volts. Thus if E_s is known, equations (8) and (9) can be solved to yield r as a function of Z.

B. THE ENERGY OF THE H_2^+

To determine E_s, the energy of the scattered H_2^+ particle, consider the following sketch of the kinematics of the reaction: $\underline{H}^+ + CH_4 \rightarrow \underline{H}_2^+ + CH_3$.

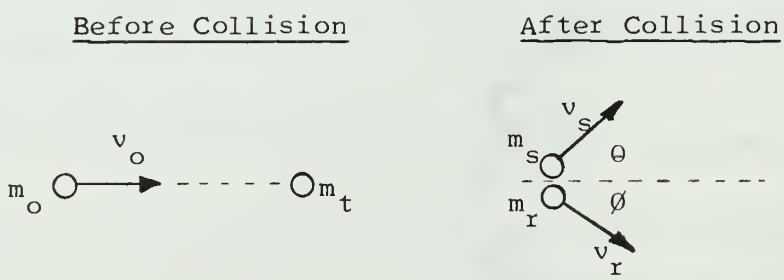

where m_o represents the mass of the H^+, the incident ion, and the m_t represents the mass of the CH_4, the target molecule, and m_s represents the mass of the H_2^+, the scattered ion, and the m_r

$$\frac{\frac{d^2 r}{dz^2}}{1+\left(\frac{dr}{dz}\right)^2}\left[k^2 - A_\phi^2\right] - \frac{dr}{dz}\left[A_\phi \frac{\partial A_\phi}{\partial z}\right] + A_\phi \frac{\partial A_\phi}{\partial r} = 0 \qquad (5)$$

where $k^2 = \frac{p^2}{q^2}$ (6)

To solve this second order nonlinear differential equation by means of the digital computer, it must be reexpressed as two first order differential equations. This is done by rewriting equation (5) as follows:

$$\frac{d}{dz}\left(\frac{dr}{dz}\right) = \frac{\frac{dr}{dz}\left[A_\phi \frac{\partial A_\phi}{\partial z}\right]}{k^2 - A_\phi^2} + \frac{\left(\frac{dr}{dz}\right)^3\left[A_\phi \frac{\partial A_\phi}{\partial z}\right]}{k^2 - A_\phi^2} - \frac{A_\phi \frac{\partial A_\phi}{\partial r}}{k^2 - A_\phi^2} - \frac{\left(\frac{dr}{dz}\right)^2\left[A_\phi \frac{\partial A_\phi}{\partial r}\right]}{k^2 - A_\phi^2} \qquad (7)$$

Define: DERY (1) = r

DERY (2) = $\frac{dr}{dz}$

FUNC (4) = $\frac{A_\phi \frac{\partial A_\phi}{\partial z}}{k^2 - A_\phi^2}$

FUNC (5) = $\frac{A_\phi \frac{\partial A_\phi}{\partial r}}{k^2 - A_\phi^2}$

Then equation (7) becomes

$$\frac{d}{dz}\left[\mathrm{DERY(1)}\right] = \mathrm{DERY(2)} \qquad (8)$$

$$\frac{d}{dz}\left[DERY(2)\right] = DERY(2) \times FUNC(4) + \left[DERY(2)\right]^3 \times FUNC(4) - FUNC(5) - \left[DERY(2)\right]^2 \times FUNC(5) \quad (9)$$

We now have two first order nonlinear differential equations which can be solved by the use of the digital computer.

From equation (6) we see we need to know the momentum of the scattered particle. But $p = \sqrt{2mE_s}$ where E_s is the energy of the scattered particle. Hence

$$k^2 = \frac{2m}{q} E_s' \quad (10)$$

where E_s' is the energy of the scattered particle expressed in electron volts. Thus if E_s is known, equations (8) and (9) can be solved to yield r as a function of Z.

B. THE ENERGY OF THE H_2^+

To determine E_s, the energy of the scattered H_2^+ particle, consider the following sketch of the kinematics of the reaction: $\underline{H}^+ + CH_4 \rightarrow \underline{H}_2^+ + CH_3$.

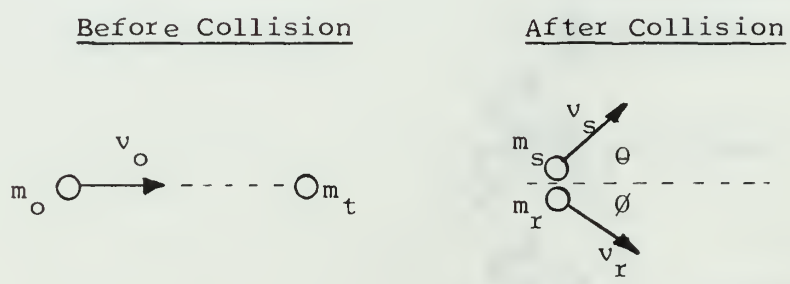

where m_o represents the mass of the H^+, the incident ion, and the m_t represents the mass of the CH_4, the target molecule, and m_s represents the mass of the H_2^+, the scattered ion, and the m_r

represents the mass of the CH_3, the remaining molecule. Ignoring the binding energies, we can write the following:

From the conservation of energy we have:

$$\tfrac{1}{2} m_o v_o^2 = \tfrac{1}{2} m_s v_s^2 + \tfrac{1}{2} m_r v_r^2 \tag{11}$$

From conservation of momentum we have:

$$m_o v_o = m_s v_s \cos \theta + m_r v_r \cos \phi \tag{12}$$

$$0 = m_s v_s \sin \theta - m_r v_r \sin \phi \tag{13}$$

We wish to solve these three equations to yield the relation:

$$E_s = E_s(E_o, m_r, m_s, m_o, \theta)$$

Squaring (12) and (13) and adding, we eliminate ϕ and get:

$$m_o^2 v_o^2 - 2m_o v_o m_s v_s \cos \theta + m_s^2 v_s^2 = m_r^2 v_r^2$$

But from (11) $m_r^2 v_r^2 = m_r m_o v_o^2 - m_r m_s v_s^2$.

Thus we have on substituting this into the above equation:

$$m_o^2 v_o^2 - 2m_o v_o m_s v_s \cos \theta + m_s^2 v_s^2 - m_r m_o v_o^2 + m_r m_s v_s^2 = 0$$

<u>or</u> $$2m_o E_o - 4 \sqrt{m_o E_o m_s E_s} \cos \theta + 2m_s E_s - 2m_r E_o + 2m_r E_s = 0$$

Thus we get on rearranging:

$$E_s(m_s + m_r) + E_o(m_o - m_r) = 2 \sqrt{m_o m_s E_o E_s} \cos \theta \tag{14}$$

Now let: $a = m_s + m_r$ and $b = m_o - m_r$ (15)

Squaring (14) we get:

$$a^2 E_s^2 + \left[2ab\, E_o - 4\, m_o m_s E_o \cos^2\theta\right] E_s + b^2\, E_o^2 = 0$$

Solving for E_s we obtain:

$$E_s = \frac{4\, m_o m_s E_o \cos^2\theta - 2abE_o \pm \sqrt{(2abE_o - 4\, m_o m_s E_o \cos^2\theta)^2 - 4a^2b^2E_o^2}}{2a^2}$$

As the + root only yields physical results, in our case we have, on substituting equation (15) for a and b:

$$E_s = E_o \left[\frac{2\, m_o m_s \cos^2\theta + (m_r - m_o)(m_s + m_r)}{(m_s + m_r)^2} + \frac{\sqrt{4\, m_o^2 m_s^2 \cos^4\theta - 4(m_s + m_r)(m_o - m_r) m_o m_s \cos^2\theta}}{(m_s + m_r)^2} \right]$$

Now: $m_r = m_{CH_3^+}$

$m_o = m_{H^+}$

$m_s = m_{H_2^+} = 2m_o$

Thus the above equation simplifies to:

$$E_s = E_o \left[\frac{m_r^2 + m_r m_o - 2m_o^2 + 4m_o^2 \cos^2\theta}{(m_r + 2m_o)^2} + \frac{2\sqrt{2}\, m_o \cos\theta \sqrt{m_r^2 + m_r m_o - 2m_o^2 + 2m_o^2 \cos^2\theta}}{(m_r + 2m_o)^2} \right] \qquad (16)$$

Thus selecting θ and E_o we can calculate E_s, the energy of the scattered H_2^+, from equation (16).

Figure 20, a plot of the ratio $\frac{E_s}{E_o}$ versus the scattering angle θ, shows that in the 10^o range from 41^o to 51^o, E_s changes by less than 3%.

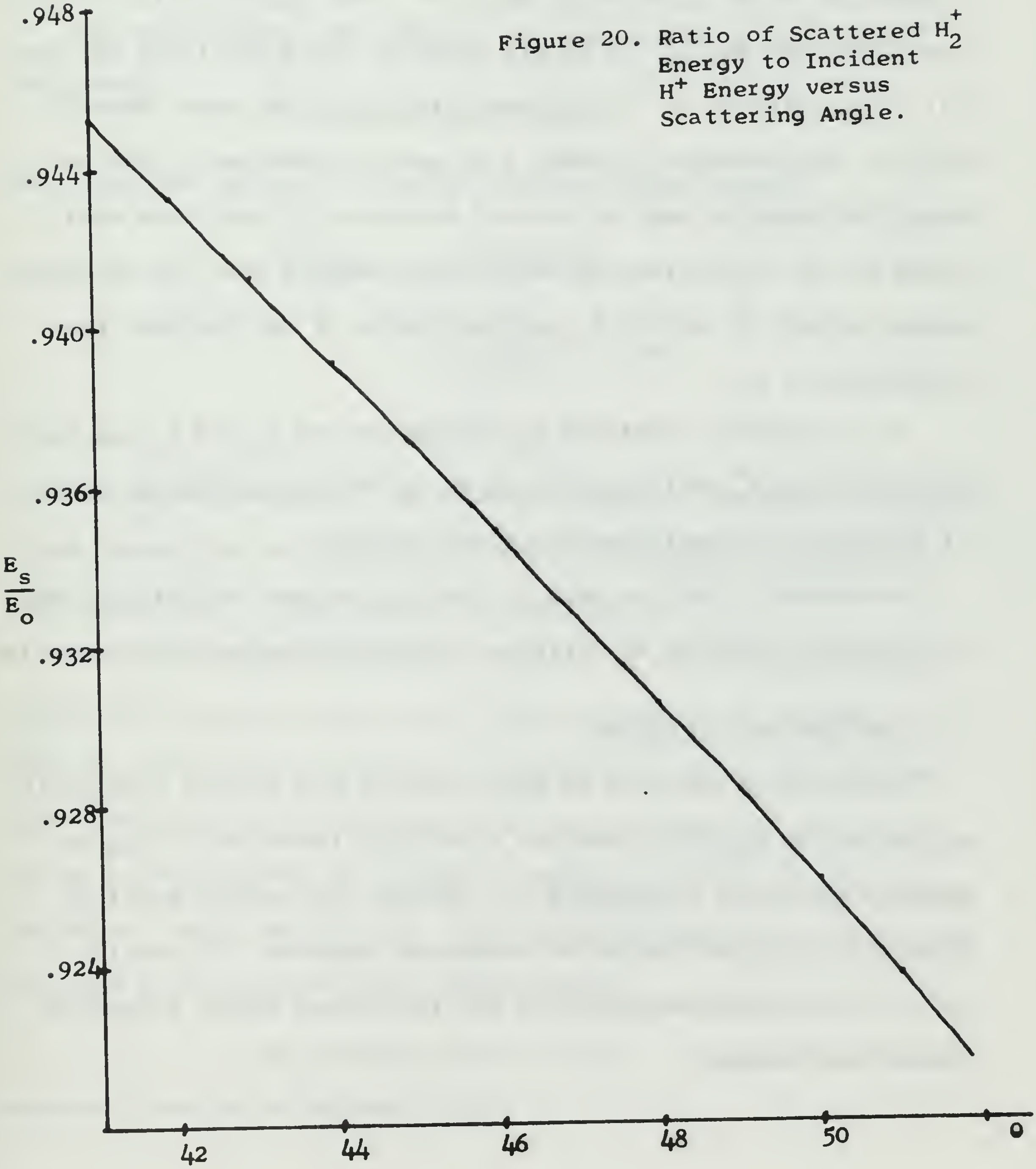

Figure 20. Ratio of Scattered H_2^+ Energy to Incident H^+ Energy versus Scattering Angle.

C. THE METHOD OF SOLUTION

Assume protons of energy E_o and a focusing magnetic current I_o to have been selected. Then equation (4) yields the magnetic field $B_z(r = 0,z)$. Equation (16) yields the energy of the H_2^+ as a function of the scattering angle, Θ. From equation (10) k^2 is then known for the H_2^+ and we are ready to solve equations (8) and (9). The solution is a trajectory similar to the ones shown in Fig. 7. The distance Z_o where r is zero is recorded. This is where the detector must be located to detect H_2^+ particles scattered out of the scattering cell at the angle Θ when the focusing magnet current is set at I_o and the energy of the incident beam of protons is E_o.

If the detector distance Z_o is changed and I_o and E_o are held constant then H_2^+ particles scattered out of the scattering cell at different scattering angles Θ are detected.

Alternately, one can hold E_o and Z_o constant and vary I_o. This also allows particles of different scattering angles to be detected.

D. THE COMPUTER SOLUTION

The computer solution of equations (8) and (9) was originally worked out by Gagliano, but has since been rewritten. Program SOLANG, explained in Appendix II, employs the Hamming Modified Predictor-Corrector method to integrate equations (8) and (9). This is the DHPGC subroutine of the IBM System 360-67 Scientific Subroutine Package.

The trajectory equations are solved for a range of scattering angles for a particular E_o and I_o. The results are stored and later used to compute the solid angle subtended by the detector as it intercepts each of these trajectories.

E. THE SOLID ANGLE

The solid angle subtended by the detector is given by the relation:

$$d\Omega(\theta,\phi) = \sin\theta \, d\theta \, d\phi$$

But since our system is axially symmetric this becomes

$$d\Omega(\theta) = \sin\theta \, d\theta \int d\phi$$

$$= 2\pi\left(\frac{290}{360}\right) \sin\theta \, d\theta$$

$$= 1.612\,\pi \sin\theta \, d\theta.$$

This is because only 290^o of the available 360^o of the axial angle ϕ are accessible to the detector due to the construction of the scattering cell. (See Chapter II, Section 3.)

From the trajectory plots on Fig. 15 it can be seen that all particles scattered into θ will cross the axis at Z_o within ΔZ_o. This ΔZ_o determines the angular resolution $\Delta\theta$ which the detector sees and so allows determination of the solid angle. But ΔZ_o is in turn determined by the detector geometry and the particular trajectory under observation. The relation between $\Delta\theta$ and ΔZ_o can be found from the functional relationship:

$$Z_o = f(E, B, \theta, \rho, \eta, C)$$

where E = energy of incident ion.

B = magnetic field

ρ = target width from system axis along a radial line

η = target thickness from system center along the Z axis

C = constant for each reaction including mass ratios, inelastic energy losses, etc.

Differentiating this gives:

$$\Delta Z_o = \frac{\partial Z_o}{\partial E}\Delta E + \frac{\partial Z_o}{\partial B}\Delta B + \frac{\partial Z_o}{\partial \theta}\Delta\theta + \frac{\partial Z_o}{\partial \rho}\Delta\rho + \frac{\partial Z_o}{\partial \eta}\Delta\eta + \frac{\partial Z_o}{\partial C}\Delta C$$

But $\Delta B = 0$ and $\Delta C = 0$ for any specific reaction and measurement. Thus, solving for $\Delta\theta$ we get:

$$\Delta\theta = \frac{\Delta Z_o - \left(\frac{\partial Z_o}{\partial E}\right)_{\theta,\rho,\eta}\Delta E - \left(\frac{\partial Z_o}{\partial \rho}\right)_{E,\theta,\eta}\Delta\rho - \left(\frac{\partial Z_o}{\partial \eta}\right)_{E,\theta,\rho}\Delta\eta}{\left(\frac{\partial Z_o}{\partial \theta}\right)_{E,\rho,\eta}}$$

No analytical expression exists for the various differentials. However, computer trajectory results obtained by varying E,θ,ρ and η show the effect of the differentials is to change $\Delta\theta$ by no more than by 10% (see Ref. 10). Thus the angular spread can be expressed as:

$$\Delta\theta \approx \left(\frac{\partial\theta}{\partial Z_o}\right)_E \Delta Z_o \qquad (17)$$

Hence the solid angle becomes

$$d\Omega(\theta) = 1.612\pi \sin\theta \left(\frac{\partial\theta}{\partial Z}\right)_E \Delta Z_o \qquad (18)$$

Now, since ΔZ_o depends on the angle θ_o (see Fig. 21 and Ref. 5 for further details) and θ_o in turn depends on the scattering angle θ we see that $d\Omega$ must be evaluated at each angle of

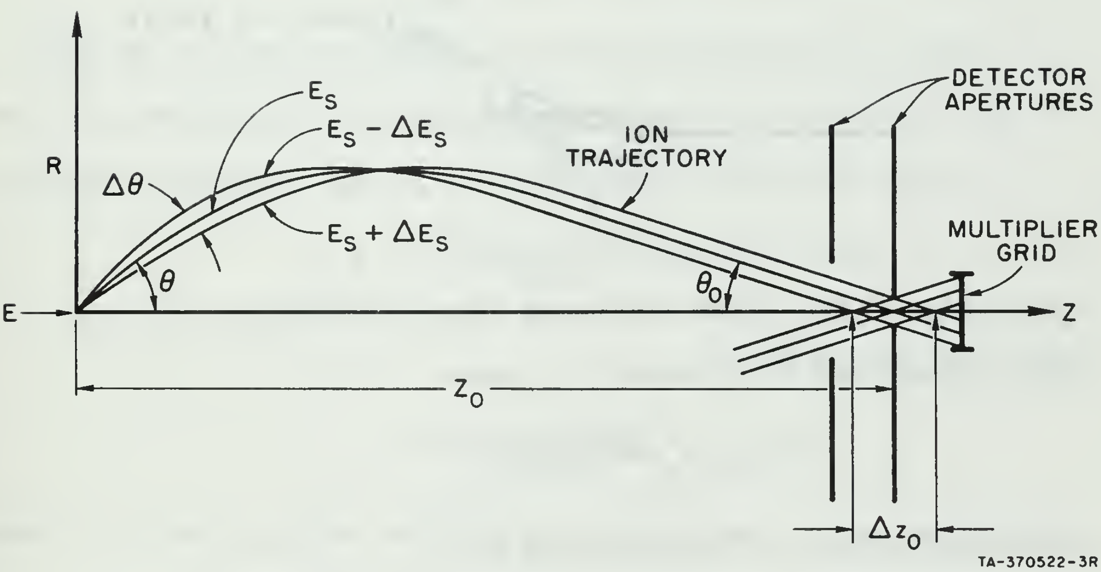

Figure 21. Angular and Energy Acceptance of Dector

scatter. This is implemented in the latter subroutine of the computer program SOLANG.

Computer results indicate that the angular resolution given by equation (17) is approximately 1^{o}.

F. THE CROSS SECTION

Consider a beam of monoenergetic ions I_i incident on a target of N_t molecules. A detector located at an angle Θ subtends solid angle $d\Omega(\Theta)$.

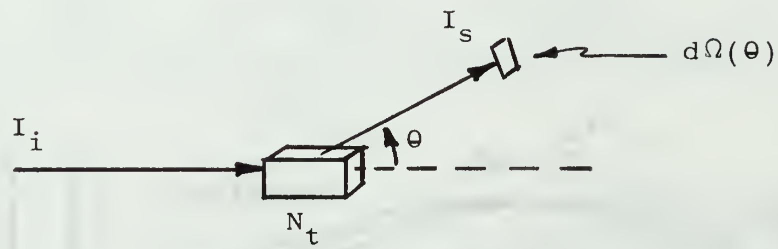

The number of particles scattered into the detector, N_s, is usually measured as a current I_s where:

$$I_s = N_s \, d\Omega(\Theta)$$

The cross section is then defined as:

$$d\sigma(\Theta) = \frac{I_s}{I_i \, N_t \, d\Omega(\Theta)} \, . \qquad (19)$$

But I_s is magnified G times by the multiplier gain. Hence I_D, the actual detector current measured is:

$$I_D = I_s \, G$$

Hence (19) becomes:

$$d\sigma(\theta) = \frac{I_D}{I_i \; G \; N_t \; d\Omega(\theta)}$$

But N_t, the number of target particles, is given by:

$$N_t = P_{sc} \rho \, t$$

Where P_{sc} = pressure of target gas in scattering cell in torr

$\rho = 3.536 \times 10^{16}$ particles/cm^3 torr

t = target length in cm

Hence we have:

$$d\sigma(\theta) = \frac{I_D}{I_i \; G \; P_{sc} \rho \, t \; d\Omega(\theta)} \; \text{cm}^2 \qquad (20)$$

Because of the construction of the scattering cell (see Section 3 of Chapter II) the target thickness depends on the scattering angle θ. Bush, has shown this relation to be:

$$t = S - \frac{2.54 \sin(36^\circ - \theta)}{\sin\theta} \quad \text{if } \theta < 36^\circ$$

$$t = S \quad \text{if } 36^\circ < \theta < 49^\circ \qquad (21)$$

$$t = S - \frac{2.0 \sin(\theta - 49^\circ}{\sin\theta} \quad \text{if } 49^\circ < \theta$$

where S is the minimum separation of the front of the scattering cell from the rear of the scattering cell, (which is adjustable from outside the vacuum system).

Computer Program CSVSZ, listed in Appendix I, calculates the differential cross section in the Lab. and Center of Mass coordinate systems using equations (20) and (21) and the solid angle determined by the program SOLANG.

V. EXPERIMENTAL RESULTS

A. ELIMINATION OF BACKGROUND

When H^+ collides with CH_4 three general types of collision may occur which can produce large detector signals.

Event (a) The rearrangement collision where the H^+ captures a proton to form H_2^+.

Event (b) A scattering collision of the H^+ with a hydrogen atom.

Event (c) A scattering collision of the H^+ with a carbon atom.

Events (b) and (c) are expected to have cross sections that are many orders of magnitude larger than those of event (a). Hence appropriate steps were taken to insure events (b) and (c) were not measured by our detector. To eliminate events (b) and (c) we look first at the energy and momentum of the scattered particles in all three events.

Consider first event (a). The capture process may be approximated by the reaction shown below:

$$\underline{H}^+ + CH_4 \rightarrow \underline{H}^+ + CH_3$$

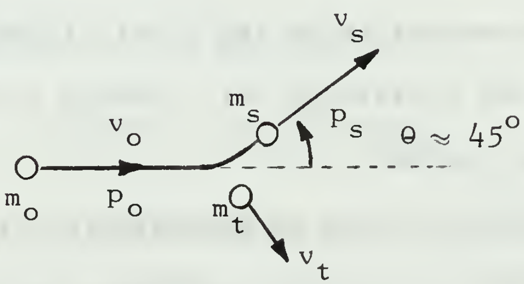

The energy of the incident H^+ particle is:

$$E_o = \tfrac{1}{2} m_o v_o^2 = \frac{p_o^2}{2m_o} \tag{1}$$

Now, from conservation of momentum we see the momentum of the scattered H_2^+ particle, represented by p_s, related to p_o by:

$$p_o \approx p_s \cos 45^o = \frac{p_s}{\sqrt{2}} \qquad (2)$$

where we assume the mass of the CH_3, represented by m_t, to be infinitely large. Hence in the capture process, the scattered particle has momentum $p_s = \sqrt{2}\, p_o$. The energy of the scattered particle is then:

$$E_s = \frac{p_s^2}{2m_s} \approx \frac{p_o^2}{m_s}$$

But for the H_2^+ particle, $m_s = 2\, m_o$

Hence:

$$E_s \approx \frac{p_o^2}{2m_o} = E_o \, . \qquad (3)$$

Consider now event (b), the scattering of the H^+ from a hydrogen atom:

$$\underline{H}^+ + H \rightarrow \underline{H}^+ + \underline{H}$$

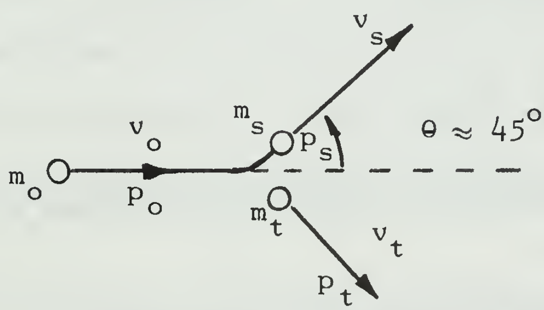

Since $m_t = m_s$ and $p_t = p_s$ we see that:

$$p_o = 2\, p_s \cos 45^o = \sqrt{2}\; p_s$$

Hence:

$$p_s = \frac{p_o}{\sqrt{2}} \qquad (4)$$

Then:

$$E_s = \frac{p_s^2}{2m_s} = \frac{p_o^2}{4m_o} = \tfrac{1}{2}\, E_o . \qquad (5)$$

Thus the elastically scattered H^+ from H has a momentum that is approximately $\frac{p_o}{\sqrt{2}}$ and an energy that is approximately $\frac{1}{2} E_o$.

Finally consider event (c), the scattering of the H^+ from a carbon atom:

$$\underline{H}^+ + C \rightarrow \underline{H}^+ + C$$

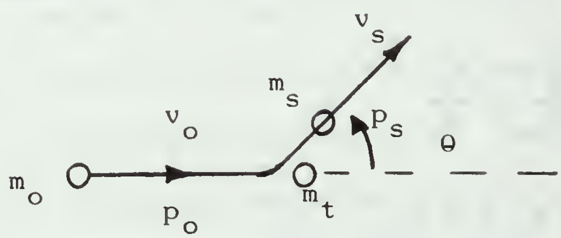

Assuming the carbon to be infinitely massive we see that:

$$E_s = E_o \tag{6}$$

Hence:
$$\frac{p_s^2}{2m_s} = \frac{p_o^2}{2m_o}$$

But:
$$m_s = m_o$$

Thus:
$$p_s = p_o \tag{7}$$

Hence the elastically scattered H^+ from C has momentum p_o and energy E_o.

Summarizing the results of this very approximate analysis in Table 1 we get for an incident beam of protons of energy E_o and momentum p_o the information shown. Note that the scattered H^+ produced in events (b) and (c) has momentum less than the H_2^+ produced in event (a).

Possible Events	Scattered Particle	Momentum of Scattered Particle	Energy of Scattered Particle
Event (a) Capture $\underline{H}^+ + CH_4 \rightarrow \underline{H}_2^+ + CH_3$	H_2^+	$\sqrt{2}\ p_o$	E_o
Event (b) Scatter $\underline{H}^+ + H \rightarrow \underline{H}^+ + \underline{H}$	H^+	$\frac{1}{\sqrt{2}}\ p_o$	$\frac{1}{2}\ E_o$
Event (c) Scatter $\underline{H}^+ + C \rightarrow \underline{H}^+ + C$	H^+	p_o	E_o

TABLE 1. The Three Possible Scattering Processess.

Plots of the scattered ion trajectories resulting from each of the three events tabulated are shown in Fig. 22, for the particular case of E_o = 100 eV and I = 6.0 amps. Note that the two elastically scattered H^+ ions cross the axis at a z less than that of the H_2^+ ion. To prevent these unwanted H^+ particles from reaching the detector, a baffle, 5 cm in radius was positioned over the beam collector as shown in Fig. 22. This allowed only the H_2^+ produced by the rearrangement collision to reach the detector.

Figure 23 contains plots of the detector current versus the detector grid voltage for the case of E_o = 100 eV and I = 6.0 amps and with the detector located at z = 46 cm (this corresponds to a scattering angle θ of 46.92^o). Figure 23 -(i) was recorded before the baffle was placed in the path of the H^+ ions and Fig. 23 - (ii) was recorded after the baffle was positioned, as shown in Fig. 22.

Consider first, Fig. 23 - (i). A grid voltage of 25 volts eliminates the slow ions. As the detector grid voltage is varied from 25 to 50 volts, we continue to collect the ions scattered from the scattering cell due to processess (a) and (b) and (c). Between 60 and 90 volts we collect only these particles with energies greater than 90 volts; ie, the ions which result from processes (a) and (c) only.

Figure 23-(ii) now shows that the baffle does indeed eliminate particles resulting from processes (b) and (c). Thus with the grid voltage set anywhere between 30 and 90 volts, and the baffel in position, we only detect the H_2^+ that results from the re-arrangement collision.

B. DEMONSTRATION OF VALIDITY OF DETECTOR SIGNAL

From equation (20) of Chapter IV we have:

$$d\sigma(\theta) = \frac{I_D}{I_i \; P_{sc} \; \rho \, tG \; d\Omega(\theta)} \quad cm^2 \tag{8}$$

If the angle of the scatter θ is held constant, then this reduces to:

$$d\sigma = K \frac{I_D}{I_i P_{sc}} \tag{9}$$

where K = constant.

Consider now the case where I_i is held constant. Then (9) reduces to:

$$I_D = C_1 \; P_{sc} \tag{10}$$

where C_1 = constant. Experimental data plotted in Fig. 24 obeys this linear relationship. The fact that I_D does not extrapolate to zero is due to the background.

Figure 22. Trajectory plots of the H_2^+ and the elastically scattered H^+ particles at $\theta = 45°$ when I = 6.0 amp. and the energy of the incident proton beam = 100 ev.

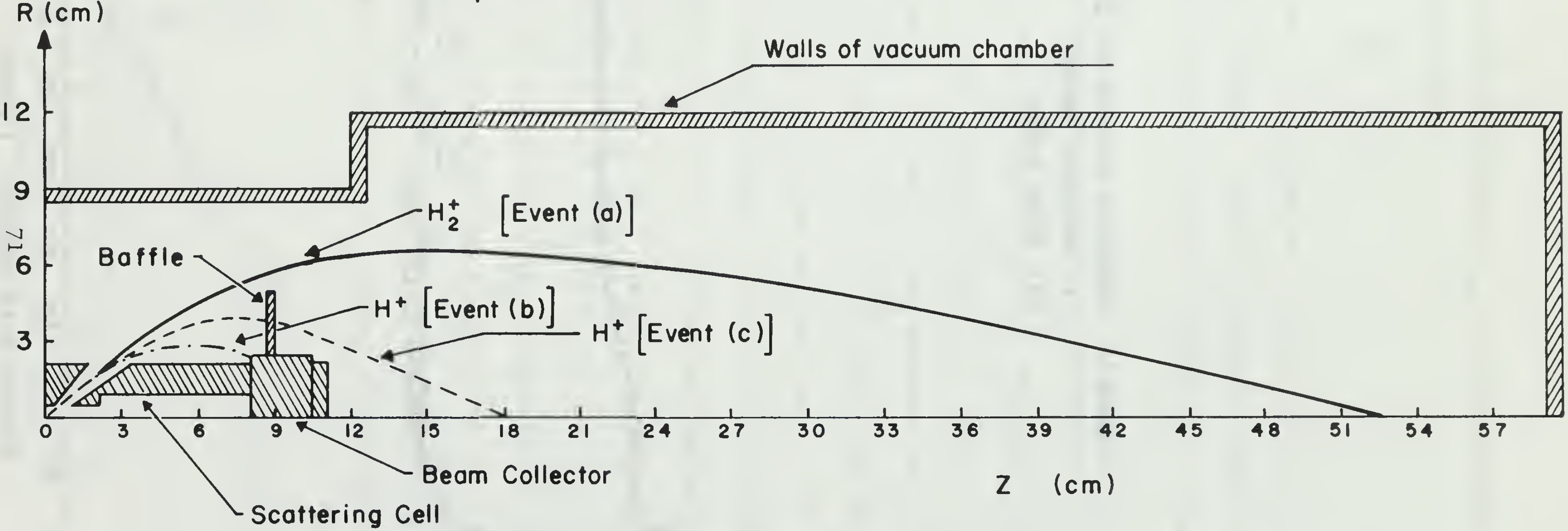

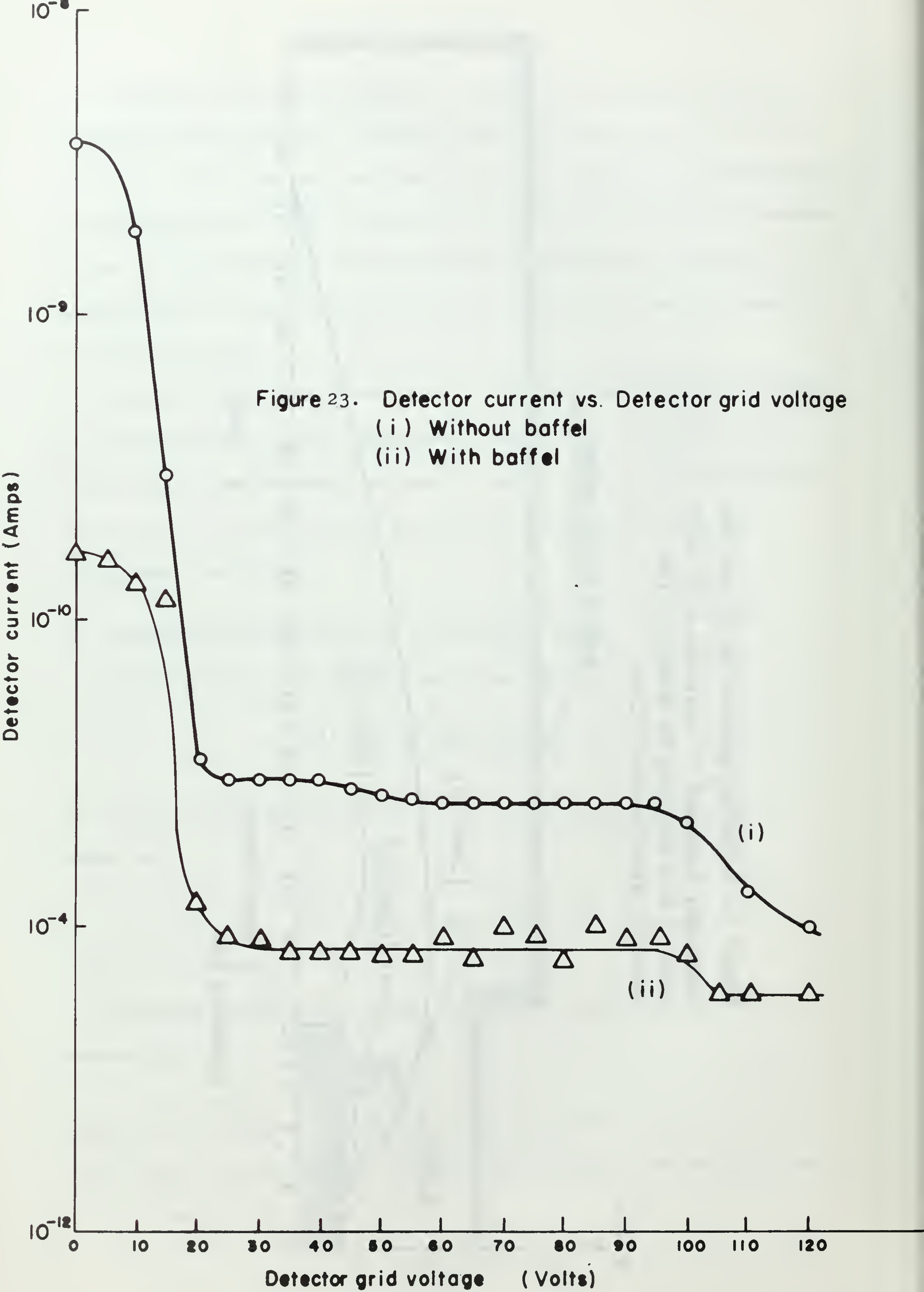

Figure 23. Detector current vs. Detector grid voltage
(i) Without baffel
(ii) With baffel
Detector current (Amps)
10^-8
10^-9
10^-10
10^-4
10^-12
(i)
(ii)
0 10 20 30 40 50 60 70 80 90 100 110 120
Detector grid voltage (Volts)

Consider next the case where P_{sc} is held constant. Then equation (9) reduces to:

$$I_D = C_2 I_i \tag{11}$$

where I_i = constant. Experimental data plotted in Fig. 25 follows this linear relationship. Thus our detector signal has the proper dependance on the various parameters and behaves like a scattered particle current.

For the differential scattering measurements made with 100 eV incident protons, the proton current at the beam collector was approximately 10^{-7} amps and the current to the rear of the scattering cell was about 10^{-8} amps. The methane gas pressure was varied from 1×10^{-4} torr to 3×10^{-3} torr. The detector signal under these operating conditions varied from 1×10^{-12} amps to 3×10^{-11} amps. This represents a flux of a few hundred particles per second. With no gas in the scattering chamber the detector current fell to about 5.0×10^{-13} amps.

The UGIA Ion Gauge used to measure the methane pressure in the scattering cell was calibrated using a Capacitance Manometer. The relationship between the pressure measured by the ion gauge ($P_{measured}$) and the actual pressure which was measured by the manometer (P_{actual}) is linear in the region of interest as is shown below.

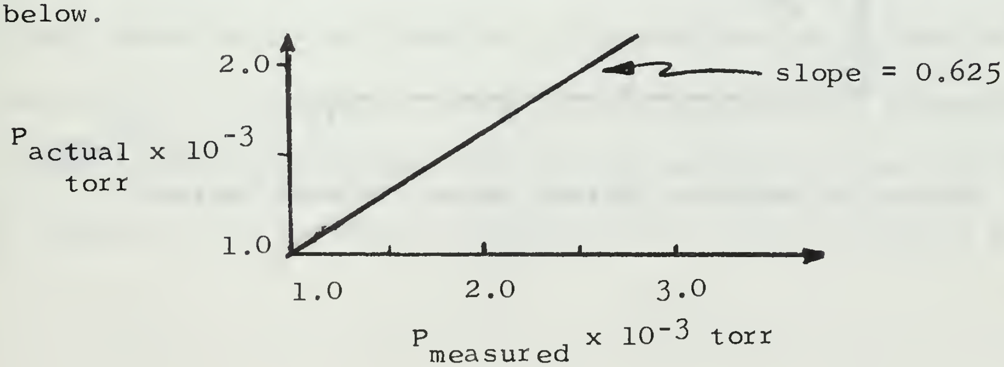

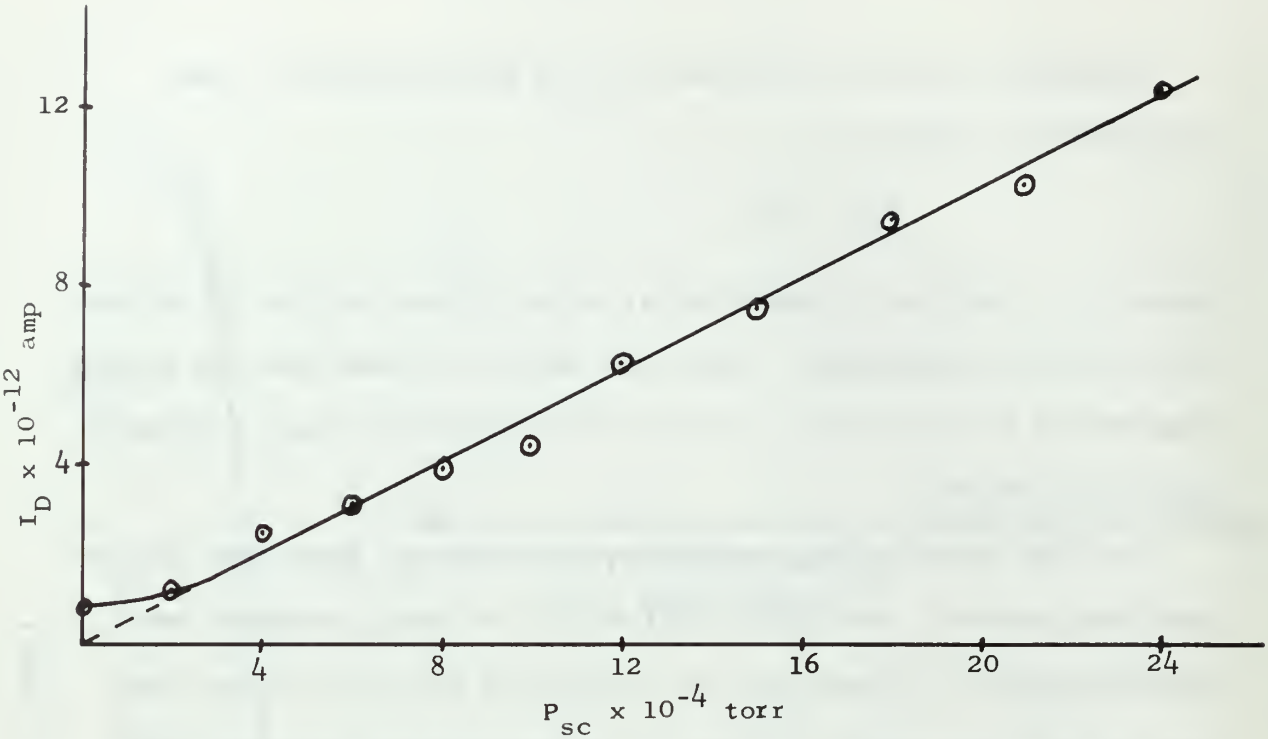

Figure 24. Detector Current versus Pressure of Target Gas

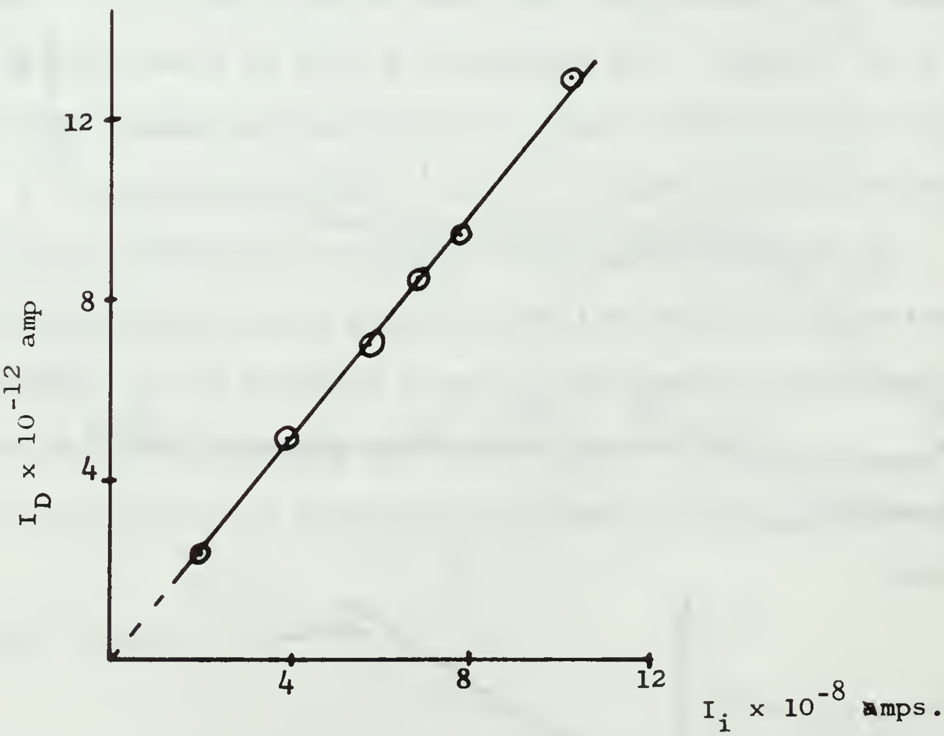

Figure 25. Detector Current versus Incident Current.

C. $H^+ + CH_4$ SCATTERING DATA

The cross section for the formation of H_2^+ was measured at different angles of scatter by varying the detector distance Z while holding the magnet current I fixed. As pointed out in Section B of Chapter II the cross section is expected to be a pronounced peak at 46.9°. Hence the detector was swept through the range of scattering angles from 43° to 49°. This was repeated for various target gas pressures for each value of the energy of the incident proton beam. The energies investigated were 70, 85, 100, 150 and 200 electron volts. The scattering data recorded at each of these energies is shown in Figs. 26, 28, 30, 32 and 33 respectively. A prominent peak exists in the 70, 85, and 100 eV data. The 150 and the 200 eV data shows no apparent peak in the cross section.

The data was analyzed in the following manner. From the cross section measurements made at each energy an average value of $\sigma(\theta)$ was computed and sketched in as a solid line. The assumed background was then drawn as a dotted line. Subtracting out the background from the 70, 85, and 100 eV data, the points connected by the solid curve in Figs. 27, 29, and 31 were obtained. To find out what the actual peak in the scattering data looked like before it was detected by our detector of approximately 1° resolution, the effect of the angular width of the detector was determined and the actual curve unfolded. The curves dotted on Figs. 27, 29, and 31 represent the unfolded original peak in the scattering data.

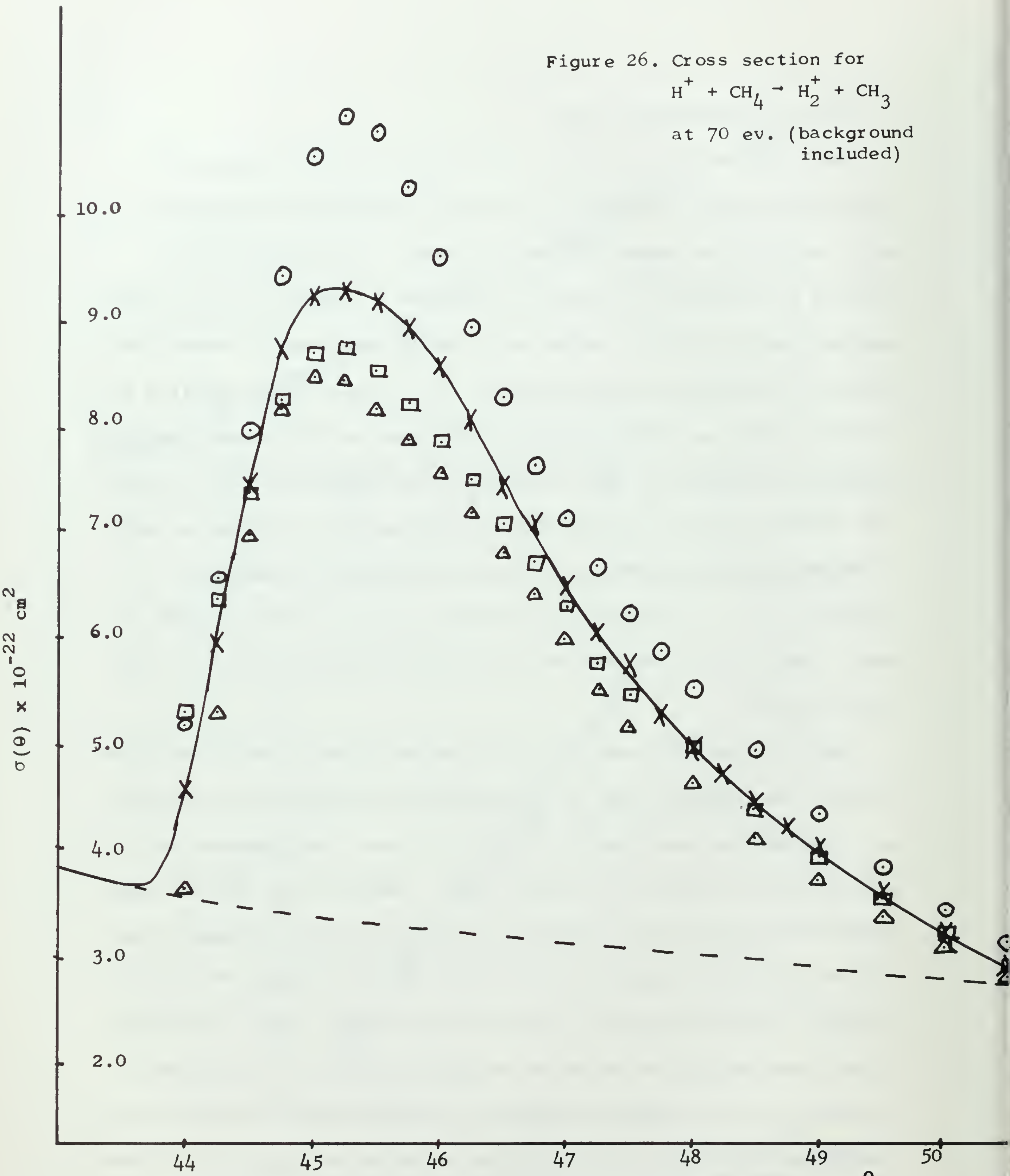

Figure 26. Cross section for $H^+ + CH_4 \rightarrow H_2^+ + CH_3$ at 70 ev. (background included)

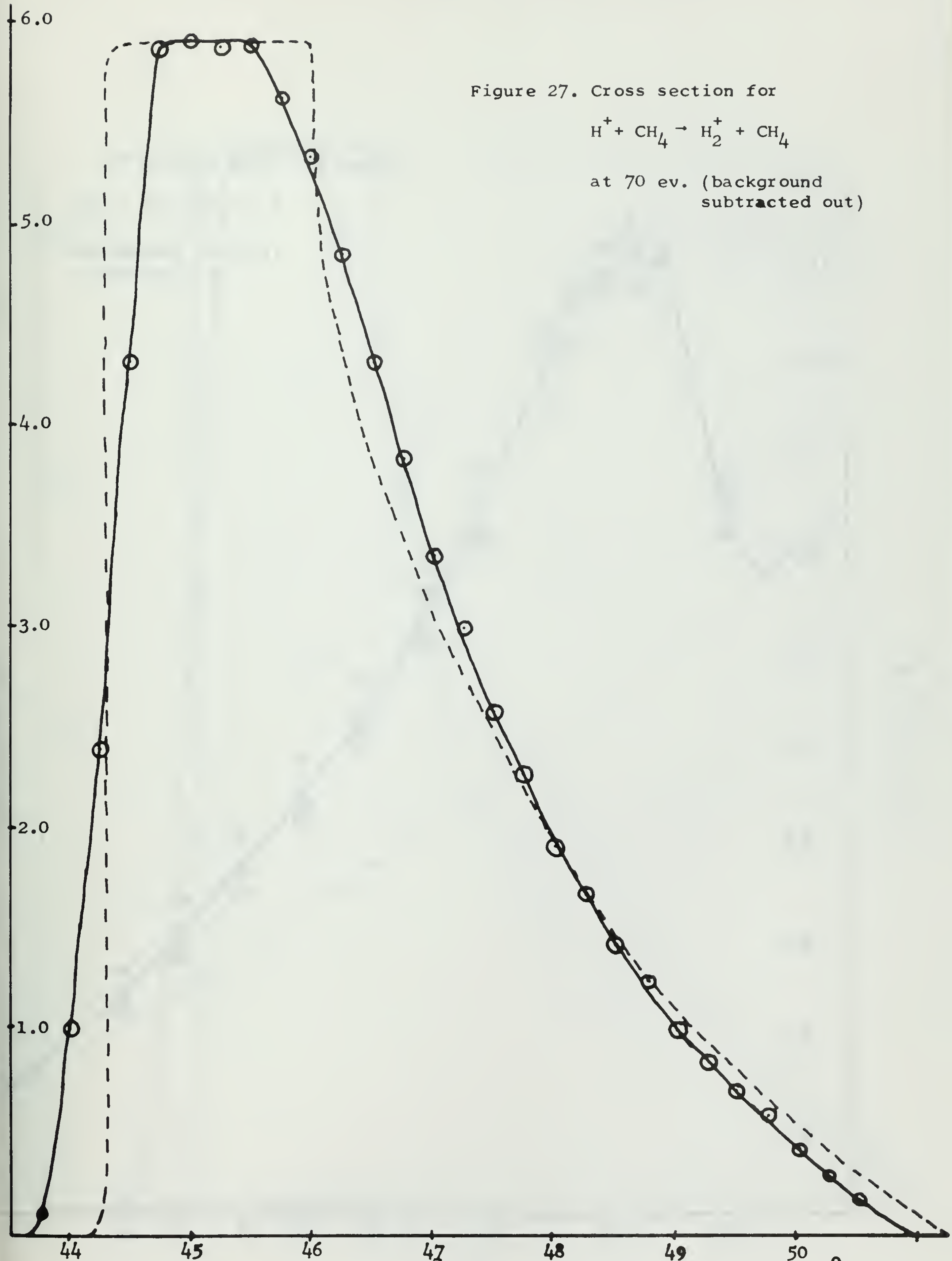

Figure 27. Cross section for

$H^+ + CH_4 \rightarrow H_2^+ + CH_4$

at 70 ev. (background subtracted out)

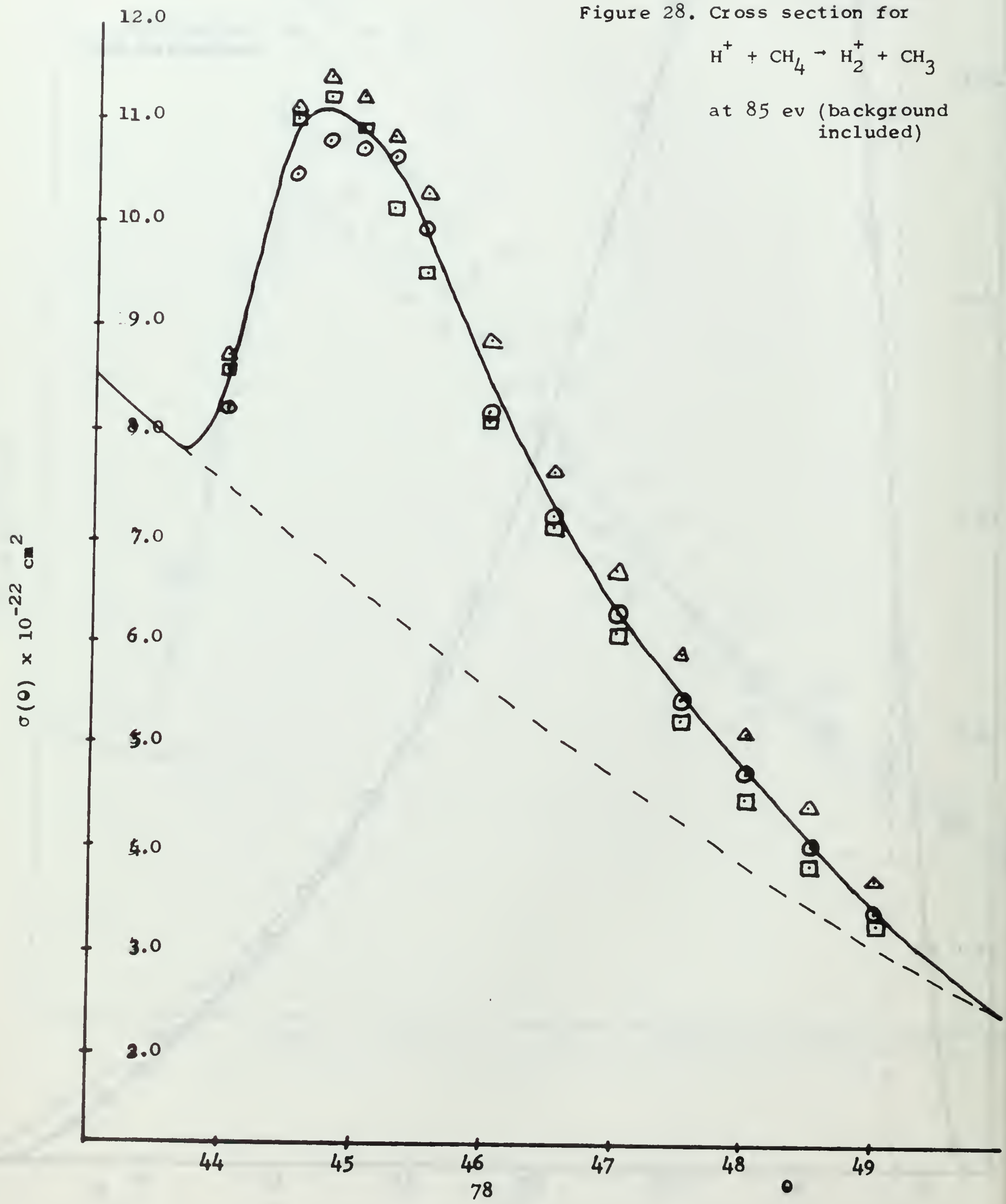

Figure 28. Cross section for $H^+ + CH_4 \rightarrow H_2^+ + CH_3$ at 85 ev (background included)

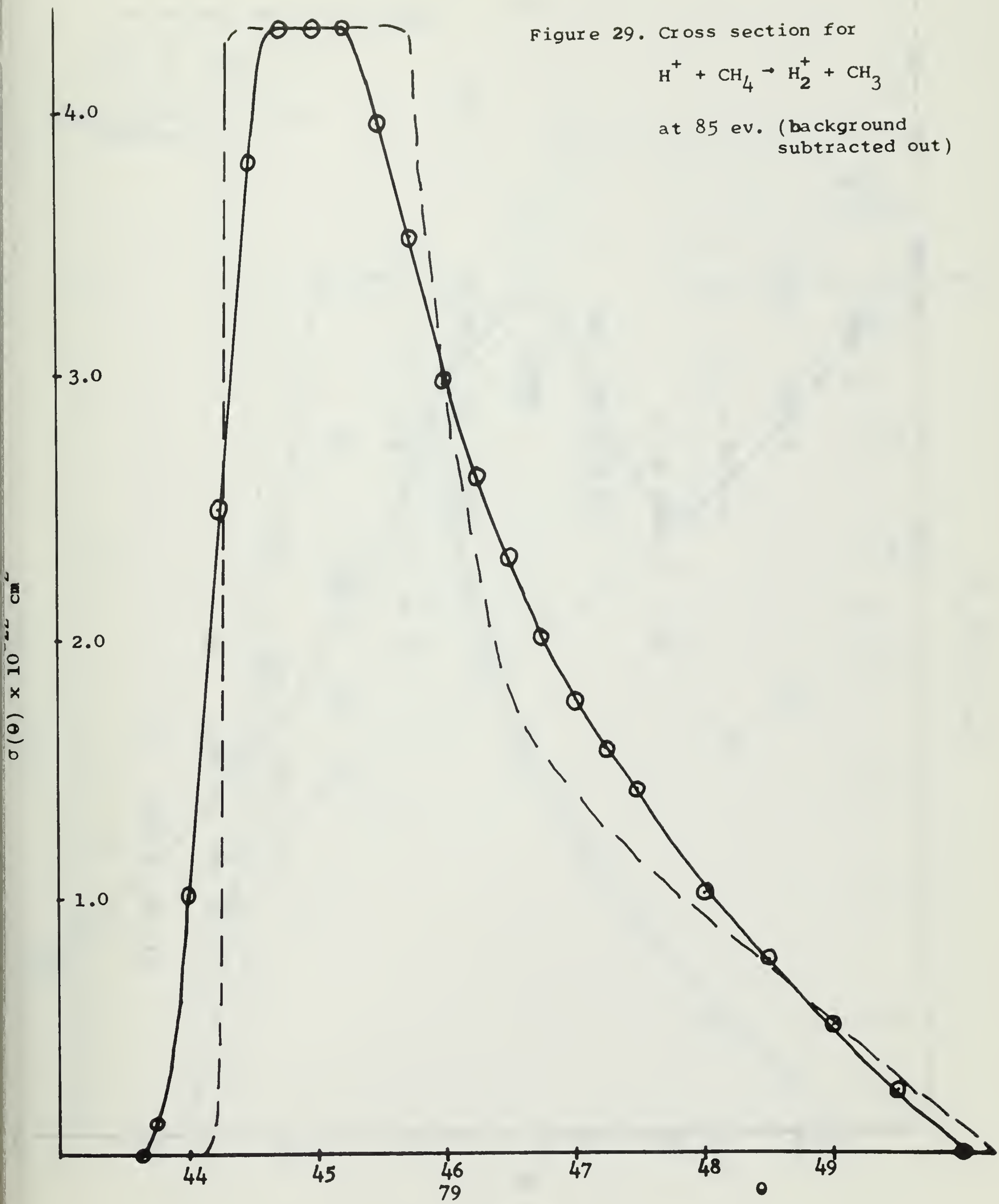

Figure 29. Cross section for $H^+ + CH_4 \rightarrow H_2^+ + CH_3$ at 85 ev. (background subtracted out)

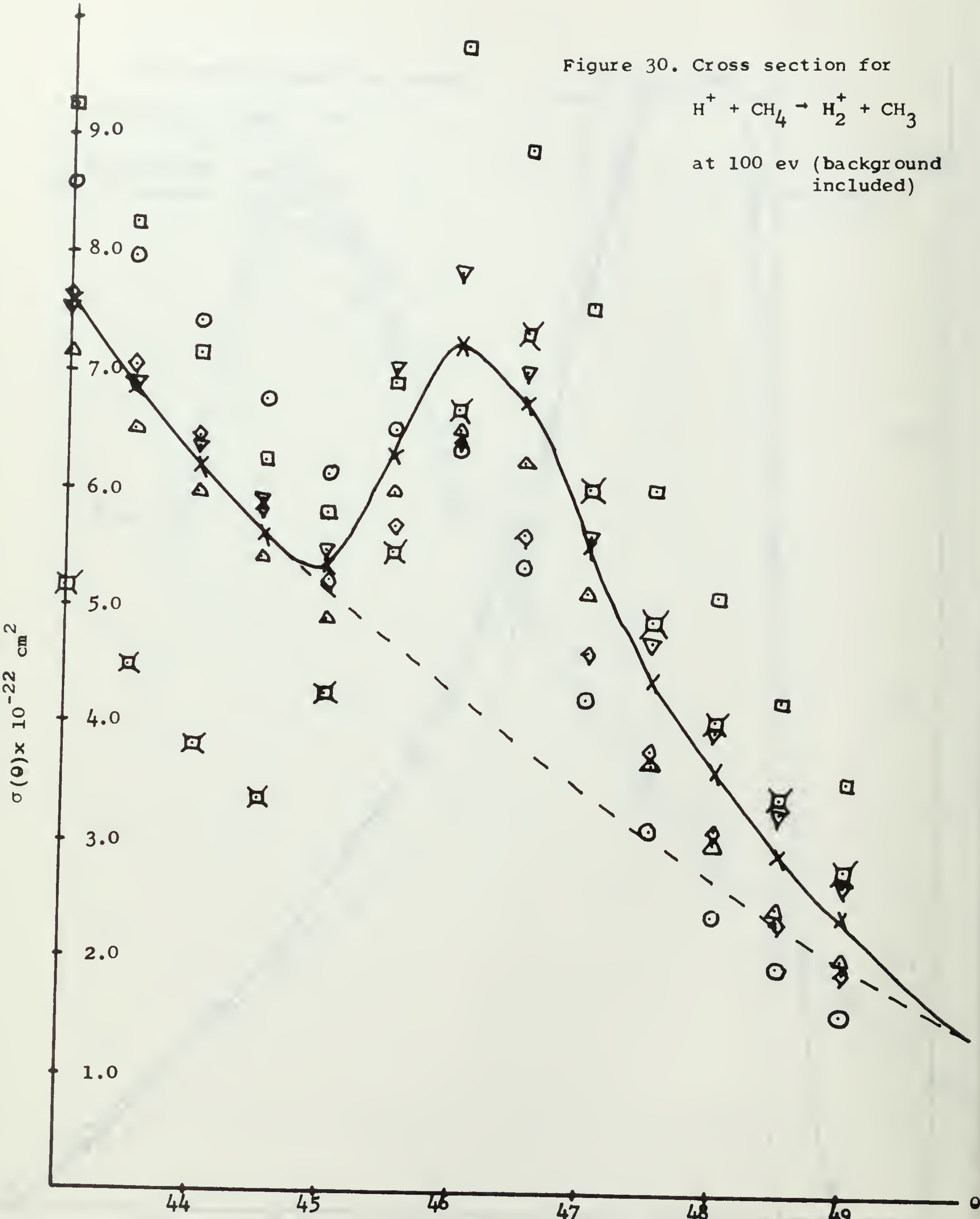

Figure 30. Cross section for $H^+ + CH_4 \rightarrow H_2^+ + CH_3$ at 100 ev (background included)

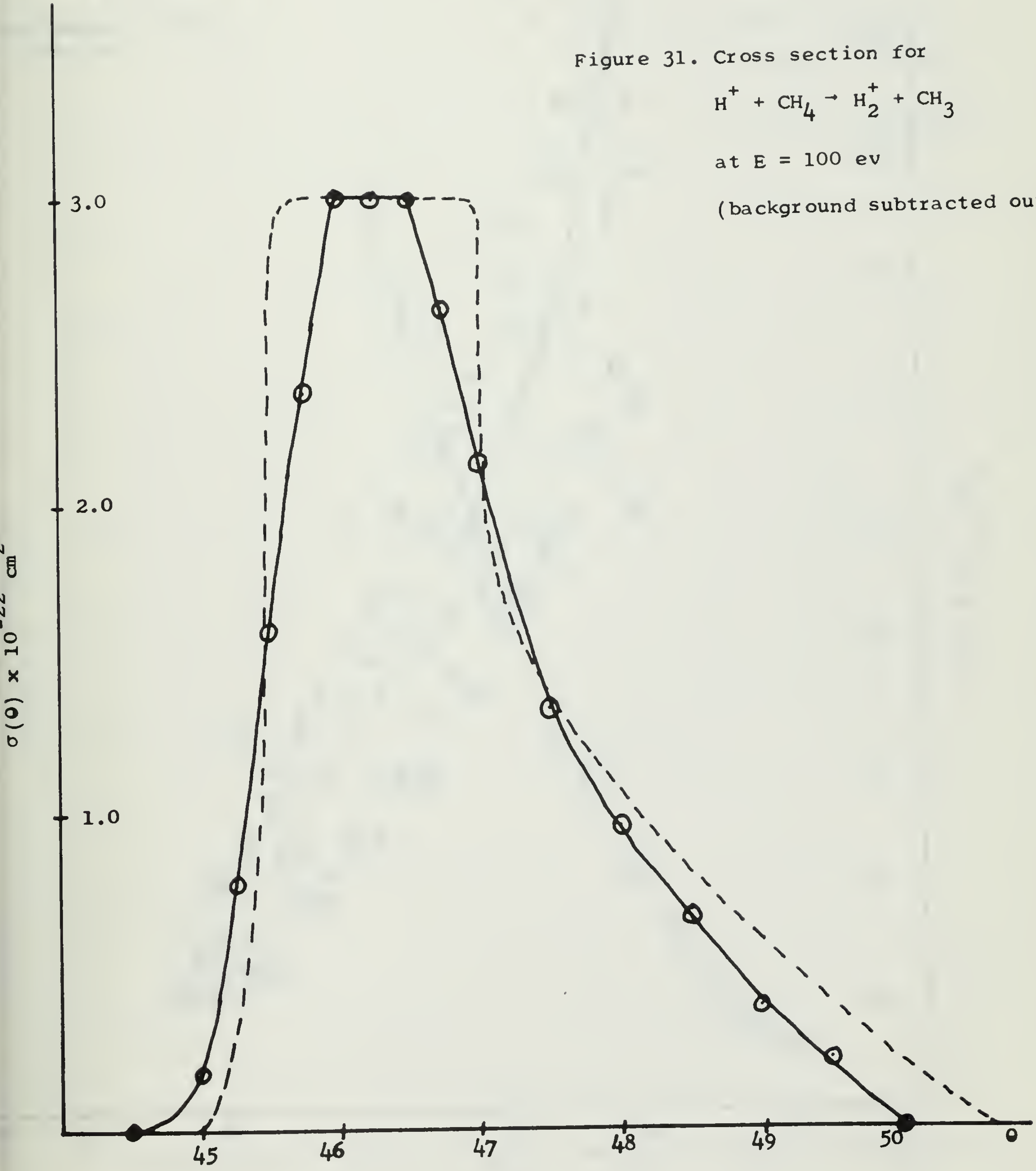

Figure 31. Cross section for

$H^{+} + CH_4 \rightarrow H_2^{+} + CH_3$

at E = 100 ev

(background subtracted out)

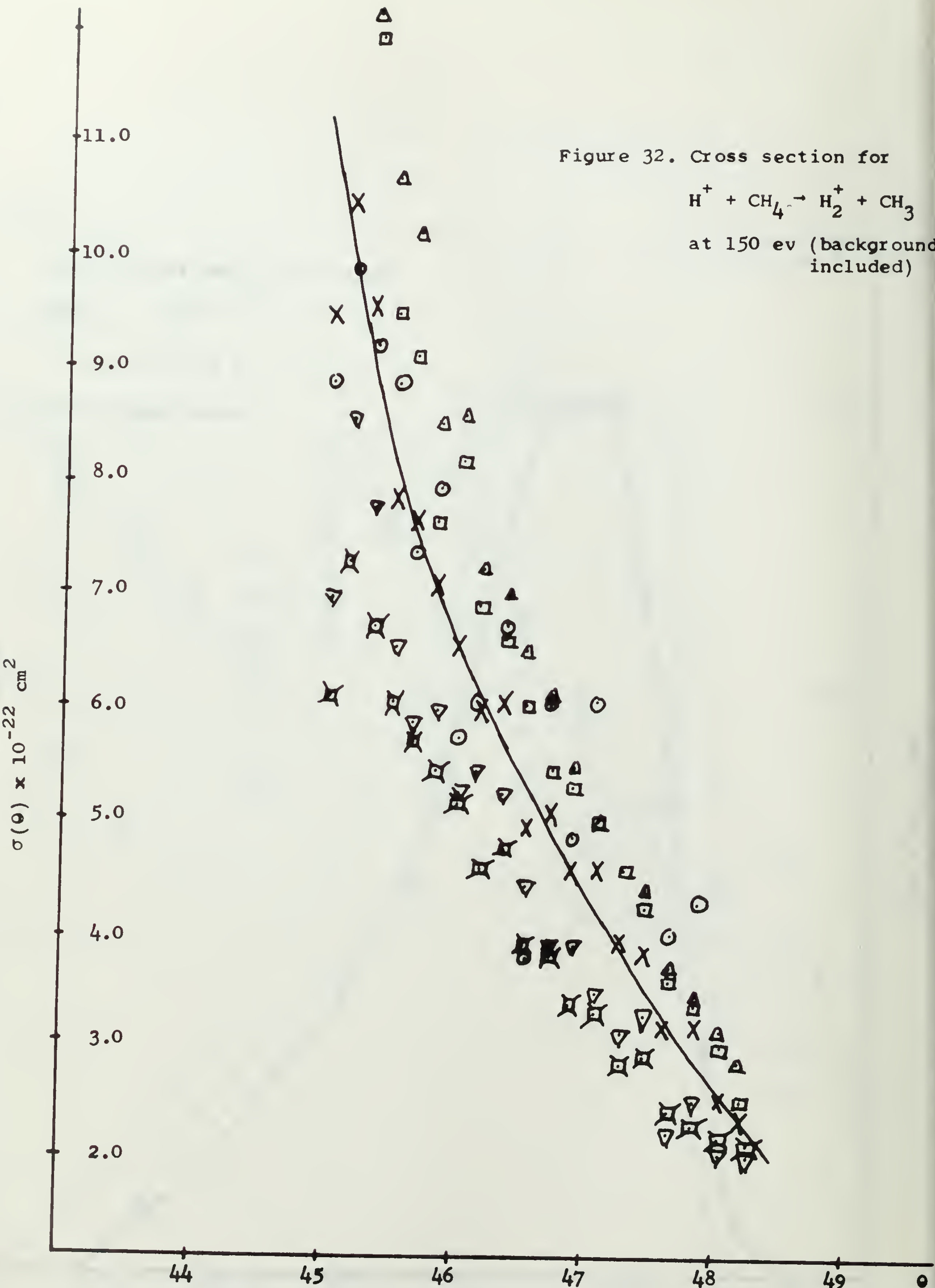

Figure 32. Cross section for $H^+ + CH_4 \rightarrow H_2^+ + CH_3$ at 150 ev (background included)

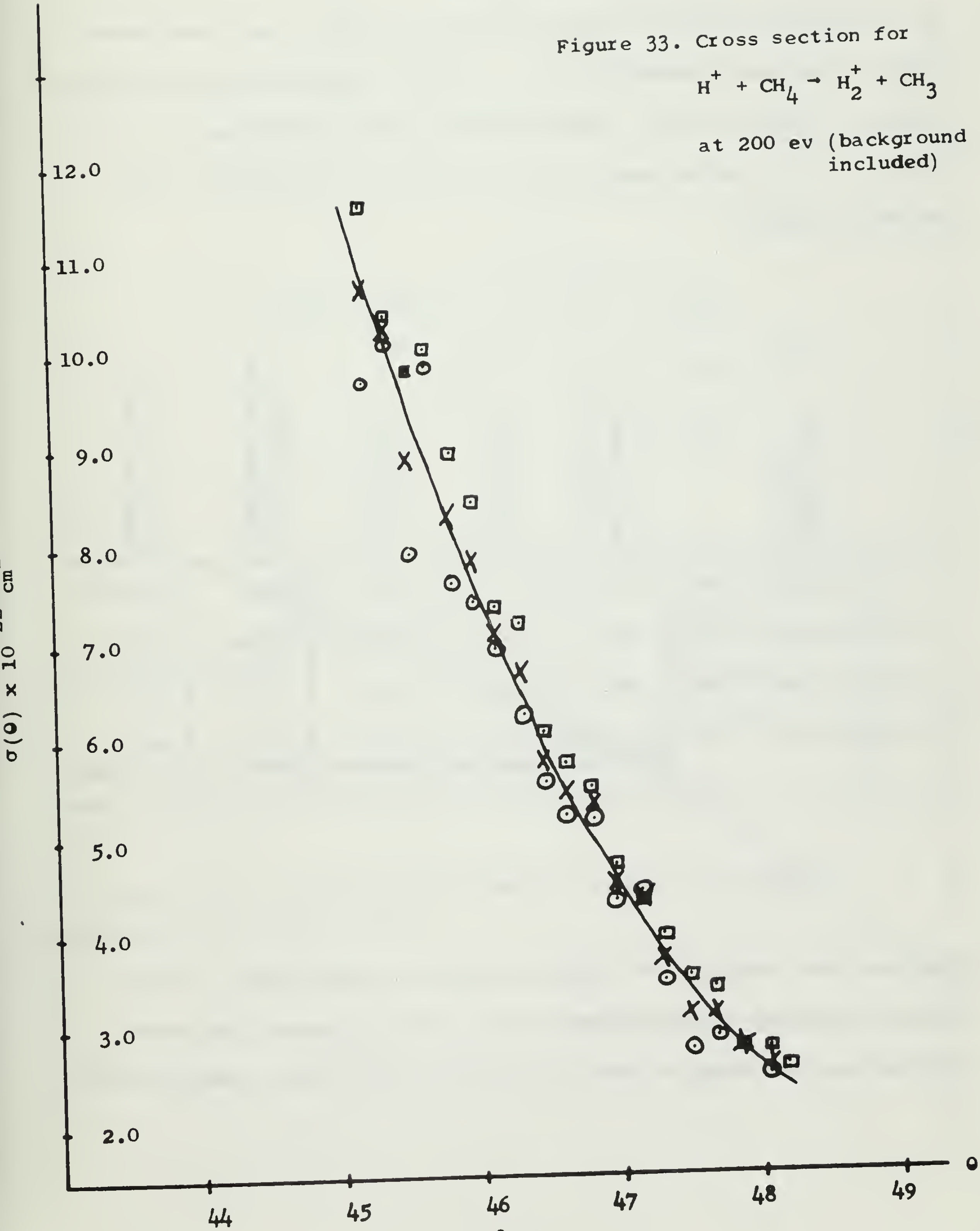

Figure 33. Cross section for $H^+ + CH_4 \rightarrow H_2^+ + CH_3$ at 200 ev (background included)

These peaks are then the actual cross sections for the rearrangement reaction:

$$\underline{H}^+ + CH_4 \rightarrow \underline{H}_2^+ + CH_3$$

as the energy of the H^+ varies from 70 to 100 eV. All the peaks exhibit the same characteristics: a sharp leading edge at the lower angles, a flat top and a long decreasing tail extending out to about 51^o. The peaks dependence on energy is exhibited in the following table:

E	Magnitude of Peak	Angle Peak Occurs	Peak Width	Area Under Peak	Area Under Complete Curve	Centroid of Complete Curve
70 eV	$5.95 \times 10^{-22} cm^2$	45.15^o	1.7^o	10.2	20.6	45.87^o
85 eV	$4.26 \times 10^{-22} cm^2$	45.1^o	1.5^o	6.56	11.56	45.6^o
100 eV	$3.0 \times 10^{-22} cm^2$	46.25^o	1.5^o	4.62	7.6	46.7^o
≥ 150 eV	$\leq 1.0 \times 10^{-22} cm^2$	Not Observed	Not Observed	Not Observed	Not Observed	Not Observed

Table II. Summary of Experimental Data

The peak does exhibit the expected physical properties. As the energy increases the magnitude of the peak decreases, the width narrows and the angle at which the peak occurs moves towards 46.9^o.

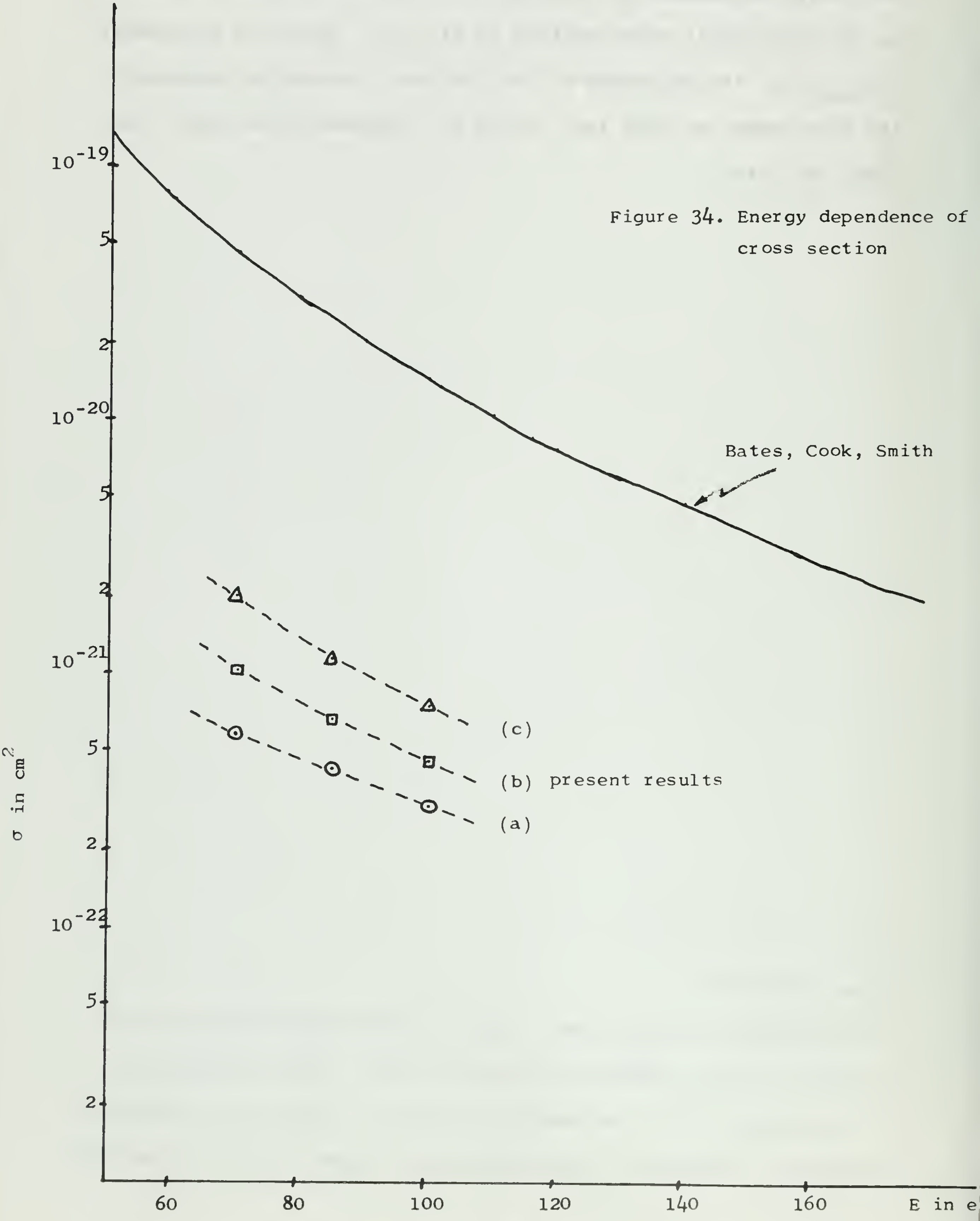

Figure 34. Energy dependence of cross section

The energy dependence of the experimental cross section is compared to the theoretical cross section in Fig. 34. Curve (a) represents $\sigma(\theta)_{max}$, ie. the magnitude of the flat top. Curve (b) represents the area under the flat top. Curve (c) represents the total area under the curve.

The energy dependence of the experimental cross section is compared to the theoretical cross section in Fig. 34. Curve (a) represents $\sigma(\theta)_{max}$, ie. the magnitude of the flat top. Curve (b) represents the area under the flat top. Curve (c) represents the total area under the curve.

Figure 34. Energy dependence of cross section

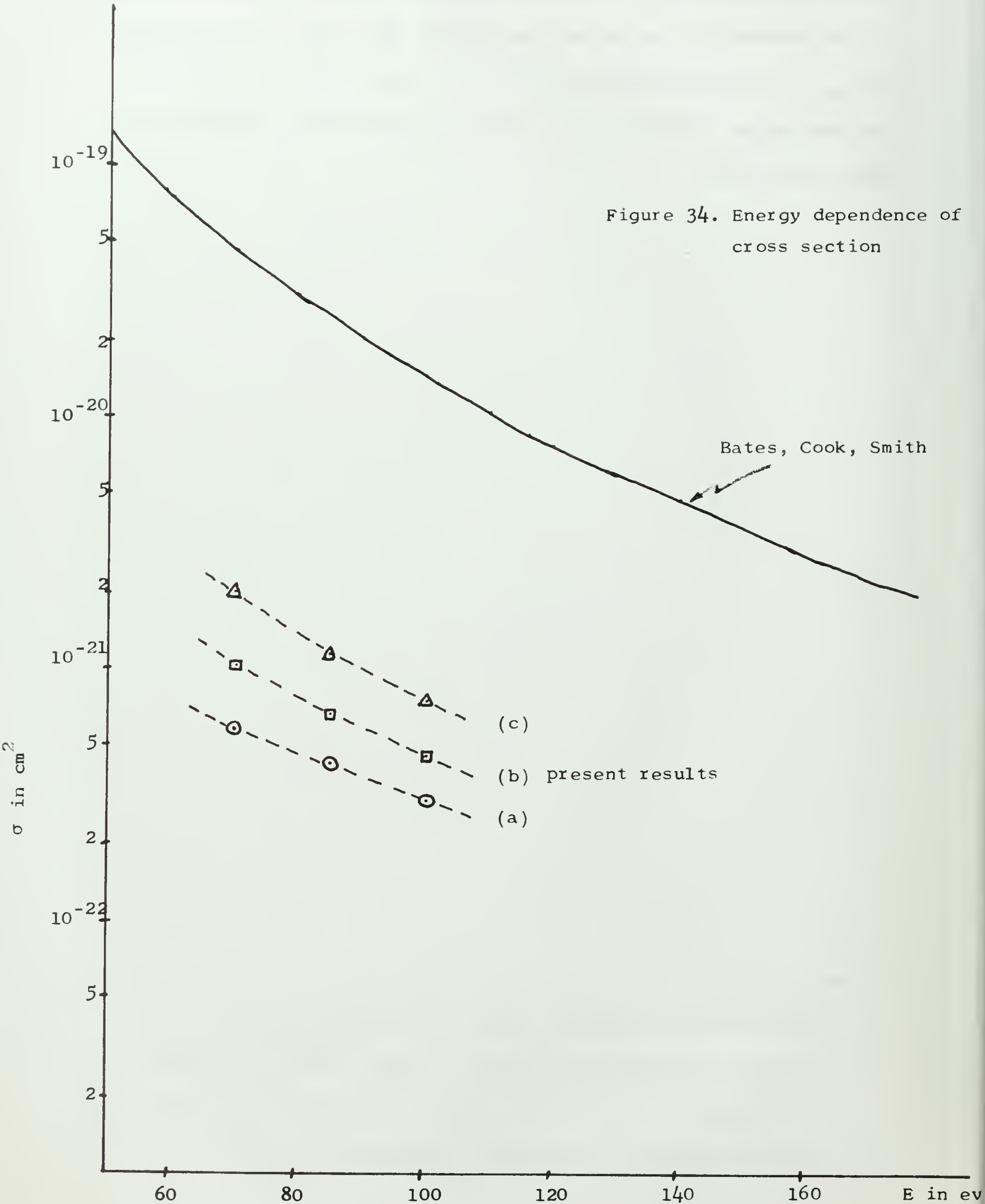

V. CONCLUSION

The close agreement between the experimental data and the predictions of the ion molecule rearrangement theory proposed by Bates, Cook and Smith is evident in the following observations:

(1) The sharp peak in the cross section predicted by Bates et.al., is observed in the 70, 85, and 100 eV data. The fact that the peak is not observed on the 150 and 200 eV data is not surprising for extrapolation of the experimental data to 150 eV shows that the magnitude of the cross section should be $1.0 \times 10^{-22} cm^2$. The 150 eV experimental data on Fig. 32 shows that a peak of this magnitude or smaller cannot be observed.

(2) The theory predicted the peak to occur at 46.9^o. The peaks observed were located between 45.1^o and 46.25^o, the latter corresponding to the higher energy. As the accuracy of the approximations made in the theory increases with higher energy, one expects the location of the peak in the experimental data to approach 46.9^o as the energy is increased. This trend is observed experimentally.

(3) As is evident from Fig. 34, the experimental cross section has an energy dependence similar to that predicted by the theory.

(4) The cross section predicted by Bates et.al., is an upper limit. Hence it is expected that the experimental cross section might be smaller than the theoretical cross section. The experimental cross section shown in Fig. 34 is in fact about a factor of 30 smaller than the theoretical upper limit.

(5) As some of the approximations made in the theory may no longer be valid at low energies one expects the peak to broaden as the energy decreases. This trend is indeed observed in the 100, 85, and 70 eV data shown in Figs. 31, 29, and 27 respectively.

It is felt that the facts mentioned above constitute a satisfactory verification of the ion molecule rearrangement theory of Bates, Cook and Smith as applied to the formation of H_2^+ in the reaction

$$\underline{H}^+ + CH_4 \rightarrow \underline{H}_2^+ + CH_3 .$$

APPENDIX I

MULTIPLIER GAIN MEASUREMENT

The following sketch shows how, in principle, the gain measurement can be made.

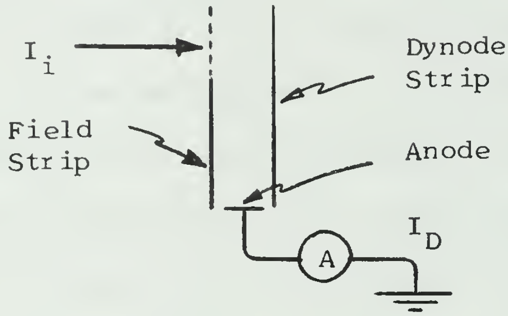

By recording the incident current I_i and the detector output I_D the gain can be computed from:

$$G = \frac{I_D}{I_i}$$

To measure I_i the Dynode Strip was used as a Faraday Cup. Two problems then arose:

(1) The Dynode Strip, because of its large resistance ($10^8\,\Omega$) retains a large residual negative charge. Thus in using the Dynode Strip as a Faraday Cup, I_i had to be greater than 10^{-10} amps so as to insure that this residual negative charge did not adversely affect the measurement.

(2) The Multiplier saturates when $I_D \geq 5 \times 10^{-6}$ amps. Thus we must have $I_i < (5 \times 10^{-6})G$.

To overcome these two difficulties the gain measurement was performed in the following sequence of steps.

Step 1. A beam of about 10^{-10} amps was focused on the Beam Collector.

Step 2. The Beam Collector was swung away from the back of the Scattering Cell. This allowed the ion beam to fall directly on the multiplier. With F.S.I. and D.S.O. grounded, (see Fig. 17) and a Keithley 610 Micro-Micro-ammeter connected to the D.S.I. this incident current was measured to be I_i' ($\approx 10^{-10}$ amps).

Step 3. The Multiplier was now restored to the configuration shown in Fig. 17. The Dynode Voltage was reduced to approximately 1,000 volts (this insured that the anode current to be measured in Step 4 was less than 10^{-6} amps the saturation current of the Multiplier).

Step 4. The Multiplier was turned on and a detector current I_D' ($\approx 10^{-7}$ amps) was measured at the anode. Thus, with the Multiplier settings as selected in Step 3 the gain was

$$G' = \frac{I_D'}{I_i'}$$

Step 5. The incident beam I_i' was now reduced by adjusting the focusing electrodes (see Fig. 5) a significant amount to cause I_D' to decrease at least two orders of magnitude. This new detector current I_D'' ($\approx 10^{-9}$ amps) was then recorded. Thus the incident beam must have been $I_i = \frac{I_D''}{G'}$.

Step 6. The Dynode Voltage was turned up to 1,500 volts. The Multiplier now had the configuration desired for the experimental measurements to be made later on. The detector signal I_D now recorded allowed the gain of the Multiplier in this configuration to be computed from:

$$G = \frac{I_D}{I_i}$$

The above procedure was repeated at various values of detector distance Z and focusing magnet current I selected so as to give a measure of G versus the axial magnetic field B. The results of such measurements is shown in Fig. 18.

APPENDIX II

The two computer programs SOLANG and CROSEC are listed in the following chapter.

SOLANG, is the program which integrates the equation of the motion of the scattered H_2^+ ion (equations (8) and (9) of Chapter IV) for predetermined values of the Focusing Magnet Current I, and the Incident Proton Energy E over a range of scattering angles θ. The integration is preformed using the D.H.P.G.C. Subroutine of the IBM System 360-67 Scientific Subroutine Package in the MAIN portion of the program, and in the two Subroutines FCT and OUTP. The resulting distances Z_o, where the trajectory crosses the magnetic axis and the corresponding angles θ_o (see Fig. 21) are stored and later tabulated.

The program now continues on to the Subroutine DOMEGA and the succeeding subroutines, to compute the solid angle $d\Omega(\theta)$ for each of the H_2^+ trajectories. The solid angle is computed using equation (18) of Chapter IV, which is:

$$d\Omega(\theta) = 1.612\pi \sin\theta \left(\frac{\partial\theta}{\partial Z_o}\right)_{E,I} \Delta Z_o$$

ΔZ_o has been determined by Bush, (Ref. 5) and is given by the following relations: (see Fig. (19) for explanation of symbols used)

I for $32.2^o \geq \theta_o \geq 26.6^o$

$$\Delta Z_o = (f+a)\cot\theta_o - 2b$$

II for $26.6^{o} \geq \theta_{o} \geq 17.3^{o}$

$$\Delta Z_{o} = (h+a) \text{ cotan } \theta_{o} - b$$

III for $17.3^{o} \geq \theta_{o} \geq 0^{o}$

$$\Delta Z_{o} = 2h \text{ cotan } \theta_{o}$$

The relation $\left(\frac{\partial \theta}{\partial Z_{o}}\right)_{E,I}$ is determined by fitting the results of Z_{o} versus θ that were obtained in the trajectory integrations by a polynomial $Z_{o} = f(\theta)$. We then evaluate $\frac{\partial Z_{o}}{\partial \theta}$ at the various θ values. In this manner the solid angle $d\Omega$ is computed for various values of θ.

In order that the results may be tabulated for various Z values it is necessary to fit the results of θ versus Z_{o} that were obtained in the trajectory integrations by a polynomial $\theta = f(Z)$. Hence, on choosing a Z, the corresponding θ can be computed and in the manner described above, the solid angle can be determined.

CROSEC is the program which computes the cross section from the experimental measurements of the Detector Current I_{D} and the Incident Proton Current I_{i} which were recorded at various detector distances Z for a particular proton energy E_{1} methane pressure P_{sc} and a particular Focusing Magnet Current B_{mag}.

Because the data is recorded at various detector distances Z, the coefficients of the polynomial $\theta = f(Z)$ that were determined in the program SOLANG are read into CROSEC on data cards and so allow the θ corresponding to each Z to be determined. Rather than read into this program the solid angle at each point Z, the coefficients of the polynomial $\theta_{o} = f(\theta)$ that were determined in SOLANG are read in on data cards. Hence using: $d\Omega(\theta) = 1.612\pi \sin \theta \left(\frac{\partial \theta}{\partial Z}\right) \Delta Z_{o}$ and

the relations for ΔZ_o referred to in the discussion of the program SOLANG, we compute the solid angle at the Θ corresponding to the Z where the data was recorded. Hence using equation (20) of Chapter IV:

$$d\sigma(\Theta) = \frac{I_D}{I_i P_{sc} \rho t \; G \; d\Omega(\Theta)}$$

we compute the cross sections.

Using the transformation from the Laboratory to the Center of Mass coordinates for the reaction $\underline{H}^+ + CH_4 \rightarrow \underline{H}_2^+ + CH_3$ we can determine $\Theta_{C \text{ of } M}$ and hence $\sigma(\Theta)_{C \text{ of } M}$. The results are both tabulated and plotted.

SOLANG

```
//  EXEC  FORTCLG,REGICN.GO=175K,TIME.GO=15
//FORT.SYSIN DD *
C
C   THIS PRCGRAM CALLS CN THE SUBROUTINE CHPCG TO SOLVE TWO DIFFERENTIAL
C   EQUATICNS DESCRIBING THE TRAJECTORY OF THE SCATTERED ION.
C
C
C
      IMPLICIT REAL*8(A-H,C-Z)
      REAL*8 ITITLE(12)/12*8H        /
      REAL*8 LABEL/8H        /
      REAL*4 THET,ZEE
      DIMENSION PRMT(9),Y(2),DERY(2),AUX(16,2),B(13),THESD(30),THEZD(30)
     *,ZERCD(30),THET(30),ZEE(30)
      COMMON B,P,OKAY
      EXTERNAL FCT,CUTP
      CALL CANCEL(2)
      B( 1)=  8.0498907D-02
      B( 2)=  2.3351831D-02
      B( 3)= -4.8664438D+00
      B( 4)=  4.2887590D+01
      B( 5)= -4.3626183D+02
      B( 6)=  3.9271101D+03
      B( 7)= -2.2648265D+04
      B( 8)=  8.2393030D+04
      B( 9)= -1.9359723D+05
      B(10)=  2.9437706D+05
      B(11)= -2.8025472D+05
      B(12)=  1.5200646D+05
      B(13)= -3.5865075D+04
      READ(5,17)P,T
   17 FORMAT(2F10.0)
C   P IS THE PROJECTILE MASS AND T IS THE TARGET MASS IN AMU.
      READ(5,4001) NCT
 4001 FORMAT(I2)
      DO 400 NO =1,NCT
      READ(5,10)(ITITLE(J),J=1,6)
   10 FORMAT(6A8)
      WRITE(6,11)(ITITLE(J),J=1,6)
   11 FORMAT(1H1,6A8,////)
      JON=1
      READ(5,3)ENIT,CUR,THINIT,THINC,THFIN
    3 FORMAT(5F10.5)
      TOM=THINIT-THINC
      NGR=(THFIN-THINIT)/THINC +1.0
      DO 50 I=1,NGR
      PRMT(1)=0.0
      PRMT(2)=0.9
```

```
      PRMT(3)=0.1D-01
      PRMT(4)=0.1D-06
      PRMT(6)=0.0
      TOM=TOM+THINC
      THESD(JCN)=TOM
      A=T*T+T*F-2.0*F*F
      GG=DCOS(THR)
      G=GG*F
      AA=A+2.0*G*G
      C=(T+2.0*F)*(T+2.0*F)
      IF(AA)50,50,20
   20 ENER=ENIT*(A+4.0*G*G+1.414214*2.0*G*DSQRT(AA))/C
      OKAY=(4.17576D-08)*ENER
      P=CUR/10.0
      Y(1)=0.0
       TILT=THESD(JCN)/57.2957795131
      STILL=DTAN(TILT)
      Y(2)=STILL
      NOGOCD=0
    4 DERY(1)=0.5
      DERY(2)=0.5
C NOW DETERMINING THE TRAJECTORY
      CALL DHPCG(PRMT,Y,DERY,2,IHLF,FCT,OUTP,AUX)
      IF(IHLF-11)30,22,22
   22 NOGOCD =NOGOCD+1
      PRMT(3)=PRMT(3)/10.0
      PRMT(4)=PRMT(4)/100.0
      IF(NOGOCD-3)21,30,30
   21 Y(1)=0.0
      Y(2)=STILL
      GO TO 4
   30 CONTINUE
C WRITE OUT RESULSS
      FRACT=PRMT(7)/(PRMT(7)-Y(1))
      Y(1)=0.0
      Y(2)=PRMT(8)+FRACT*(Y(2)-PRMT(8))
      ZEROD(JCN)=(PRMT(6)+FRACT*(PRMT(9)-PRMT(6)))*100.0
      THO=DATAN(Y(2))
      THOD=THO*57.2957795131
      THEZD(JCN)=DABS(THOD)
      WRITE(6,5)  I,CUR,ENIT,ENER,THESD(JCN),ZEROD(JCN),Y(1),THEZD(JCN)
    5 FORMAT(     2X,'RUN=',I2,T12,'CURRENT=',F4.1,T26,'E(INITIAL)=',F5.
     *1,T46,'E(SCAT)=',F5.1,T62,'THETA(S)=',F4.1,//,10X,'Z(ZERO)=',F6.2,
     *T32,'ZERO RADIUS=',D9.2,T58,'THETA(ZERO)=',F5.2)
      IF(IHLF.GE.11.OR.ZEROD(JCN).GE.80.0)GO TO 7
      WRITE(6,6)IHLF
    6 FORMAT(/,10X,'IHLF=',I2,5X,'THIS RUN IS GOOD',////)
    9 FORMAT(/,10X,'IHLF=',I2,5X,'THIS RUN IS IGNORED',////)
```

```
      GO TO 8
    7 WRITE(6,9)IHLF
      GO TO 50
    8 JON=JON+1
   50 CONTINUE
      JON=JON-1
      DO 12 K=1,JON
      THET(K)=THESD(K)
   12 ZEE(K)=ZEROD(K)
      CALL DRAW(JON,THET,ZEE,0,0,LABEL,ITITLE,0,0,0,0,1,1,9,15,1,LAST)
      WRITE(6,13)LAST
   13 FORMAT(2X,'GRAPH OF Z VS THETA HAS LAST=',I2)
      ZINT=ZEE(1)
      ZFIN=ZEE(1)
      DO 54 I =1,JON
      IF(ZINT-ZEE(I))54,54,55
   55 ZINT=ZEE(I)
   54 CONTINUE
      DO 56 I =1,JON
      IF(ZFIN-ZEE(I))51,56,56
   51 ZFIN=ZEE(I)
   56 CONTINUE
      CALL SOLID(THESD,ZEROD,THEZD,JON,ZINT,ZFIN)
  400 CONTINUE
      RETURN
      END


      SUBROUTINE FCT(X,Y,DERY)
      IMPLICIT REAL*8(A-H,O-Z)
      DIMENSION Y(2),DERY(2),B(13),F(6),G(7)
      COMMON B,F,CKAY
      F(1)=B(2)+2.*B(3)*X+3.*B(4)*X**2+4.*B(5)*X**3+5.*B(6)*X**4+6.*B(7)
     1*X**5+7.*B(8)*X**6+8.*B(9)*X**7+9.*B(10)*X**8+10.*B(11)*X**9+11.*B
     2(12)*X**10+12.*B(13)*X**11
      F(2)=6.*B(4)+24.*B(5)*X+60.*B(6)*X**2+120.*B(7)*X**3+210.*B(8)*X**
     14+336.*B(9)*X**5+504.*B(10)*X**6+720.*B(11)*X**7+990.*B(12)*X**8+1
     2320.*B(13)*X**9
      F(3)=120.*B(6)+720.*B(7)*X+2520.*B(8)*X**2+6720.*B(9)*X**3+15120.*
     1B(10)*X**4+30240.*B(11)*X**5+55440.*B(12)*X**6+95040.*B(13)*X**7
      F(4)=5040.*B(8)+40320.*B(9)*X+181440.*B(10)*X**2+604800.*B(11)*X**
     13+1663200.*B(12)*X**4+3991680.*B(13)*X**5
      F(5)=362880.*B(10)+3628800.*B(11)*X+19958400.*B(12)*X**2+79833600.
     1*B(13)*X**3
      F(6)=39916800.*B(12)+479001600.*B(13)*X
      VECDZ=Y(1)*F(1)/2.-F(2)*Y(1)**3/16.+F(3)*Y(1)**5/384.-F(4)*Y(1)**7
```

```
      1/18432.+F(5)*Y(1)**9/1474560.-F(6)*Y(1)**11/176947200.
       G(1)=B(1)+B(2)*X+B(3)*X**2+B(4)*X**3+B(5)*X**4+B(6)*X**5+B(7)*X**6
      1+B(8)*X**7+B(9)*X**8+B(10)*X**9+B(11)*X**10+B(12)*X**11+B(13)*X**1
      22
       G(2)=2.*B(3)+6.*B(4)*X+12.*B(5)*X**2+20.*B(6)*X**3+30.*B(7)*X**4+4
      12.*B(8)*X**5+56.*B(9)*X**6+72.*B(10)*X**7+90.*B(11)*X**8+110.*B(12
      2)*X**9+132.*B(13)*X**10
       G(3)=24.*B(5)+120.*B(6)*X+360.*B(7)*X**2+840.*B(8)*X**3+1680.*B(9)
      1*X**4+3024.*B(10)*X**5+5040.*B(11)*X**6+7920.*B(12)*X**7+11880.*B(
      213)*X**8
       G(4)=720.*B(7)+5040.*B(8)*X+20160.*B(9)*X**2+60480.*B(10)*X**3+151
      1200.*B(11)*X**4+332640.*B(12)*X**5+665280.*B(13)*X**6
       G(5)=40320.*B(9)+362880.*B(10)*X+1814400.*B(11)*X**2+6652800.*B(12
      1)*X**3+19958400.*B(13)*X**4
       G(6)=3628800.*B(11)+39916800.*B(12)*X+239500800.*B(13)*X**2
       G(7)=479001600.*B(13)
       VECDR=G(1)/2.-3.*G(2)*Y(1)**2/16.+5.*G(3)*Y(1)**4/384.-7.*G(4)*Y(1
      1)**6/18432.+9.*G(5)*Y(1)**8/1474560.-11.*G(6)*Y(1)**10/176947200.+
      213.*G(7)*Y(1)**12/29727129600.
       VECPT=Y(1)*G(1)/2.-G(2)*Y(1)**3/16.+G(3)*Y(1)**5/384.-G(4)*Y(1)**7
      1/18432.+G(5)*Y(1)**9/1474560.-G(6)*Y(1)**11/176947200.+G(7)*Y(1)**
      213/29727129600.
       FUNC1=CKAY-VECPT*VECPT*P*P
       FUNC2=VECPT*VECDZ*P*P
       FUNC3=VECPT*VECDR*P*P
       FUNC4=(FUNC2)/(FUNC1)
       FUNC5=(FUNC3)/(FUNC1)
       DERY(2)=Y(2)*(FUNC4)+Y(2)*Y(2)*Y(2)*(FUNC4)-Y(2)*Y(2)*(FUNC5)-(FUN
      1C5)
       DERY(1)=Y(2)
       RETURN
       END


       SUBROUTINE CUTP(X,Y,DERY,IHLF,NDIM,PRMT)
C
       REAL*8 Y,PRMT,X
       DIMENSION Y(2),PRMT(9)
       IF((Y(1).LE.0.0).AND.(X.GE.0.5D-01))GO TO 1
       GO TO 2
     1 PRMT(5)=1.0
       PRMT(9)=X
       RETURN
     2 PRMT(6)=X
       PRMT(7)=Y(1)
       PRMT(8)=Y(2)
```

```
      RETURN
      END


      SUBRCUTINE SOLID(X,ZZ,YY,M,ZINT,ZFIN)
C  PROGRAM TO COMPUTE THE COEFFICENTS CZ AND CT OF THE LEAST SQUARES
C  FITTED POLYNOMIALS Z(ZERO) VS THETA(S) AND THETA(O) VS THETA(S)
C  RESPECTIVELY.  X(I) IS THETA(S),ZZ(I) IS  Z(O),YY(I) IS THETA(O)
C  KM IS THE MAXIMUM DEGREE OF FIT  ANC M IS THE NUMBER OF DATA POINTS-
C  LIMITED TO 500.   FROM THESE POLYNOMIALS THE SOLID ANGLE OCME IS
C  COMPUTED IN THE SUBROUTINE OCMEGA
      IMPLICIT REAL*8(A-H,O-Z)
      DIMENSION X(100),F(100),W(100),YY(99),DELY(100),B(20),SB(20),T(20)
     1,ST(20),C(20),SC(20),A(30,30),CZ(11),CT(11),ZZ(99),Y(100),CTZ(11)
      READ(5,1)KM
    1 FORMAT(I1)
      IR=KM+1
      JIM=-1
      DO 3 I=1,11
      CZ(I)=0.0
      CTZ(I)=0.0
    3 CT(I)=0.0
   11 IF(JIM)21,22,23
   21 DO 6 I=1,M
    6 F(I)=ZZ(I)
      GO TC 7
   22 DO 8 I=1,M
    8 F(I)=YY(I)
      GO TC 7
   23 DO 16 I=1,M
      F(I)=X(I)
   16 X(I)=ZZ(I)
    7 CALL LSCPCL(M,KM,0,1,1,SIGMA,X,F,W,Y,DELY,B,SB,T,ST,C,SC,A)
      JIM=JIM+1
      IF(JIM-1)9,12,14
    9 DO 10 I=1,IR
   10 CZ(I)=B(I)
      GO TC 11
   12 DC 13 I=1,IR
   13 CT(I)=B(I)
      GO TC 11
   14 DO 15 I=1,IR
   15 CTZ(I)=B(I)
      CALL COMEGA(CZ,CT,CTZ,ZINT,ZFIN)
      RETURN
      END
```

```
      SUBROUTINE CCMEGA(CZ,CT,CTZ,ZINT,ZFIN)
C   PROGRAM TO CCMPUTE THE SCLIC ANGLE CCME
C   LIMITED TO 900 ITERATIONS BETWEEN THETA INITIAL AND THETA FINAL
C   MAX DEGREE OF PCLYNCMIALS 10
C
      IMPLICIT REAL*8(A-H,O-Z)
      REAL*8 ITITLE(12)/12*8H        /
      REAL*8 LABEL/8H        /
      REAL*4 X,Y
      DIMENSION X(900),Y(900),CZ(20),CT(20),T(900),DOME(900),TR(900),THE
     *T(900),CTZ(20),Z(900)
      IZINT=ZINT
      IZFIN=ZFIN+1.0
      ZINT=IZINT
      ZFIN=IZFIN
      IF(ZFIN-55.0)21,21,22
   22 ZFIN=55.0
   21 CONTINUE
      ZINC=1.0
      Z(1)=ZINT
      K1=(ZFIN-ZINT)/ZINC +1.0
      DO 3 I =2,K1
      J=I-1
    3 Z(I)=Z(J)+ZINC
      READ(5,5)(ITITLE(J),J=1,6)
    5 FORMAT(6A8)
      WRITE(6,11)(ITITLE(J),J=1,6)
   11 FORMAT(1H1,6A8,//)
C COMPUTE THE SOLIC ANGLE FCR VARICUS VALUES OF Z
      WRITE(6,6)
    6 FORMAT(4X,'Z',T11,'THETA',T17,'SCLIC ANGLE',T29,'D(THETA)/DZ',T41,
     *'DZ',T45,'THETA(0)',//)
      DO 7 I =1,K1
      T(I)=ANG(CTZ,Z(I))
      SLOP=SLCPE(CZ,T(I))
      TR (I)=T(I)/57.2957795131D+00
      D=DELZ(CT,T(I),TR(I))
      S=DSIN(TR(I))
      P=0.08731D+00
      DOME(I)=DABS(P*S*SLOP*D)
    7 WRITE(6,8)Z(I),T(I),DOME(I),SLOP,D
    8 FCRMAT(1H+,2X,F4.1,T10,F7.4,T19,F8.6,T31,F7.4,T41,F3.1,T46,F5.2)
      DO 9 I=1,K1
      THET(I)=T(I)
```

```
      RETURN
      END


      SUBROUTINE SOLID(X,ZZ,YY,M,ZINT,ZFIN)
C     PROGRAM TO COMPUTE THE COEFFICENTS CZ AND CT OF THE LEAST SQUARES
C     FITTED POLYNOMIALS Z(ZERO) VS THETA(S) AND THETA(O) VS THETA(S)
C     RESPECTIVELY.  X(I) IS THETA(S),ZZ(I) IS  Z(0),YY(I) IS THETA(0)
C     KM IS THE MAXIMUM DEGREE OF FIT  AND M IS THE NUMBER OF DATA POINTS-
C     LIMITED TO 500.   FROM THESE POLYNOMIALS THE SOLID ANGLE DOME IS
C     COMPUTED IN THE SUBROUTINE DOMEGA
      IMPLICIT REAL*8(A-H,O-Z)
      DIMENSION X(100),F(100),W(100),YY(99),DELY(100),B(20),SB(20),T(20)
     1,ST(20),C(20),SC(20),A(30,30),CZ(11),CT(11),ZZ(99),Y(100),CTZ(11)
      READ(5,1)KM
    1 FORMAT(I1)
      IR=KM+1
      JIM=-1
      DO 3 I=1,11
      CZ(I)=0.0
      CTZ(I)=0.0
    3 CT(I)=0.0
   11 IF(JIM)21,22,23
   21 DO 6 I=1,M
    6 F(I)=ZZ(I)
      GO TO 7
   22 DO 8 I=1,M
    8 F(I)=YY(I)
      GO TO 7
   23 DO 16 I=1,M
      F(I)=X(I)
   16 X(I)=ZZ(I)
    7 CALL LSQPOL(M,KM,0,1,1,SIGMA,X,F,W,Y,DELY,B,SB,T,ST,C,SC,A)
      JIM=JIM+1
      IF(JIM-1)9,12,14
    9 DO 10 I=1,IR
   10 CZ(I)=B(I)
      GO TO 11
   12 DO 13 I=1,IR
   13 CT(I)=B(I)
      GO TO 11
   14 DO 15 I=1,IR
   15 CTZ(I)=B(I)
      CALL DOMEGA(CZ,CT,CTZ,ZINT,ZFIN)
      RETURN
      END
```

```
      SUBROUTINE CCMEGA(CZ,CT,CTZ,ZINT,ZFIN)
C   PROGRAM TO COMPUTE THE SCLIC ANGLE CCME
C   LIMITED TO 900 ITERATIONS BETWEEN THETA INITIAL AND THETA FINAL
C   MAX DEGREE OF PCLYNOMIALS 10
C
      IMPLICIT REAL*8(A-H,O-Z)
      REAL*8 ITITLE(12)/12*8H        /
      REAL*8 LABEL/8H        /
      REAL*4 X,Y
      DIMENSION X(900),Y(900),CZ(20),CT(20),T(900),DOME(900),TR(900),THE
     *T(900),CTZ(20),Z(900)
      IZINT=ZINT
      IZFIN=ZFIN+1.0
      ZINT=IZINT
      ZFIN=IZFIN
      IF(ZFIN-55.0)21,21,22
   22 ZFIN=55.0
   21 CONTINUE
      ZINC=1.0
      Z(1)=ZINT
      K1=(ZFIN-ZINT)/ZINC +1.0
      DO 3 I =2,K1
      J=I-1
    3 Z(I)=Z(J)+ZINC
      READ(5,5)(ITITLE(J),J=1,6)
    5 FORMAT(6A8)
      WRITE(6,11)(ITITLE(J),J=1,6)
   11 FORMAT(1H1,6A8,//)
C COMPUTE THE SOLIC ANGLE FCR VARICUS VALUES OF Z
      WRITE(6,6)
    6 FORMAT(4X,'Z',T11,'THETA',T17,'SCLIC ANGLE',T29,'D(THETA)/DZ',T41,
     *'DZ',T45,'THETA(0)',//)
      DO 7 I =1,K1
      T(I)=ANG(CTZ,Z(I))
      SLOP=SLCPE(CZ,T(I))
      TR (I)=T(I)/57.2957795131D+00
      D=DELZ(CT,T(I),TR(I))
      S=DSIN(TR(I))
      P=0.08731D+00
      DOME(I)=DABS(P*S*SLOP*D)
    7 WRITE(6,8)Z(I),T(I),DCME(I),SLOP,D
    8 FCRMAT(1H+,2X,F4.1,T10,F7.4,T19,F8.6,T31,F7.4,T41,F3.1,T46,F5.2)
      DO 9 I=1,K1
      THET(I)=T(I)
```

```
      X(I)=T(I)
    9 Y(I)=DOME(I)
      CALL DRAW(K1,X,Y,0,0,LABEL,ITITLE,0,0,0,0,1,1,9,15,1,LAST)
      WRITE(6,10)LAST
   10 FORMAT(//,5X,'LAST=',I5)
      RETURN
      END


      FUNCTION ANG(CTZ,Z)
      IMPLICIT REAL*8(A-H,O-Z)
      DIMENSION CTZ(11)
      ANG=CTZ(1) +CTZ(2)*Z +CTZ(3)*Z**2 +CTZ(4)*Z**3 +CTZ(5)*Z**4 +CTZ(6
     *)*Z**5 +CTZ(7)*Z**6 +CTZ(8)*Z**7 +CTZ(9)*Z**8 +CTZ(10)*Z**9 +CTZ(1
     *1)*Z**10
      RETURN
      END


      FUNCTION SLOPE(CZ,F)
      IMPLICIT REAL*8(A-H,O-Z)
      DIMENSION CZ(11)
      DZDT=CZ(2)+2.0*CZ(3)*F   +3.0*CZ(4)*F**2   +4.0*CZ(5)*F**3   +5.0*
     1CZ(6)*F**4   +6.0*CZ(7)*F**5   +7.0*CZ(8)*F**6   +8.0*CZ(9)*F**7
     8 +9.0*CZ(10)*F**8   +10.0*CZ(11)*F**9
      SLOPE=1.0/DZDT
    4 RETURN
      END


      FUNCTION DELZ(CT,G,TR)
      IMPLICIT REAL*8(A-H,O-Z)
      DIMENSION CT(11),T(900)
      TZERO= CT(1) +CT(2)*G +CT(3)*G**2 +CT(4)*G**3 +CT(5)*G**4 +CT(6)*G
     1**5 +CT(7)*G**6 +CT(8)*G**7 +CT(9)*G**8 +CT(10)*G**9 +CT(11)*G**10
      TZERR=TZERO/57.2957795131
      WRITE(6,9)TZERO
    9 FORMAT(46X,F5.2)
      IF(TZERO-1.0)11,12,12
   11 GO TO 7
   12 CONTINUE
      IF(TZERO-17.3)1,1,2
```

```
1 DELZ=0.635*DCCTAN(TZERR)
  GO TC 7
2 IF(TZERD-26.6)3,3,4
3 DELZ=1.0318*DCOTAN(TZERR)-1.27
  GO TC 7
4 IF(TZERD-33.2)5,5,6
5 DELZ=1.6668*DCCTAN(TZERR)-2.54
  GO TC 7
6 WRITE(6,8)
8 FORMAT(1H+,5X,'THETA(ZERC) GREATER THAN 33.2 DEGREES',/)
7 CONTINUE
  RETURN
  END
```

CROSEC

```
// EXEC FORTCLGP,REGION.GO=100K
//FORT.SYSIN DD *
C     CSVSZ - THIS PROGRAM CALCULATES THE  CROSS SECTION  WHEN THE DATA
C             WAS TAKEN BY KEEPING THE CURRENT  FIXED AND VARYING THE
C             DETECTOR DISTANCE
C
C
      IMPLICIT REAL*8 (A-H,O-Z)
      REAL*8 ITITLE(12),IBLANK/8H        /,LABEL/8H        /
      REAL*4 SLB,SCM,PSSG,BCS,DS
      DIMENSION F(13),TL(100),SLA(100),CT(9),B(13),TD(9),TCM(100),
     1          SCM(100),TLB(100),SLB(100)
      RHO=3.536D+16
C
C     THE B(I) COEFFICIENTS ARE THE AXIAL MAGNETIC FIELD STRENGTH VS Z
C     12TH ORDER POLYNOMIAL FIT.
      B( 1)=  8.0498907D-02
      B( 2)=  2.3351831D-02
      B( 3)= -4.8664438D+00
      B( 4)=  4.2887590D+01
      B( 5)= -4.3626183D+02
      B( 6)=  3.9271101D+03
      B( 7)= -2.2648265D+04
      B( 8)=  8.2393030D+04
      B( 9)= -1.9359723D+05
      B(10)=  2.9437706D+05
      B(11)= -2.8025472D+05
      B(12)=  1.5200646D+05
      B(13)= -3.5865075D+04
C
C     THE F(I) COEFFICIENTS ARE LOG10(MULTIPLIER GAIN) VS AXIAL
C     FIELD STRENGTH  12TH ORDER POLYNOMIAL FIT FOR
C     INPUT DIFFERENTIAL=250V.
C     DYNODE STRIP POT  =1500V.
C     OUTPUT DIFFERENTIAL=250V.
      F( 1)= 2.8128368D+02
      F( 2)=-4.6963571D+01
      F( 3)= 3.4654789D+00
      F( 4)=-1.4672706D-01
      F( 5)= 3.9711700D-03
      F( 6)=-7.2495145D-05
      F( 7)= 9.1801618D-07
      F( 8)=-8.1561429D-09
      F( 9)= 5.0665520D-11
      F(10)=-2.1546053D-13
      F(11)= 5.9758605D-16
      F(12)=-9.7372900D-19
      F(13)= 7.0695689D-22
```

```
C
C     TM IS TARGET MASS IN AMU.  PM IS ION MASS IN AMU.
      READ(5,103)PM,TM
  103 FORMAT(2F10.0)
C
C     THE CT(I) COEFFICIENTS GIVE THETA VS Z.
      READ(5,101)(CT(I),I=1,7)
C
C     THE TO(I) COEFFICIENTS GIVE THETA ZERO VS THETA
      READ (5,101)(TO(I),I=1,7)
  101 FORMAT(3D20.7)
      READ(5,105)NR
  105 FORMAT(I2)
      DO 99 K=1,NR
      READ(5,100) NRPTS,S,PSCG,BMAG,PGC
  100 FORMAT(I5,F5.0,D10.3,2F5.0)
      PSC=PSCG*PGC
      TGTPT =PSCG*RHO*PGC
      WRITE(6,112) TM,PM,S,PSC,BMAG
  112 FORMAT(1H1,///,T10,'TGT  MASS(AMU)  =',1PD13.6,/,
     1               T10,'PROJ MASS(AMU)  =',1PD13.6,/,
     2               T10,'CELL OPENING    =',1PD13.6,/,
     3               T10,'CELL PRESSURE   =',1PD13.6,/,
     4               T10,'MAGNET CURRENT  =',0PF5.1)
      WRITE(6,110)
  110 FORMAT(/////,T2,'Z ',T6,'THETA(L)',T16,'SIGMA(L)',T26,'THETA(CM)',
     1        T36,'SIGMA(CM)',T46,'COLL CUR',T56,'DET CUR',T66,'DOME',
     2        T75,'GAIN',T85,'T',//)
      DO 51 I=1,NRPTS
      READ(5,102)Z,BCI,DI
  102 FORMAT(F5.0,2D10.3)
      Z=Z+15.5
      ZM=Z
      Z=Z/100.
      HO = B(1)+B(2)*Z+B(3)*Z**2+B(4)*Z**3+B(5)*Z**4+B(6)*Z**5+B(7)*Z**6
     1+B(8)*Z**7+B(9)*Z**8+B(10)*Z**9+B(11)*Z**10+B(12)*Z**11+B(13)*Z**1
     22
      HO=HO*BMAG*1000.
      G=F(1)+F(2)*HO+F(3)*HO**2+F(4)*HO**3+F(5)*HO**4+F(6)*HO**5
     1+F(7)*HO**6+F(8)*HO**7+F(9)*HO**8+F(10)*HO**9+F(11)*HO**10
     2+F(12)*HO**11+F(13)*HO**12
      G = 10.**G
      Z=ZM
      THETA  = CT(1)+CT(2)*Z+CT(3)*Z**2+CT(4)*Z**3+CT(5)*Z**4+CT(6)*Z**5
     1        +CT(7)*Z**6
      THL= THETA*3.14159/180.
      IF(THETA-49.)11,11,12
   11 IF(THETA-36.)13,14,14
```

```
C
C      T WHEN THETA IS GREATER THAN 49 DEG.
   12 T=S-1.3122+1.5094*DCOTAN(THL)
      GO TO 16
C
C      T WHEN THETA IS LESS THAN 36 DEG.
   13 T=S-1.493*DCOTAN(THL)+2.0548
      GO TO 16
C
C      T WHEN THETA LIES BETWEEN 36 AND 49 DEGREES.
   14 T=S
   16 IF(T-.01)18,17,17
   18 WRITE(6,115)Z,THL
  115 FORMAT(F5.1,T8,F5.2,T15,'..T IS LESS THAN 0.01 CM.',/)
      GO TO 51
   17 DTDZ = CT(2) +2.*CT(3)*Z +3.*CT(4)*Z**2 +4.*CT(5)*Z**3 +5.*CT(6)
     1*Z**4+6.*CT(7)*Z**5
      DTDZ =DABS(DTDZ)
      THO = TO(1)+TO(2)*THETA+TO(3)*THETA**2+TO(4)*THETA**3+TO(5)*THETA*
     1*4+TO(6)*THETA**5+TO(7)*THETA**6
      THOR = THO*3.14159/180.
   30 IF(THO-17.3)31,31,32
   31 DZ = 0.635*DCOTAN(THOR)
      GO TO 35
   32 IF(THO-26.6)33,33,34
   33 DZ = 1.0318*DCOTAN(THOR)-1.27
      GO TO 35
   34 DZ = 1.6668*DCOTAN(THOR)-2.54
   35 DOME = 0.08731281*DSIN(THL)*DTDZ*DZ
      SL=DI/(G*BCI*TGTPT*T*DOME)
      A=TM*TM+TM*PM-2.0*PM*PM
      GAG=DCOS(THL)
      GC=GAG*PM
      AA=A+2.0*GC*GC
      CAT=DSQRT(A+4.0*GC**2+1.414214*2.0*GC*DSQRT(AA))
      BETA=DSQRT(2.0*PM**2)/CAT
      FIG=DSIN(THL)/(DCOS(THL)-BETA)
      THC=DATAN(FIG)
      GAM=DSQRT(2.0*PM**2/(TM*PM+TM**2))
   21 A=1.0+GAM*DCOS(THC)
      A=DABS(A)
      BA=1.0+GAM**2+2.0*GAM*DCOS(THC)
      BAD=BA**3
      SC=SL*A/BAD
      THL=THL*180./3.14159
      THC=THC*180./3.14159
      TLB(I)=THL
      SLB(I)=DLOG10(SL)
```

```
      TCM(I)=THC
      SCM(I)=DLOG10(SC)
   50 WRITE(6,111)Z,THL,SL,THC,SC,BCI,DI,DOME,G,T
  111 FORMAT(F5.1,T8,F5.2,T15,1PD10.3,T27,0PF6.2,T35,1P3D10.3,
     1       T66,0PF6.4,1PD10.3,0PF8.5,/)
   51 CONTINUE
      READ(5,104)(ITITLE(J),J=1,12)
  104 FORMAT(6A8)
   52 IF(ITITLE(1)-IBLANK)60,61,60
   60 CALL DRAW(NRPTS,TLB,SLB,0,1,LABEL,ITITLE,0,0,0,0,1,1,9,15,1,LAST)
  113 FORMAT(T10,'LAST = ',I1)
      WRITE(6,113)LAST
      CALL DRAW(NRPTS,TCM,SCM,0,2,LABEL,ITITLE,0,0,0,0,1,1,9,15,1,LAST)
      WRITE(6,113)LAST
      GO TO 99
   61 WRITE(6,114)
  114 FORMAT(///,T5,'... NO GRAPH REQUESTED.')
      WRITE(6,104)(ITITLE(J),J=1,12)
   99 CONTINUE
      RETURN
      END
```

LIST OF REFERENCES

1. Bates, D.R.; Cook, C.J.; Smith, F.J.; "Classical Theory of Ion-Molecule Rearrangement Collisions at High Impact Energies", Proc. Phys. Soc., Vol. 83, p. 49, 1964.

2. Thomas, L.H.; "On the Capture of Electrons by Swiftly Moving Electrified Particles", Roy. Soc. Proc., Vol. A114, p. 561, 1927.

3. Byatt, W.J.; "Analytical Representation Hartree Potentials and Electron Scattering", Physical Review, Vol. 104, No. 5, Dec 1, 1956.

4. McDaniel, E. W.; "Collision Phenomena in Ionized Gases", J. Wiley, 1964.

5. Bush, T.O.; "Large Angle Scattering of Lithium Ions by Helium Atoms", Unpublished Ph.D. Thesis, Naval Postgraduate School, Monterey, California, 1968.

6. Carter, T.L.; "Ion Sources for the Production of Low Energy Beams", Unpublished Masters Thesis, Naval Postgraduate School, Monterey, California, 1968.

7. Strohsahl, G.H.; "Construction and Calibration of a Mass Spectrometer for the Analysis of Light Ions", Unpublished Masters Thesis, Naval Postgraduate School, Monterey, California, 1967.

8. Kelly, P.J.; "Analogue Measurements of Charged Particle Trajecteries in an Inhomogeneous Magnetic Field", Unpublished Masters Thesis, Naval Postgraduate School, Monterey, California, 1965.

9. Gagliano, R.A.; "Theoretical Trajectories of Charged Particles in an Inhomogeneous Magnetic Field", Unpublished Masters Thesis, Naval Postgraduate School, Monterey, California, 1966.

10. Bush, T.O.; Heinz, O.; Rodeback, G.W.; Cook, C.J.; "Measurements of Large Angle Atomic Scattering Using Axially Symmetric Magnetic Fields", Submitted for Publication.

INITIAL DISTRIBUTION LIST

		No. of Copies
1.	Defense Documentation Center Cameron Station Alexandria, Virginia 22314	20
2.	Library Naval Postgraduate School Monterey, California 93940	2
3.	Dr. Otto Heinz Department of Physics Naval Postgraduate School Monterey, California 93940	5
4.	Dr. Charles J. Cook Stanford Research Institute (A220) Menlo Park, California 94025	3
5.	Capt. Norman R.A. Smyth DMCS 2 Canadian Forces Headquarters Ottawa 4, Canada	3
6.	Dr. Don E. Harrison, Jr. Department of Physics Naval Postgraduate School Monterey, California 93940	1
7.	Mr. Thomas Maris Department of Physics Naval Postgraduate School Monterey, California 93940	1
8.	Lt. Thomas O. Bush, USN 1017 Laguna Livermore, California 94550	1
9.	Lt. E.V. Snotherly 1144 Spruance Monterey, California 93940	1

Unclassified

Security Classification

DOCUMENT CONTROL DATA - R & D

(Security classification of title, body of abstract and indexing annotation must be entered when the overall report is classified)

ORIGINATING ACTIVITY (Corporate author)

Naval Postgraduate School
Monterey, California 93940

2a. REPORT SECURITY CLASSIFICATION

Unclassified

2b. GROUP

REPORT TITLE

The Cross Section for the Formation of H_2^+ in the Reaction of Fast Protons with Methane

DESCRIPTIVE NOTES (Type of report and, inclusive dates)

Master's Thesis; June 1969

AUTHOR(S) (First name, middle initial, last name)

Norman R.A. Smyth

REPORT DATE

June 1969

7a. TOTAL NO. OF PAGES

108

7b. NO. OF REFS

10

8a. CONTRACT OR GRANT NO.

b. PROJECT NO.

c.

d.

9a. ORIGINATOR'S REPORT NUMBER(S)

9b. OTHER REPORT NO(S) (Any other numbers that may be assigned this report)

10. DISTRIBUTION STATEMENT

Distribution of this document is unlimited.

11. SUPPLEMENTARY NOTES

12. SPONSORING MILITARY ACTIVITY

Naval Postgraduate School
Monterey, California 93940

13. ABSTRACT

The capture cross section for the formation of H_2^+ in the reaction $H^+ + CH_4 \rightarrow H_2^+ + CH_3$ was measured at incident proton energies of 70, 85, 100, 150 and 200 eV and covering the scattering angles of 43° to 49.5° (lab coordinates). At 100 eV and below the curve of the cross section versus angle shows a sharp peak at about 46° whose position approaches the theoretical limit of 46.9° with increasing energy. Above 100 eV the peak was too small to be observed and only an upper limit can be placed on the value of the cross section. Typical values of the total cross section are 2.0×10^{-21} cm^2 at 70 eV and 7.6×10^{-22} at 100 eV. The magnitude and energy dependence of the cross section as well as the angular position of the peak all are in essential agreement with the classical theory of ion-molecule rearrangement collisions proposed by Bates, Cook and Smith.

14 KEY WORDS	LINK A		LINK B		LINK C	
	ROLE	WT	ROLE	WT	ROLE	WT
Atomic collision processes						
ion-atom rearrangement collision						
classical impulse approximation						
capture process						
Axially symmatric magnetic field						
Cross section for H_2^+ formation						
Large angle scattering						